

**DEVELOPMENT OF A NANOGEL BASED TOPICAL DRUG FORMULATION FOR  
THE TREATMENT OF NEOVASCULAR AGE-RELATED MACULAR  
DEGENERATION (nAMD)**

by

HANDE EDA ŞUTOVA

Submitted to the Graduate School of Engineering and Natural Sciences

in partial fulfillment of the requirements for the degree of

Master of Science

Sabancı University

**July 2022**

**DEVELOPMENT OF A NANOGEL BASED TOPICAL DRUG FORMULATION  
FOR THE TREATMENT OF NEOVASCULAR AGE-RELATED MACULAR  
DEGENERATION (nAMD)**

APPROVED BY:

DATE OF APPROVAL: **25/07/2022**

© Hande Eda Şutova

2022 All Rights Reserved

## **Abstract**

# **DEVELOPMENT OF A NANOGEL BASED TOPICAL DRUG FORMULATION FOR THE TREATMENT OF NEOVASCULAR AGE-RELATED MACULAR DEGENERATION (nAMD)**

HANDE EDA ŞUTOVA

Molecular Biology, Genetics and Bioengineering, M.Sc. Thesis, July, 2022

Thesis Supervisor: Assist. Prof. Sibel Çetinel

**Keywords:** HRH peptide, nanogel, age-related macular degeneration, penetratin

Age-related macular degeneration (AMD) is a complex eye disease leading irreversible vision loss of mostly 65 years-old or older individuals. AMD accounts for 8.7 % of blindness globally and an estimate of one of five people in aging populations (60-year-old or more), one of five people may have this disease. AMD is classified into two main types: early AMD and late AMD. Late AMD may be distinguished in two forms: wet (neovascular) and dry (non-neovascular) AMD. Early stages AMD is characterized by changes occurred in retinal pigment epithelium (RPE) and drusen (small yellowish white deposits) formations. Laser photocoagulation and injection of VEGF inhibitors (ranibizumab, bevacizumab, aflibercept, and pegaptanib, brolocizumab, abicipar, conbercept, faricimab, pazaopanib) are the approaches for AMD treatment. However, there are several patients, who do not respond well to these treatments or face with side effects such as pain and infection. In addition, the treatment is costly and experienced professionals are required to perform intravitreal injections. The aim of this study is to develop a topical nanodrug formulation with less cost of production, capable of crossing the anatomical and physiological barriers of the eye. To this aim, an anti-VEGF peptide that has high affinity to VEGF-Fc receptor was used as the bioactive agent to control neovascularization of retina. In this nano formulation, a cell penetrating peptide (penetratin peptide) and hyaluronic acid (HA), which is specific to retina were combined with the anti-VEGF peptide. To increase the stability and control the size of the nanodrug, divinyl sulfone (DVS) and cholesterol were used, respectively. Initial results on HUVE cells and ARPE-19 cells indicate that nanodrug inhibits HUVE cell proliferation in a dose dependent manner, whereas it does not affect ARPE-19 cells proliferation. Encapsulation efficacy of nanogels

were 65 % and 53 % for nanogel 1 and nanogel 2, respectively. Drug release was 34,72 % from nanogel 1 at the end of 192 hours, and 36% of drug was released from nanogel 2 at the end of 24 hours. We believe that nanogels formulated in this study can be improved and investigated further as a potential AMD treatment approach. The promising data obtained from *in vitro* studies should also be validated with *in vivo* models to confirm the efficiency of the nanodrugs.

## Özet

# NEOVASKÜLER YAŞA BAĞLI MAKULAR DEJENERASYON TEDAVİSİ İÇİN TOPIKAL BİR İLAÇ FORMÜLASYONUNUN GELİŞTİRİLMESİ

HANDE EDA ŞUTOVA

Moleküler Biyoloji, Genetik ve Biyomühendislik, Yüksek Lisans Tezi,

2022 Tez Danışmanı: Dr. Öğretim Üyesi Sibel Çetinel

Anahtar kelimeler: HRH peptid, nanojel, yaşa bağlı maküla  
dejenarasyonu, penetratin

Yaşa bağlı macula dejenerasyonu, çoğunlukla 60 yaş ve üzeri kişilerde geri dönüşü olmayan görme kaybına yol açan karmaşık bir göz hastalığıdır. Yaşa bağlı maküle dejenerasyonu, dünyada kişilerde görülen görme kayıplarının % 8.7'sini oluşturmaktadır. Yaşlanan popülasyonlarda her beş kişiden birinin bu hastalığa sahip olabileceği tahmin edilmektedir. Yaşa bağlı maküla dejenerasyonu iki ana tipte sınıflandırılır: erken ve geç maküla dejenerasyonu. Geç maküla dejenerasyonu ıslak (neovasküler) ve kuru (neovasküler olmayan) olmak üzere iki şekilde sınıflandırılabilir. Erken evre maküla dejenerasyonu, retina pigment epitelinde meydana gelen değişiklikler ve küçük, sarımsı beyaz birikintilerin oluşumu ile karakterize edilir. Lazer fotokoagülasyon, VEGF inhibitörleri, ranibizumab, bevacizumab, aflibercept, pegaptanib, brolucizumab, abicipar, conbercept, faricimab, pazopanib ve bazı anti-VEGF peptidleri yaşa bağlı maküla dejenerasyonu tedavisinde kullanılan yöntemlerdir, ancak bu tedavilere yanıt vermeyen veya ağrı, enfeksiyon gibi yan etkilerle karşılaşan çok sayıda hasta bulunmaktadır. Ayrıca tedavi oldukça maliyetlidir ve intravitreal enjeksiyonlar yapmak için deneyimli profesyonellere ihtiyaç vardır. Bu çalışmanın amacı, daha az üretim maliyeti olan ve anatomik ve fizyolojik bariyerleri aşabilen topical bir nano-ilaç formülasyonu geliştirmektir. Bu amaçla, VEGF-Fc reseptörüne yüksek afinitesi olan bir anti-VEGF peptidinin maküla dejenerasyonu tedavisinde kullanılması düşünülmüştür. Bu nanoformülasyonda, hücreye nüfuz etme kabiliyeti olan bir peptid (penetratin) ve retinaya spesifik hyaluronik asit ve anti-VEGF peptid birleştirilirken, nanoilacın stabilitesini arttırmak

için divinyl sulfone, hidrofobitesini arttırmak için ise kolesterol kullanılmıştır. HUVEC ve ARPE-19 hücreleri üzerindeki ilk sonuçlar, nanoilacın HUVEC hücre proliferasyonunu doza bağlı bir şekilde inhibe ettiğini, buna karşın ARPE-19 hücrelerinin proliferasyonunu etkilemediğini göstermektedir. HUVEC ve ARPE-19 hücreleri üzerinde denenen nanojellerin (nanojel 1 ve nanojel 2) enkapsülasyon verimliliğinin ise sırasıyla % 65 ve % 53 olduğu sonucuna ulaşılmıştır. 192 saat sonunda ilaç salımı nanojel 1'den %34.72 iken 24 saat sonunda nanojel 2'den gerçekleşen ilaç salımı %36 olarak saptanmıştır. Bu çalışmada formülize edilen nanojellerin, enjekte edilebilir monoclonal antikorlara alternatif AMD tedavisi olarak geliştirilebileceği ve araştırılabileceği sonucuna varılmıştır. *In vitro* çalışmalardan elde edilen umut verici veriler, nanoilaçların etkinliğini doğrulamak için *in vivo* modellerle doğrulanmalıdır.

*“To my mother, brother, and my dearest father whose soul is always with me...”*

*“Canım anneme, canım kardeşime, yakın zamanda kaybettiğim, çok özlediğim, herkesten çok sevdiğim ve ruhunun her zaman benimle olduğuna inandığım en kıymetlim babama...”*

## Acknowledgements

I would like to express my sincere gratitude to my supervisor Assist. Prof. Sibel Çetinel for her infinite support, guidance, and motivation. I am grateful for her endless patience and encouragement. I realized her believe in me when I faced with several troubles during my research, and she gave me every possible opportunity to improve my abilities in the project. It was a great opportunity to work under her supervision. I also would like to thank my co-advisor Assoc. Prof. Özlem Kutlu for her believe in me and giving serious responsibilities in a second project. I also thank to my master thesis committee, Assoc. Prof. Özlem Kutlu, Assist. Prof. Nur Mustafaoğlu Varol, Assoc. Prof. Emrah Şefik Abamor, and Assist. Prof. Cavit Ağca for spending their valuable time to evaluate my thesis and to provide valuable comments and advice.

I would like to give grateful thanks to my lab members Sevilay Burcu Şahin, Abuzer Alp Yetişgin, Hale Kesim, and Saliha Durak who have been a great support mechanism to me as I need solutions. I shared every moment in the lab and in our social lives and had so much fun. Thank you so much for letting me experience a cornea dissection process! I would also like to thank present members of Çetinel Lab for giving me valuable advice during preparation of my thesis.

Finally, I would like to express my deepest appreciation to my dearest father, Atila Şutova, who passed away 4 months before my graduation, I know you are always with me, and I cannot thank enough you to make me the luckiest person as I am your daughter. I also would like to thank to my mother, Şengül Şutova, and my brother, Talat Şutova, who always makes me out loud even in my most stressful days, for their endless love and support and showing how strong bonds we have as a family. I love you and I am grateful to have you. Thank you for being a wonderful family and thank you for your kindness and patience.

## **Table of Contents**

<b>1.</b>	<b>Introduction</b>	<b>13</b>
<b>1.1.</b>	<b>Age-Related Macular Degeneration</b>	<b>13</b>
<b>1.1.1</b>	<b>Structure of Macula</b>	<b>14</b>
<b>1.1.2</b>	<b>Pathophysiology of AMD</b>	<b>15</b>
<b>1.1.3</b>	<b>Treatment of AMD</b>	<b>16</b>
<b>1.2.</b>	<b>Anti-VEGF Therapies in Ophthalmology</b>	<b>17</b>
<b>1.2.1</b>	<b>Topical drug delivery for the posterior segment eye diseases</b>	<b>22</b>
<b>1.3</b>	<b>Cell-penetrating peptides (CPPs)</b>	<b>26</b>
<b>1.3.1</b>	<b>CPP Penetration Mechanisms</b>	<b>27</b>
<b>1.3.2</b>	<b>CPP for Biomedical Applications</b>	<b>29</b>
<b>1.3.3</b>	<b>CPPs in Ophthalmology</b>	<b>29</b>
<b>1.4</b>	<b>Hyaluronic acid (HA)</b>	<b>31</b>
<b>1.4.1</b>	<b>HA in drug delivery systems</b>	<b>32</b>
<b>1.4.2</b>	<b>HA in Ophthalmology</b>	<b>33</b>
<b>1.5</b>	<b>Nanogels</b>	<b>34</b>
<b>1.5.1</b>	<b>Nanogels in Ophthalmology</b>	<b>35</b>
<b>3.</b>	<b>Materials</b>	<b>37</b>
<b>4.</b>	<b>Methods</b>	<b>38</b>
<b>4.1</b>	<b>Nanogel Characterization</b>	<b>43</b>
<b>5.</b>	<b>Results</b>	<b>45</b>
<b>5.1</b>	<b>Cell proliferation ability of co-cultured ARPE-19 and HUVE cells</b>	<b>45</b>
<b>5.2</b>	<b>Cell Viability Assay with bioactive peptides (HRH and CPP)</b>	<b>47</b>
<b>5.3</b>	<b>Nanogel generation</b>	<b>47</b>
<b>5.3.1</b>	<b>HA-Poly-L-lysine (PLL) formulation</b>	<b>47</b>
<b>5.3.2.</b>	<b>HA-Cholesterol-PLL and HA-EDC/NHS-Cholesterol-PLL formulations</b>	<b>50</b>
<b>5.3.3.</b>	<b>HA-DVS-PLL Nanogel formulation</b>	<b>51</b>
<b>5.3.4.</b>	<b>HA-EDC/NHS-Cholesterol-HRH-CPP nanogel formulation</b>	<b>52</b>
<b>5.3.5.</b>	<b>HA-DVS-Cholesterol-HRH-CPP nanogel formulation</b>	<b>54</b>
<b>5.4</b>	<b>Encapsulation Efficacy and Release Profile of Nanogels</b>	<b>57</b>
<b>5.5</b>	<b>Treatment of HUVECs and ARPE-19 cells with nanodrug formulation</b>	<b>58</b>
<b>5.7.</b>	<b>Nanogel penetration to ARPE-19 and HUVE cells</b>	<b>64</b>
<b>7</b>	<b>Conclusion and Future Perspective</b>	<b>70</b>
<b>8</b>	<b>References</b>	<b>71</b>

## List of Tables

<b>Table 1.</b> Anti-VEGF peptides for inhibition of vascularization	22
<b>Table 2.</b> DLS analysis of HA-PLL interactions at different pH at 25 and 37 °C	48
<b>Table 3.</b> DLS analysis of HA-Cholesterol-PLL and HA-EDC/NHS-Cholesterol-PLL interactions at pH 7.4.and 25 °C.	50
<b>Table 4.</b> DLS analysis of HA-DVS-PLL interactions at pH 6 and pH 11 at 25 °C.	51
<b>Table 5.</b> DLS analysis of HA-EDC/NHS-Cholesterol-HRH-CPP interactions at pH 6.and 25 °C.	53
<b>Table 6.</b> DLS analysis of HA-DVS-Cholesterol-HRH-CPP interactions at pH 11.and 25 °C.	55
<b>Table 7.</b> TEER measurements of cocultured cells after nanogel 1 and nanogel 2 treatment.	62

## List of Figures

<b>Figure 1</b> Multimodal imaging of AMD.	14
<b>Figure 2.</b> Schematic representation of wet AMD.	15
<b>Figure 3.</b> Anti-VEGF therapies.	19
<b>Figure 4.</b> Representative scheme of human corneal layers	23
<b>Figure 5.</b> Alternative topical routes of drug absorption from the cornea/conjunctiva to the vitreous humour	25
<b>Figure 6.</b> Cellular uptake mechanisms of CPPs	28
<b>Figure 7.</b> Nanogel formulation composed of HA, HRH peptide, and CPP	37
<b>Figure 8.</b> Chemical structure of penetration peptide	37
<b>Figure 9.</b> Schematic representation of HA-PLL nanogel formation	38
<b>Figure 10.</b> Chemically crosslinked HA, cholesterol, and PLL nanogel formation	39
<b>Figure 11.</b> HA, cholesterol, and PLL nanogel generation	40
<b>Figure 12.</b> HA-DVS-PLL nanogel generation	40
<b>Figure 13.</b> HA-EDC/NHS-Cholesterol-HRH-CPP nanogel generation	41
<b>Figure 14.</b> HA-DVS-Cholesterol-HRH-CPP nanogel generation	42
<b>Figure 15.</b> Co-culture experiments on ARPE-19 and HUVE cells in different culture media conditions and numbers of ARPE-19 cells and HUVE cells	46
<b>Figure 16.</b> CCK-8 on HUVECs and ARPE-19 cells treated with different concentrations of HRH peptide.	47
<b>Figure 17.</b> Representative DLS data of HA-PLL nanogel formation	49
<b>Figure 18.</b> SEM images of HA-PLL nanogels	49
<b>Figure 19.</b> A representative DLS data of HA-Cholesterol-PLL and HA-EDC/NHS-Cholesterol-PLL nanogels	50
<b>Figure 20.</b> SEM images of HA-Cholesterol-PLL	51
<b>Figure 21.</b> Representative DLS data of HA-DVS-PLL nanogel formation	52
<b>Figure 22.</b> SEM images of HA-DVS-PLL nanogels	52
<b>Figure 23.</b> The mechanism of HA-EDC/NHS interaction	53
<b>Figure 24.</b> A representative DLS data of HA-EDC/NHS-Cholesterol-HRH-CPP interaction	53
<b>Figure 25.</b> SEM images of HA-EDC/NHS-Cholesterol-HRH-CPP	54
<b>Figure 26.</b> HA-DVS crosslinking mechanism	54
<b>Figure 27.</b> A representative DLS data of HA-DVS-Cholesterol-HRH-CPP interaction	55
<b>Figure 28.</b> A representative DLS data of HA-DVS-Cholesterol-HRH-CPP interactions	56
<b>Figure 29.</b> SEM images of HA (21-40 kDa)-DVS-Cholesterol-HRH-CPP nanogels	56

<b>Figure 30.</b> FTIR analysis of nanogel 1 (A) and nanogel 2	57
<b>Figure 31.</b> Nanogel release profile in 24 hours	58
<b>Figure 32.</b> A representative data of HUVECs (E) treated with nanogel	59
<b>Figure 33.</b> CCK-8 assays and cell numbers of HUVECs and ARPE-19 cells	60
<b>Figure 34.</b> TEER measurement device designed in the laboratory	61
<b>Figure 35.</b> TEER measurements of ARPE-19 and HUVECs treated with nanogel	62
<b>Figure 36.</b> The images of ARPE-19 and HUVECs treated with nanogel	63
<b>Figure 37.</b> The images of ARPE-19 and HUVECs treated with nanogel	63
<b>Figure 38.</b> HUVEC and ARPE-19 cells treated with nanogel with CPP	65
<b>Figure 39.</b> HUVEC and ARPE-19 cells treated with nanogel with no CPP	65
<b>Figure 40.</b> The red dots representing the amount of nanogels that penetrated the HUVE cells and ARPE-19 cells	66

## 1. Introduction

Eye is a complex organ of the body. It is anatomically divided into three areas: precorneal area, anterior and posterior segments. Each area is a center for different types of diseases to arise, and these diseases may need to be medicated with different route of administrations (Al-Kinani et al., 2018). Eye has static (including the conjunctiva, sclera, and cornea), dynamic, and metabolic barriers and topical administrations are quite challenging due to their thickness, surface charge, hydrophilicity, and collagen content (Patel, Cholkar, Agrahari, & Mitra, 2013). When the eye is medicated with topical administration, most of the drug is washed away by tear and blinking and subjected to systemic circulation before affecting the eye. If the mucoadhesive drug molecule can stay on the tear film, it can penetrate to the inner layers through the cornea, conjunctiva or sclera. Sclera is known to be more permeable to hydrophilic drugs, while the corneal epithelium is more suitable for the permeation of lipophilic drugs. On the other hand, human eye has esterase and carbonic anhydrase enzymes that can deactivate drug molecules (Urtti, 2006). Consequently, these drawbacks cause poor patient compliance due to the reduced precorneal residence time, necessity of frequent drug administration, and low bioavailability.

### 1.1. Age-Related Macular Degeneration

Age-related macular degeneration (AMD) is a complex eye disease leading irreversible vision loss of mostly 60 years-old or older individuals. AMD accounts for 8.7 % of blindness globally (Rama D. Jager, 2008; Rozing *et al.*, 2020). It is estimated that in aging populations (>60 years old), one of five people may have this disease. Besides age being a major risk factor for AMD progression; life style, blood pressure, race (Varma *et al.*, 2004), cigarette smoking (Group, 2005; Johanna M. Seddon, 2006), oxidative stress, cardiovascular diseases, high-density lipoprotein (HDL), obesity, diabetes (Jae Kyung Choi, 2010; Srinivasan *et al.*, 2017), atherosclerosis, and genetic dysregulations of lipid, complement, and angiogenic pathways are other factors that increase the risk for development of AMD (Deng *et al.*, 2021).

AMD is classified into two main types: early AMD and late AMD. Late AMD may be distinguished in two forms: wet (neovascular) and dry (non-neovascular) AMD. Early stages AMD is characterized by changes occurred in the retinal pigment epithelium (RPE) and by drusen (small yellowish white deposits) formations. In the intermediate stage, drusen are observed more confluent in a larger area as can be seen in **Figure 1** (Rozing *et al.*, 2020). In wet AMD, blood vessels abnormally grow from the choroid into the retina, resulting in a total loss of neuroretinal tissue, consisting of ganglion cells, muller cells, amacrine cells, bipolar

cells, horizontal cells, and retinal pigment epithelium cells. Since these vessels are fragile and easy to break, vascular fluid leaks and causes rapid vision loss (Ferrington, Fisher, & Kowluru, 2020). Although almost 85% of AMD cases are diagnosed as dry AMD, about 80% of vision loss is a result of wet AMD, which only accounts 15% of diagnosed cases (de Jong, Geerlings, & den Hollander, 2020; Thomas, Mirza, & Gill, 2021).

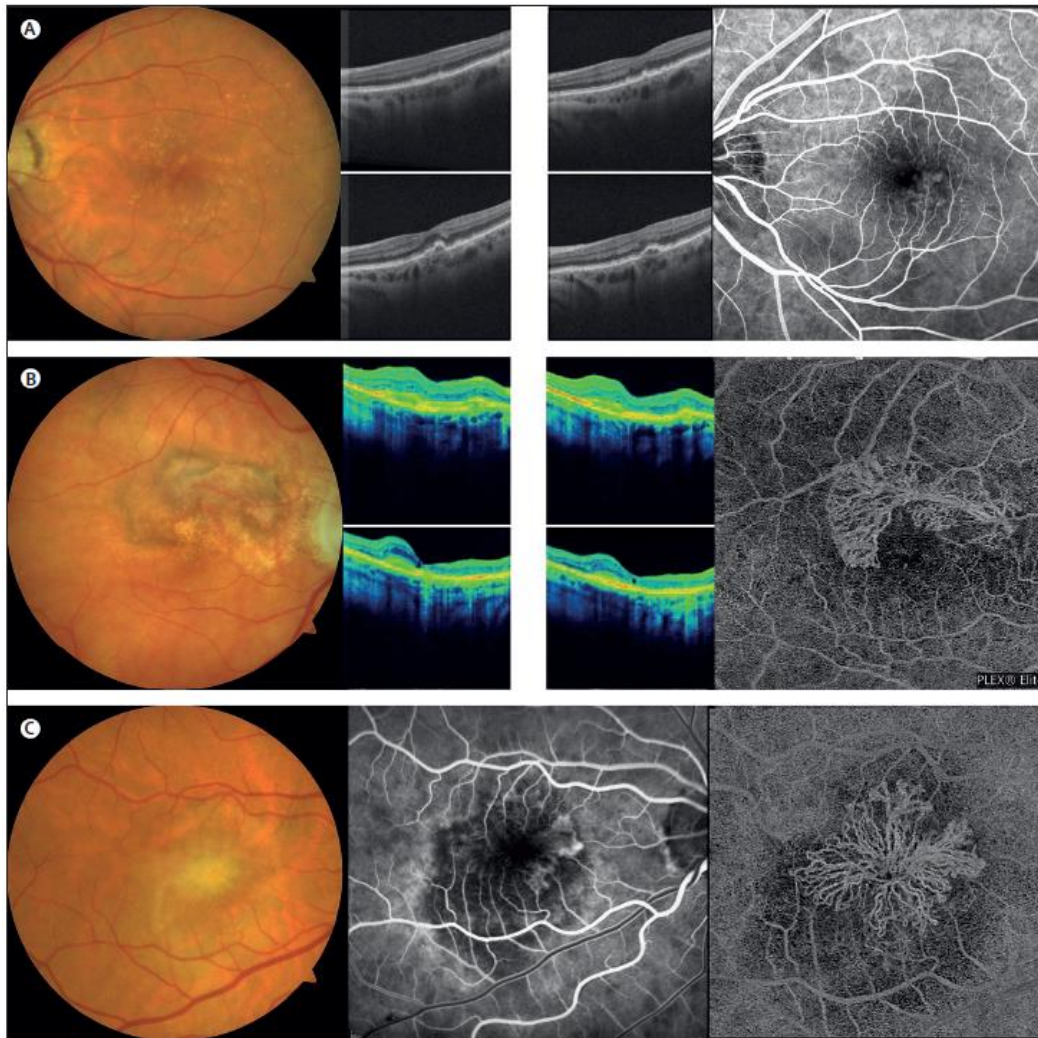


**Figure 1. Multimodal imaging of AMD.** (A) Large soft drusen on colour photography (left), spectral-domain optical coherence tomography (middle), and fluorescein angiography (right). (B) Recent on-set neovascular AMD on colour photography (left), spectral-domain optical coherence tomography (middle), and optical coherence tomography angiography showing appearance of choroidal new vessels (right). (C) Longer-standing neovascular AMD with fibrous scar on colour photography (left), fluorescein angiography (middle), and optical coherence tomography angiography showing Medusa-like appearance of choroidal new vessels (right). Adapted with permission from reference (Mitchell, Liew, Gopinath, & Wong, 2018), copyright 2018, Elsevier.

### 1.1.1 Structure of Macula

Macula is located at the center of the retina. It is responsible for central high-resolution with highly concentrated photoreceptors, rods and cons, within the retina and providing a good vision. There are retinal pigment epithelium (RPE) cells located at the posterior of the photoreceptors. RPE cells are the most important component of the blood-retinal-barrier (BRB)

and provide maintenance of photoreceptor cells (S. M. George, Lu, Rao, Leach, & Gross, 2021). RPE cells function in photoreceptor phagocytosis, nutrient transport, and cytokine secretion. Bruch's membrane is found in the posterior of the RPE. It is a semipermeable membrane that functions as a barrier between RPE and choroid, supplying blood to the outer layers of the retina (Rama D. Jager, 2008) (**Figure 2**).

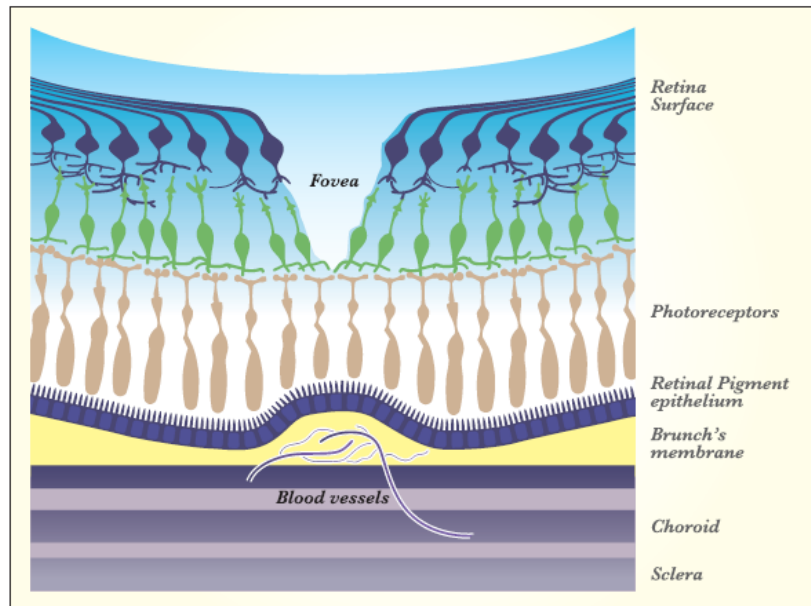


**Figure 2. Schematic representation of wet AMD.** Blood vessels present in the retina ruptures the Bruch's membrane and damages the macula. The fovea is located in the center of macula and contains a high concentration of cones in the retina, enabling high-resolution vision. Cone photoreceptors are present in the center of fovea. Cone photoreceptors are attached to RPE cell layer. Bruch's membrane is an elastic, semi-permeable barrier, functioning in major metabolic transport and exchange. Choroid provides blood supply to the RPE and the macula.

### 1.1.2 Pathophysiology of AMD

Both dry AMD and wet AMD show degenerative effects in the ocular fundus, the macula that is the area playing role for central vision (Klettner *et al.*, 2013). In AMD, there is an accumulation of cellular debris on both sides of the RPE membrane affecting the macula. Hypothetically, AMD progression is sequestered in six events, including, dysfunction of RPE, intracellular material accumulation, accumulation of extracellular materials, alterations in Bruch's membrane permeability, and then RPE response (Zarbin, 1998). The senescence of RPE cells changes the balance between enzymes in the extracellular matrix in the macula. With RPE aging, mitochondrial defects, such as decrease in number and size, change in form (oval or round form) and randomly distributed peroxisomes in the basal cytoplasm of RPE cells (Feher *et al.*, 2006) are accumulated. Due to metabolic complications, cell metabolites (drusen) are deposited between the Bruch's membrane and RPE layer, resulting in adjacent retinal tissue damage, decrease of blood supply to retina, and formation of vitreous warts (Deng *et al.*, 2021; Ferrington *et al.*, 2020). Additionally, immunogenic processes play role in AMD pathogenesis

within Bruch's membrane with dendritic cells and macrophages, in macula complement and microglial activation (Kinnunen, Petrovski, Moe, Berta, & Kaarniranta, 2012). The degeneration of RPE cells lead to the progression of disease to early-stage AMD and finally it progresses to late AMD (de Jong *et al.*, 2020; Deng *et al.*, 2021). Dry AMD can also progress to wet form and cause hemorrhaging and exudation throughout central choroidal neovascular (CNV) membranes in the retina and result in vision loss (Thomas *et al.*, 2021). The reason of CNV formation is excessive vascular proliferation or angiogenesis because of vascular endothelial growth factor (VEGF) release (Thomas *et al.*, 2021).

### **1.1.3 Treatment of AMD**

Laser photocoagulation in 1980s and photodynamic therapy in 1990s had been introduced for AMD treatment. Laser photocoagulation is the first approach for AMD treatment to slow down disease progression by cauterizing the ocular blood vessels (Virgili G, 2007). However, the outcomes of this method were quite limited. Since VEGF has a key role in choroidal neovascularization, VEGF inhibitors were under investigation and administered to the patients via intravitreal injection (Laurence S. Lim, Mitchell, Seddon, Holz, & Wong, 2012) becoming an alternative treatment for AMD.

The intravitreal agents are administrated to the patients by using a topical or subconjunctival anesthetic (Rama D. Jager, 2008). Pegaptanib (Macugen, Pfizer), ranibizumab (Lucentis, Genentech/Novartis), and aflibercept (VEGF Trap-Eye Rgeneron/Bayer) are FDA approved anti-VEGF drugs. However, there are two important issues about using these drugs for AMD treatment. The first issue is safety. It is known that ranibizumab and bevacizumab enter bloodstream and systemic circulation after ocular injection. It was observed that there is suppression of plasma VEGF levels for 28 days after injection of bevacizumab but not ranibizumab and theoretically, systemic inhibition of VEGF levels may increase the risk of cardiovascular and cerebrovascular diseases. (L. S. Lim, Cheung, Mitchell, & Wong, 2011). The second disadvantage for use of anti-VEGF drugs is that the patients need repeated drug administration strictly every month (Laurence S. Lim *et al.*, 2012). In addition, despite the patients are treated with intravitreal injections of anti-VEGF antibodies timely, it has been observed that the vision may still be lost in many patients (Brynskov, Munch, Larsen, Erngaard, & Sorensen, 2020).

Besides anti-VEGF drugs, the progression of the disease can be slowed by modifying or eliminating some risk factors, such as smoking or diet. Additionally, antioxidant supplements

such as vitamin C, vitamin E, beta carotene, zinc oxide have been used to prevent AMD progression (Liew, Joachim, Mitchell, Burlutsky, & Wang, 2016; Rama D. Jager, 2008). The effect of antioxidant supplements is dependent on the stage of AMD (Evans & Lawrenson, 2017).

## **1.2. Anti-VEGF Therapies in Ophthalmology**

VEGFs are a family of polypeptide growth factors including six polypeptides, VEGF-A, -B, -C, -D, -E, and placental growth factor (PlGF). VEGF family has a key role in angiogenesis, vasculogenesis and lymph angiogenesis (Roskoski, 2007). VEGF is secreted by macrophages, stromal cells, retina epithelial cells, malignant cells, and endothelial cells. VEGFs specifically bind to differentiating and mature endothelial cells and hematopoietic cells (Grunewald, Prota, Giese, & Ballmer-Hofer, 2010). VEGF stimulates the secretion and activation of proteolytic enzymes and degradation of extracellular matrix (ECM). Thereby, VEGF provides proliferation migration and tube formation of vascular endothelial cells (Bremnes, Camps, & Sirera, 2006; Chang *et al.*, 2012; M.S.Pepper, 1992).

VEGFs are expressed from various genes functioning and causing both pathological and normal angiogenesis (Grunewald *et al.*, 2010; Ng, Krilleke, & Shima, 2006). Among different VEGF molecules, alternative splicing creates a further variety. Human VEGF-A has several isoforms including VEGF<sub>121</sub>, VEGF<sub>145</sub>, VEGF<sub>165</sub>, VEGF<sub>183</sub>, VEGF<sub>189</sub>, and VEGF<sub>206</sub>. VEGF<sub>121</sub>, VEGF<sub>145</sub>, and VEGF<sub>165</sub> stimulate angiogenesis, while VEGF<sub>189</sub> and VEGF<sub>206</sub> are located mostly in the ECM. They are strongly cell-associated and bound to extracellular heparin-containing proteoglycans (John E. Park, 1993). VEGF<sub>165</sub> is the isoform secreted by both benign and malignant cells (Bremnes *et al.*, 2006).

VEGFs can make specific interactions with three different type V receptor tyrosine kinases (RTKs) namely VEGFR-1, -2, -3, and neuropilins and heparan sulfate proteoglycans (HSPG) (Grunewald *et al.*, 2010; Roskoski, 2007; Terri Davis-Smyth & Ferrara, 1996). These receptors are perpetually expressed (independent from proliferation) and lies throughout the vascular system (Bremnes *et al.*, 2006). VEGFR2 is known as the main VEGF receptor. When VEGF binds to VEGFR2, dimerization and autophosphorylation of receptors by kinase domains are activated, causing a mitogenic and proliferative signal (Chang *et al.*, 2012; Klettner & Roider, 2009).

VEGF-A has important functions in the retina. It is secreted by RPE cells and functions as a neuroprotective factor with a protective effect on Müller cells, neuronal and RPE cells and

choriocapillaris. However, alterations in Bruch's membrane and increased VEGF-A secretion by RPE cells can lead to choroidal neovascularization (Byeon *et al.*, 2010; Klettner *et al.*, 2013). VEGF-A production in the retina can be triggered by hypoxia, cytokines, oxidative stress, and hyperglycemia.

The upregulation of VEGFs in retinal cells, especially in RPE can also be a result of metabolic changes in the cell such as lysosomal dysfunction due to lipofuscin accumulation, or lipid peroxidation (Klettner *et al.*, 2013).

Since VEGF upregulation leads to formation of wet AMD in the eye, VEGFs are great targets for neovascularization inhibition (Ciulla, Hussain, Pollack, & Williams, 2020).

Anti-VEGF therapies for ocular diseases are considered as important advances (Cheung, Wong, & Wong, 2014). Anti-VEGF therapies have been extensively used in clinic for various eye diseases, including diabetic retinopathy (Zhao & Singh, 2018), neovascular age-related macular degeneration (Finger *et al.*, 2020), corneal neovascularization (Yi Lu, 2015), and choroidal neovascularization (Su *et al.*, 2021). Anti-VEGF therapeutics can be in various structures including antibody molecules, peptides, or aptamers (**Figure 3**). Among them pegaptanib, ranibizumab, brolucizumab and aflibercept have been approved by FDA as anti-VEGF therapeutic molecules for ocular disease treatments. These therapeutics inhibit the binding of VEGF signaling peptide to its receptors and prevent VEGF to generate leaky blood vessels (Ferrara & Adamis, 2016).

Pegaptanib is a pegylated anti-VEGF aptamer. It binds to VEGF-A isoform VEGF165, which is responsible for mediating neovascularization in the eye. Pegaptanib can also prevent VEGF-mediated cell proliferation (Cunningham *et al.*, 2005). Although there are several studies about the therapeutic effects of pegaptanib, there are some concerns about intraocular pressure increase in the eye after pegaptanib injection (Frenkel, Mani, Toler, & Frenkel, 2007).

Ranibizumab is the second FDA approved drug for AMD treatment. It is a recombinant monoclonal antibody fragment that binds to and neutralizes all VEGF isoforms. Thus, it was considered as a therapeutic for nAMD treatment. According to the studies done to evaluate the safety, efficacy, and pharmacokinetic profile of ranibizumab, it is suitable for clinical use for nAMD treatment (Gaudreault, Fei, Rusit, Suboc, & Shiu, 2005; Ho *et al.*, 2014; Staurenghi *et al.*, 2018).

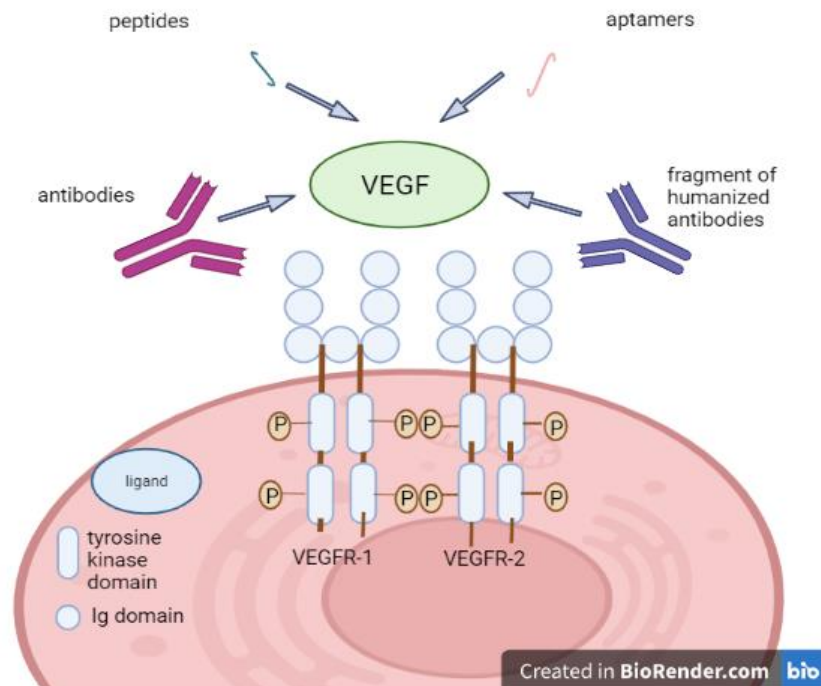


**Figure 3. Anti-VEGF therapies.** A) Antibodies, which are VEGF antagonist and bind to VEGFR, B) peptides, which are small sequences and bind to VEGFR with high affinity. C) Fragments of humanized antibodies, which are designed to inhibit all isoforms of VEGF-A. D) Aptamers, which inhibits key VEGF actions as promotion of endothelial cell proliferation and survival and vascular permeability. Created by BioRender.com. The figure was modified from (A. Pandey, 2013).

Bevacizumab (Avastin, Genentech) is a full-length antibody that binds to all VEGF isoforms as ranibizumab and is the third approved anti-VEGF drug for AMD treatment. Bevacizumab is an alternative to ranibizumab since it is cheaper and has an equal efficacy. There are several studies that evaluate the safety and efficacy of intravitreal injection of ranibizumab for AMD treatment. The results showed that bevacizumab can be used as an alternative therapeutic drug for the treatment of AMD (Brechner, Rosenfeld, Babish, & Caplan, 2011; Comparison of Age-related Macular Degeneration Treatments Trials Research *et al.*, 2012; Krebs *et al.*, 2009).

Aflibercept is an engineered fusion protein that binds to VEGF, and it is the fourth anti-VEGF drug approved by FDA for AMD treatment. Aflibercept inhibits the angiogenic response by acting as a receptor for VEGF, and prevents inflammation and retinal damage (Traynor, 2012).

Brolucizumab is a humanized, single-chain antibody fragment, VEGF inhibitor developed by Novartis for wet AMD, diabetic macular oedema, and macular oedema secondary to retinal vein occlusion. Brolucizumab inhibits VEGF-A isoforms; VEGF<sub>110</sub>, VEGF<sub>121</sub>, and VEGF<sub>165</sub> (Dugel *et al.*, 2017; Markham, 2019). It is the smallest antibody (26 kDa) among anti-VEGF antibodies. Since it is smaller compared to aflibercept (115 kDa) and ranibizumab (48 kDa), it is easier to concentrate brolucizumab up to 120 mg/mL, which enables 6 mg administration in a 50- $\mu$ L intravitreal injection, while the same amount of brolucizumab equals to 12 times the

2.0-mg and 22 times the 0.5-mg doses of aflibercept and ranibizumab, respectively. Small molecular weight of brolocizumab and its administration in high drug concentrations are important advantages of brolocizumab. Comparable half-life of brolocizumab and its higher doses of administration may lead a slower clearance of drug from the eye, enabling prolonged duration of action (Dugel *et al.*, 2017). A recent study accomplished with 1817 participants showed brolocizumab's continues inhibitory effect on vascularization up to 48 weeks (Dugel *et al.*, 2020).

Abicipar pegol (Allergan Inc, Switzerland) is a non-monoclonal anti-VEGF antibody and it is the most recent antibody in the pipeline for intravitreal therapy (Klein *et al.*, 2019). Abicipar is a molecule composed of designed ankryn repeat proteins (DARPin), which are derived from naturally occurring ankryn protein repeats. The number of repeats is limited by four to six in number and these repeating numbers are generated by protein engineering and recombinant DNA technology (Sharma, Kumar, Kuppermann, & Bandello, 2020). It can bind to all VEGF-A isoforms like ranibizumab but exhibit a longer half-life (Moisseiev & Loewenstein, 2020).

Conbercept is a recombinant fusion protein composed of VEGF receptor domains. It exhibits higher binding affinity to VEGF-A165 compared to ranibizumab and bevacizumab and a comparable binding affinity with aflibercept. Conbercept has been considered as a potential anti-VEGF drug for AMD treatment due to its inhibitory effect on VEGF-induced HUVEC proliferation (Lu & Sun, 2015).

Faricimab is a unique bispecific mAb developed to simultaneously inhibit Ang2 and VEGF-A (Stahl *et al.*, 2013). The simultaneous neutralization of angiopoietin-2 and VEGF-A is considered as sustained efficacy through extended durability and a potential for further investigation.

In a phase II clinical study, the safety and efficacy of faricimab was assessed for neovascular AMD in comparison to ranibizumab. Faricimab showed no new or unexpected safety signals (Sahni *et al.*, 2020). In another phase II trial, faricimab provided maintenance in initial vision and anatomic improvements compared to ranibizumab monthly treatment in a 52-week period (Khanani *et al.*, 2020).

Pazopanib is a multitarget tyrosine kinase inhibitor effective on both VEGF receptors and proangiogenic platelet-derived growth factor pathway. To evaluate the efficacy of pazopanib in diabetic retinopathy, an eye drop form of pazopanib suspension was designed and tested on rat models. It was indicated that the eye drop formulation significantly reduced leukostasis in

rat models and pazopanib eye drops may alleviate retinal complications of diabetic retinopathy (Thakur, Scheinman, Rao, & Kompella, 2011).

These biopharmaceutical agents have been considered as effective therapeutics for AMD treatment and other ocular neovascularization disease including diabetic retinopathy, retinal vascular occlusions, neovascular glaucoma, retinopathy of prematurity (Chakravarthy *et al.*, 2021; Kim & D'Amore, 2012; Schargus & Frings, 2020). However, there are several patients, who do not respond to these treatments or face with side effects such as pain and infection. In addition, the treatment is costly and experienced professionals are required to perform intravitreal injections (Mandal *et al.*, 2018). Due to these disadvantages, novel therapeutics and administration routes are in need for treatment of ocular neovascularization disorders.

The main disadvantage of anti-VEGF therapies is intravitreal injection, which may lead to infections, increase in intraocular pressure and inconsistent administration intervals due to patient compliance. The reason behind this route of administration is the high molecular weight of the active molecules, which cannot pass through the barriers of the eye and reach to retina. Therefore, there are two strategies for the development of new generation therapeutics; (1) discovery of smaller molecules, which could be formulated into topical drugs, (2) engineering long-term sustained release systems to extend the injection intervals.

Some novel small molecules, mostly peptides are under development as anti-VEGF molecules (**Table 1**). In 2015, Lu *et al.* studied on a novel 20-amino acid antiangiogenic peptide H-KI20 to treat corneal neovascularization. According to the experiment conducted on mouse and rat corneas, H-KI20 administration showed a considerable inhibition on corneal neovascularization induced by VEGF (Yi Lu, 2015). In another study, pigment epithelium-derived factor (PEDF)-derived synthetic peptides were administrated topically on rat eyes. It was shown that these peptides have potential to inhibit corneal neovascularization by suppressing VEGF expression through providing anti-oxidative properties by regulating the NF- $\kappa$ B pathway, when designed as PEDF nanoparticles (Matsui *et al.*, 2012; (Yi, 2014)). For tumor growth inhibition, the effects of anti-VEGF peptides were investigated with anti-Flt1 peptide and reported that anti-Flt1 peptide has an inhibitory anticancer effect by blocking VEGFR1-mediated endothelial cell migration (Dong-Goo Bae, 2005).

HRHTKQRHTALH (HRH peptide) is another novel peptide which inhibits human umbilical vein endothelial cells (HUVECs) proliferation stimulated by VEGF. HRH peptide has affinity to VEGFR-Fc and prevents VEGF-A and VEGF-B binding to VEGFR-1, and VEGF-C binding

to VEGFR-2, resulting in its anti-angiogenesis function. It also inhibits the corneal neovascularization in rat corneal models, indicating that HRH peptide possess anti-angiogenic effect both *in vitro* and *in vivo*. HRH peptide is considered as a promising angiogenic inhibitor for ophthalmic disease treatment induced by excessive angiogenesis (Y. Zhang *et al.*, 2017).

Topical administration of small molecules to the eye is straightforward but not sufficient. Corneal epithelium limiting molecular diffusion, continuous tear film and washing of anterior surface with constant blinking are the main factors limiting the absorption of drugs through the anterior segments of the eye (Sharaf *et al.*, 2014). Due to these barriers, only 5% of the active molecule in topical drugs can reach to the ocular tissues. Nanotechnology applications such as nanodrug formulations pave the way to increase therapeutic efficacy of topical eye drugs, mainly by obviating the aforementioned obstacles.

**Table 1. Anti-VEGF peptides for inhibition of vascularization.** Peptides discovered for anti-VEGF activity are listed with their respective *in vitro* and *in vivo* applications.

Peptide	Application	Reference	<i>In vivo/ex vivo</i>
H-KI20 (20aa)	Corneal neovascularization	(Yi Lu, 2015)	<i>In vitro</i>
P5-2, P5-3 (5 and 6 aa, respectively)	Corneal angiogenesis	(Matsui, Nishino, Maeda, & Yamagishi, 2012)	<i>In vivo</i>
Anti-Flt1 (6aa)	Tumor growth	(Dong-Goo Bae, 2005)	<i>In vitro</i>
Pan-VEGF inhibitory peptides (6aa)	VEGF-receptor interaction	(Jussara S. Michaloski, 2016)	<i>In vivo</i>
Anti-integrin oligopeptide	Choroidal retinal neovascularization	(By Hugo Quiroz-Mercado, 2013)	<i>In vivo</i>
iVR1	Colorectal cancer	(Valeria Cicatiello, 2015)	<i>In vivo</i>
WHLPFKC and WHKPFRF	Inhibition of HUVEC proliferation	(Berrin Erdag, 2007)	<i>In vitro</i>
HRH (12aa)	Angiogenesis inhibition	(Y. Zhang <i>et al.</i> , 2017)	<i>In vitro</i> and <i>in vivo</i>

### 1.2.1 Topical drug delivery for the posterior segment eye diseases

Posterior segment of the eye consists of vitreous humor, retina, choroid, and the optic nerve. Posterior segment eye diseases (PSEDs) are the disorders that cause visual impairment by affecting the posterior segment of the eye. The most common PSEDs are AMD, glaucoma, and diabetic retinopathy. Intravitreal injection of drugs is the most preferred way of treating PSEDs (Varela-Fernandez, 2020). Other routes for direct injections to the eye are periorbital, subretinal, and suprachoroidal administrations. In these routes, drug or system is injected in the surroundings of the target site. These methods are highly invasive and may still require the drug to cross a variety of barriers to reach to the target site (Varela-Fernandez, 2020). For instance, vitreous humor, the transparent jelly-like structure composed of collagen II, IX, and

V/XI fibers, and hyaluronic acid, acts both as a static and a dynamic barrier. It is a static barrier due to its viscous structure and a dynamic barrier due to the flow and clearance process. The retina is the innermost layer of the eye and composed of several layers including photoreceptors, glial cells, retinal pigment epithelium (RPE) and nerve fibers. The choroid is a barrier that lies between the RPE and the sclera and supplies nutrients and oxygen to the retina. Choroid functions as a static barrier with its suprachoroidal structure and dynamic barrier due to high choriocapillaris-layer blood flow (Varela-Fernandez, 2020).

Topical administration of drugs is mostly used for anterior-segment diseases of the eye, affecting the cornea, conjunctiva, iris, or ciliary body. Ocular barriers limit the adsorption and penetration of drug molecules to the eye. Different glands and Goblet cells secrete a thin precorneal tear film, acting as a barrier to eliminate drug absorption to the anterior tissues of the eye. Additionally, a high percentage of the drug molecules are washed away with tear drainage through nasolacrimal duct. The tear drainage results in the loss of drug into the systemic circulation. Despite being the most challenging route to treat posterior eye diseases, topical administration is the least invasive method and enables high patient compliance due to ease of administration.

The cornea is a six-layer collagen structure composed of Epithelium, Bowman's membrane, stroma, Dua's layer, Descemet's membrane, and Endothelium (**Figure 4**). The physicochemical characteristics of the drugs are critical for their absorption onto the cornea. Only hydrophilic molecules may diffuse through the stroma since hydrated collagen has a hydrophilic nature. The molecules with a 500 Da molecular weight or a  $<5.5\text{\AA}$  size are allowed to penetrate across tight junctions via the paracellular route. Also, the charge of the drug is an important factor since cornea has a negatively charged surface and decreases the absorption of negatively charged molecules.

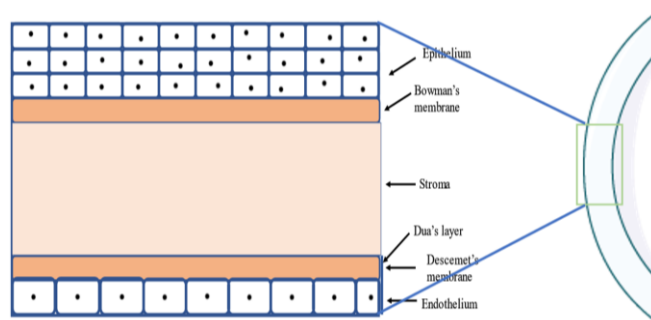


**Figure 4. Representative scheme of human corneal layers.** The outermost layer is composed of 4-6 layers of epithelial cells. The middle stroma later is  $\sim 600\ \mu\text{m}$  thick and composed of keratocyte cells. The innermost layer is formed by endothelial cells. Drawn by the author.

The conjunctiva is a thin epithelial layer that covers the eyelids and exposed sclera adjacent to the cornea. This structure has a much greater surface area and higher drug absorption compared to cornea. Conjunctiva allows drug molecules penetration up to 10kDa. However, drugs penetrate through the conjunctiva may rapidly cleared through the systemic circulation due to the presence of blood and lymphatic vessels in the conjunctiva (Varela-Fernandez, 2020).

The absorption of topically administrated drugs into the posterior segment of the eye depends on which route the drug was distributed through (**Figure 5**). Drug exposure to the cornea would enable higher concentrations of drug to be present in the aqueous humor, whereas direct exposure on the conjunctival surface would enable higher drug concentrations to be in the posterior segment of the eye. Topically administrated drugs would penetrate from the cornea/conjunctiva surface to the retina through transvitreal, uvea-scleral, or periocular routes (**Figure 5**). In the transvitreal absorption pathway, drug diffuses through the cornea, iris, and ciliary body until it reaches to the vitreous humor. Drug may diffuse to the anterior chamber with the passage through the corneal epithelium either by using transcellular or paracellular route. Lipophilic drugs use the transcellular route to cross the epithelial barrier, while hydrophilic drugs pass the corneal epithelium via the paracellular route. After corneal penetration and reaching to the aqueous humor, the drug is distributed within the surrounding tissues, which are ciliary, iris, crystalline body, and diffuses to the vitreous humor. In uveal-scleral route, drug molecules reach to the anterior chamber through transcorneal diffusion as well. Then, the drug reaches to uveal-scleral tissue, suprachoroidal space, with the drainage through the aqueous humour. Drug diffusion from the choroid to the posterior of the eye is inefficient due to the drug elimination through systemic circulation. In the periocular drug absorption, the drug diffuses through the conjunctiva to reach to the Tenon's capsule. Thereafter, drug may diffuse through the sclera, choroid, and retina (Varela-Fernandez, 2020).

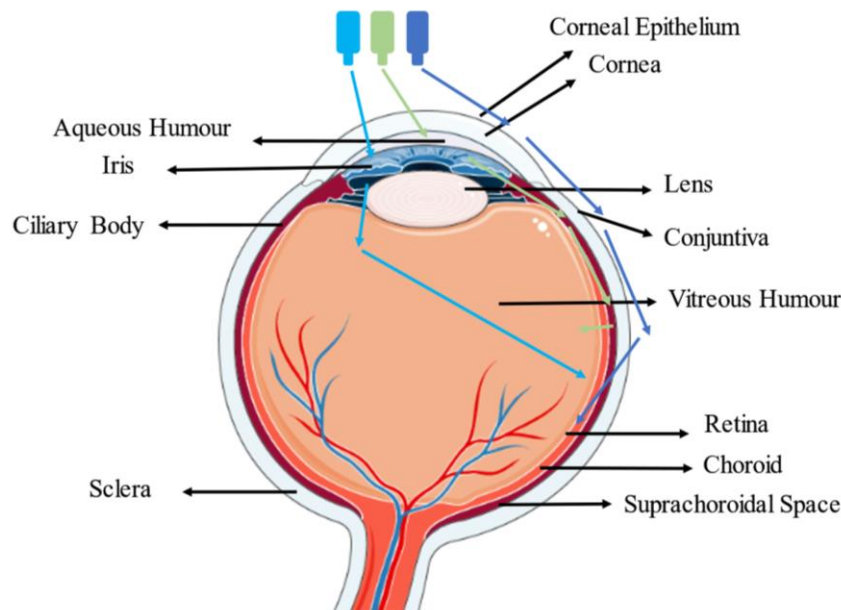


**Figure 5. Alternative topical routes of drug absorption from the cornea/conjunctiva to the vitreous humour.** Transvitreal route is shown in light blue, uvea-scleral route in green and periocular route in purple. Drawn by using smartservier.com.

In recent years, to increase the corneal residential time, corneal absorption and penetration, several drug delivery systems have been developed. These systems including nanoparticles, emulsions, liposomes and niosomes advanced topical drug delivery to the back of the eye. Penetration enhancer peptides enabled further engineering of such nano drug carriers to enhance their penetration through the ocular tissues. The first paper exploring the topical application performance of penetration peptides was published by Wang *et al.* aiming to deliver a protector against retinal ischemia (RI) reperfusion injury. In that study, TAT peptide was conjugated with human acidic fibroblast growth factor (aFGF) and administrated in male Sprague-Dawley rats. aFGF was detectable in the retina up to 8 hours after topical administration indicating that TAT peptide improved the permeation across ocular tissue and a periocular penetration route was suggested (Guo, Hutcheon, & Zieske, 2004). Similarly, De Cogan *et al.* reported that high molecular weight proteins (bevacizumab and ranibizumab) might have been delivered to the posterior of the eye with topical administration using a polyarginine peptide as the penetration enhancer. Pharmacokinetic studies on rat models after topical application of cell penetrating peptide-bevacizumab showed elevated diffusion rates to the retina and vitreous humor. Detection of the drug in aqueous humor made authors suggest a corneal route for penetration (de Cogan *et al.*, 2017). In another recent study, Huang *et al.* decorated poly-(ethylene glycol)-distearoylphosphatidylethanolamine nanoparticles with penetratin peptide to enhance their penetration to the posterior segments of the eye. The

nanoparticles loaded with anti-vascular drug Axitinib were successfully penetrated to the retina and control fundus neovascularization in rat models (Huang *et al.*, 2022).

### 1.3 Cell-penetrating peptides (CPPs)

In drug delivery approaches, translocation efficacy of drugs throughout the plasma membrane is known as a major challenge. Proteins, peptides, and nucleic acids are macromolecular compounds studied as therapeutic molecules. However, their cellular uptake is inefficient because of their poor *in vivo* stability and limited target specificity (Ruseska & Zimmer, 2020). It is crucial to transport therapeutics into cells in high quantities to obtain desired biological effect (Vives, Schmidt, & Pelegrin, 2008). CPPs are very useful basic peptides to translocate different molecules into various cell types. Since 1990s, several cell penetrating peptides were discovered to be used as enhancer for drug cellular uptake. Especially, Tat protein from HIV-1 virus and Antennapedia from *Drosophila melanogaster* have been widely studied to define structural or sequence elements of translocation (A. Joliot, 1991; Pabot, 1988). To define the minimal length domain that is required for translocation, structure-activity relationship studies were performed on Tat proteins (101 amino acids) and Antennapedia (60 amino acids) (Vives *et al.*, 2008). These studies result in short sequences of 10 to 16 amino acids, hence it leads to chemical synthesis of different mutants and analogues called “cell-penetrating peptides”. CPPs can be classified according to the characteristics of their amino acid sequences as cationic (Tat, penetratin, R9), amphiphatic (MPG, Pep-1, transportan-10 and PepFect6) and proline-rich (Bac7) CPPs (Ruseska & Zimmer, 2020). Originated and inspired by natural cell-penetrating moieties, rationally designed peptide sequences such as polyarginine and polylysine are generated and been used for efficient drug delivery (Shiroh Futaki, 2002).

Antennapedia peptide has been commercialized as “Penetratin”. Likewise, Pep-1 was named “Chariot” in the market. This peptide can internalize cargo molecule just by mixing with the drug (Deshayes, Morris, Divita, & Heitz, 2006). After all, CPPs can interact with their cargo so strongly that a disruption mechanism might be required for correct subcellular translocation of the cargo (Bippes *et al.*, 2021). Besides physically interacting with their cargo, CPPs can be used to covalently decorate nanocarriers as well as. Thereby, they are utilized to improve cellular internalization of various cargos (peptide, protein, DNA) in various nano-carriers (nanoparticles, liposomes, vesicles, niosomes, etc.). Additionally, CPPs are shown to increase absorption and penetration of macromolecules across a variety of tissues including skin, intestine, nasal and ocular tissues. In this case, cellular uptake might be avoided and CPPs carry their cargo through paracellular penetration (Pescina, 2016).

### 1.3.1 CPP Penetration Mechanisms

There are three possible pathways for the transport of cell penetrating peptides through the cell membrane: (i) direct penetration, (ii) endocytosis pathway, and (iii) translocation through the formation of a transitory structure (Derakhshankhah & Jafari, 2018). These pathways have been selected according to peptide concentration and sequence, and lipid components in each membrane. At low peptide concentrations, the preferred uptake mechanism is endocytosis, while at higher peptide concentrations translocation mechanism is cytosolic uptake (Duchardt *et al.*, 2009; Kärt Padari, 2010).

Direct penetration is an energy-independent pathway with a variety of mechanisms, including carpet-like model (Yehonathan Pouny, 1992), pore formation (Lee, Hung, Chen, & Huang, 2005), and membrane thinning model (Lee *et al.*, 2005). At the first step, negatively charged membrane components and positively charged CPP interacts, and cell membrane destabilize with CPP folding on the lipid membrane (Derakhshankhah & Jafari, 2018; Ruseska & Zimmer, 2020). Pore formation may occur in 2 forms: barrel stave and toroidal. On membrane thinning and carpet-like models, interactions between CPP and negatively charged phospholipids generates membrane thinning and carpet-like structure, respectively (**Figure 6**) (Derakhshankhah & Jafari, 2018; Ruseska & Zimmer, 2020). To summarize, these mechanisms include electrostatic interactions between CPPs and cell membranes.

Unlike direct penetration, endocytosis pathway is energy dependent. This pathway has three classes, including pinocytosis, phagocytosis, and receptor-mediated endocytosis. Plasma membrane takes large particles and solutes with pinocytosis and phagocytosis, respectively. In receptor-mediated endocytosis mechanism, clathrin and caveolin pits play important role in uptake mechanism, which covers the intracellular sides of the bio membranes (**Figure 6**) (Ruseska & Zimmer, 2020). In this process, there is a strong interaction between arginine rich CPP and the specific cell surface receptor.

Translocation through the formation of a transitory structure can also be classified under direct penetration and composed of three steps: (1) CPPs are trapped into the micelle core's hydrophilic environment, (2) membrane components interact with inverted micelle, resulting in destabilization of micelles, and (3) CPPs are released into the cytoplasm (**Figure 6**). This mechanism is not suitable for highly cationic CPPs such as Tat since the interaction between CPP and hydrophobic part of the membrane occurs besides electrostatic interactions (Derakhshankhah & Jafari, 2018). However, inverted micelle model is described for penetratin,

which is a cationic and a secondary amphipathic peptide containing Tryptophan residues that would enable interactions with membrane lipids and GAG (Pescina *et al.*, 2018).

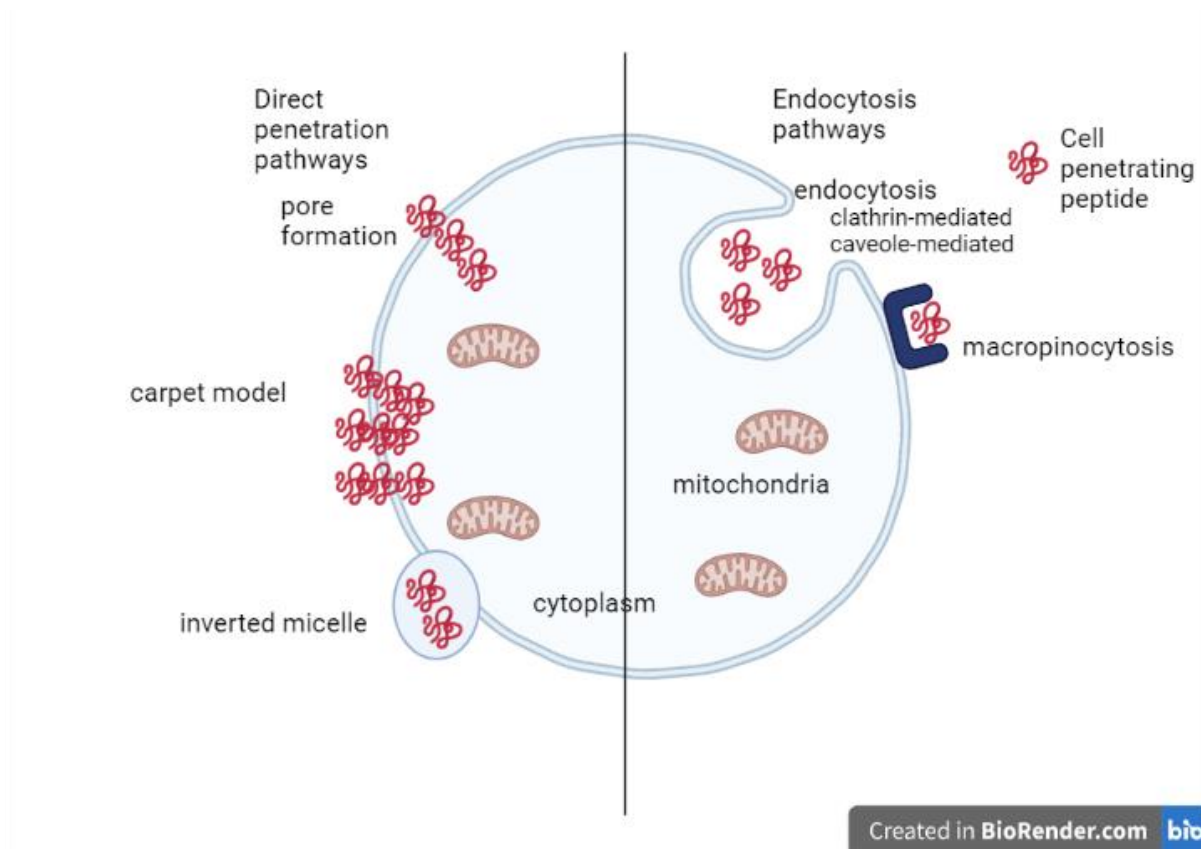


**Figure 6. Cellular uptake mechanisms of CPPs and their conjugates.** CPPs can penetrate into the cells with direct penetration and endocytosis pathways. In direct penetration, cell penetrating peptides pass through the membrane by pore formation or carpet model. In endocytosis pathways, cell penetrating peptides are *taken inside* the cell by clathrin-mediated, caveole-mediated, or micropinocytosis. In the inverted micelle model, CPP-membrane interaction leads to the formation of a micellar structure, which in turn inverted and release the CPP into the cytosol. Drawn by BioRender.com. The figure was modified from (Layek, Lipp, & Singh, 2015).

The amino acid sequence, secondary structure, hydrophobicity, and charge are the determining factors for the penetration mechanism of CPPs. Besides these physico-chemical characteristics, the environment where the penetration occurs is also critical. For instance, the concentration of CPP affects their translocation. When the peptide concentration is higher than the cell amount proportionally, direct penetration can be the preferred pathway rather than endocytosis for a particular CPP. Additionally, the cell type is definitive for cellular uptake mechanism, thus non-adherent cells are reported to be more sensitive to CPPs and high concentrations can lead to cytotoxicity. Most importantly, the type and the size of the cargo carried by the CPPs is prevalent to determine the penetration pathway.

Not always the CPP mediated penetration occurs through the transcellular route. It was shown that pep-7 (hydrophobic) and PEP-1 (amphipathic) peptides were localized in the extracellular matrix of corneal epithelial suggesting a paracellular route for penetration (Pescina, 2016). It

was particularly surprising since PEP-1 was able to be internalized by HeLa cells. Consequently, it is suggested that CPPs' penetration route may differ among different cells due to cell characteristics, glycoconjugate compositions and adjacent tissue compositions.

### **1.3.2 CPP for Biomedical Applications**

Some CPPs are effective molecules in antifungal and antimicrobial applications. For instance, Liu *et al.* designed an antimicrobial silver nanoparticle by using CPP for catalyzation (L. Liu *et al.*, 2013). Nonetheless, their main application is the field of drug delivery. They are used for the delivery of peptide, nucleic acid, and protein drugs either being conjugated with the drug molecule or the drug carrier (Derakhshankhah & Jafari, 2018). Similarly, they are used as carriers to translocate imaging agents into the cells (Rudolph L Juliano, 2009). Perillo *et al.* utilized gH625 CPP for functionalization of polyethylene glycol (PEG) for delivery of anticancer drug mitoxantrone (MTX) to HeLa cells (Perillo *et al.*, 2015). TAT peptide has been used for gene delivery to epidermal stem cells, after being conjugated with cationic noble metal nanoparticles (Peng *et al.*, 2014). Micelles were modified with CPPs and used as a carrier of siRNA/drug co-delivery to the brain for malignant glioma treatment (Kanazawa, Morisaki, Suzuki, & Takashima, 2014).

There are some limitations for biomedical application of CPPs due to their functional and chemical properties. They are not specific to cells, tissues, and organs. Thus, they need auxiliary compounds for fusion protein formation such as conjugation or noncovalent bindings. However, these compounds may show toxic effect on the cells. Additionally, the experiments need to be excessively conducted to determine the most suitable CPP and the required amount for a certain cell type or cargo (Reissmann, 2014).

### **1.3.3 CPPs in Ophthalmology**

Ocular tissues are composed of challenging barriers. Even though there are numerous effective therapeutics for ocular disease treatments, including proteins, small molecules, and oligonucleotides, the efficacies are limited due to the dynamic (tear turnover, choroidal blood flow, lymphatic clearance), static (sclera, corneal stroma, stratified corneal epithelium layers), and metabolic barriers (efflux pumps and enzymes) of the eye decreasing the bioavailability of therapeutics (S. H. Kim, Lutz, Wang, & Robinson, 2007; Pescina *et al.*, 2018). The physiology and anatomy of each barrier is different and CPPs have been considered as enhancers for ophthalmic delivery due to their ability to cross biological membranes.

To treat posterior segment diseases, local injections have been utilized, while topical applications are traditionally preferred to treat anterior segment eye diseases. However, topical administration is the least invasive and highest patient compliance approach for ocular treatment. To achieve required bioavailability of drugs for the treatment of posterior segment eye diseases, CPP mediated drug delivery is considered.

A variety of CPPs were evaluated as conjugates with the drug molecules to deliver them to the back of the eye. Among them, the conjugate of an Arginine-rich CPP with bevacizumab resulted in fast diffusion to the vitreous humor and retina. Bevacizumab-CPP complex administered two times a day for 10 days, considerably decreased the CNV area, compared to the untreated eyes (de Cogan *et al.*, 2017). Similarly, Tat peptide (GRKKRRQRRRPQ) conjugated with acidic FGF increased the penetration of FGF to the retina of Sprague-Dawley rats (Wang *et al.*, 2010).

CPPs are also actively investigated to enhance penetration of nanomedical drug delivery systems to the back of the eye. Nanoparticles, liposomes, vesicles etc. are highly preferred to provide sustained drug release and increase drug stabilities. Besides the physical characteristics of nanoparticles that would be helpful for their targeted delivery, addition of CPPs is shown to increase their penetration ability, particularly in ocular tissues. Suda *et al.* utilized penetratin, Tat and polyarginine peptides as CPPs for high-density lipoprotein (HDL) mutant transportation to treat posterior segment eye diseases as an eye drop formulation. Penetration with penetratin was the highest compared to other CPPs and CNV size was significantly decreased after administration (Suda *et al.*, 2017). In another study, Tat was conjugated with PEG-PLGA nanoparticles. Tat-NP was distributed within retina and choroid, 30 min after administration in rats with laser-induced CNV (Chu, 2017).

In various comparative studies, penetratin peptide was shown to be a better penetration enhancer, particularly than TAT, polyarginine, polyserine and proteamine (Suda *et al.*, 2017; Liu, 2014). Better performance of penetratin was explained by its structural properties, particularly higher lipophilicity compared to other CPPs evaluated. Additionally, presence of tryptophan is considered to enhance the uptake of cationic CPPs.

On the other hand, not all CPPs are effective for the delivery to the retina. Studies on POD and nucleolin binding peptide (NBP) indicated their ocular tissue localization in corneal epithelium or optic nerve sheath but no data is found on their penetration to the retina (Johnson, 2008, Binder, 2011).

#### 1.4 Hyaluronic acid (HA)

Hyaluronic acid (HA) is an anionic, non-sulphated glycosaminoglycan (GAG) that is composed of N-acetyl glucosamine D-glucuronic acid groups with interchanging  $\beta$ -1,4 and  $\beta$ -1,3 glycoside bonds. HA is a mucoadhesive, biocompatible, biodegradable, viscoelastic linear polymer, which has a variety of molecular weight ranging from 1 to 10,000 kDa and it may be chemically modified easily (Jin, Ubonvan, & Kim, 2010). HA is biologically synthesized by HA synthase (HAS) enzymes: HAS1, HAS2, and HAS3. These enzymes transport HA into the extracellular space and they are responsible for molecular size and concentrations of HA in the tissue (Huerta Angeles & Nesporova, 2021). HA is metabolized by hyaluronidase enzymes that are present in mammalian tissues.

HA is one of the crucial elements of extra cellular matrix (ECM) (X. Zhang, Wei, Xu, & Zhu, 2021). It is distributed throughout the connective tissues and organs of all animals. It plays important roles in structure formation and hydration of the ECM and enables the mechanical functionality and stability of tissues in the body (Guter & Breunig, 2017). HA is present in epithelial and connective tissues in large quantities, and it has a key role in cell propagation and migration. HA also has key roles on epithelial tissue cells growth, macrophages, and eosinophils (Vasvani, Kulkarni, & Rawtani, 2020).

There are receptors present on the cell surface and HA can interact with these receptors such as CD44, HA receptor for endocytosis (HARE), lymphatic vessel endothelial hyaluronan receptor-1 (LYVE-1), and receptor from hyaluronate-mediated motility (RHAMM) (Misra *et al.*, 2011; Vasvani *et al.*, 2020; X. Zhang *et al.*, 2021). These receptors link cells to ECM and have other multiple biological functions such as stimulating signaling processes (Misra *et al.*, 2011; X. Zhang *et al.*, 2021).

HA has been used for a variety of medical applications due to its non-toxic, non-immunogenic and non-inflammatory properties. (Jin *et al.*, 2010; Tezel & Fredrickson, 2008). Becker *et al.* reported that the use of HA and its potassium and sodium salts are nontoxic and unlikely to stimulate adverse reactions in cosmetic applications (Becker *et al.*, 2009). HA is also a widely used polysaccharide for wound healing applications. HA was grafted with pullulan (a polysaccharide polymer produced from starch and used as thickener, binder, or coater) as a biofilm exhibiting high biocompatibility and considerably promoting wound healing process (H. Li *et al.*, 2018). Mencucci *et al.* determined the safety and efficacy of HA artificial tears for tear-film stability and eliminate ocular discomfort in eyes after cataract surgery. Artificial

tear is administrated to the patient eyes, and it was observed that HA ophthalmic solution was well-tolerated and effectively reduced dry-eye diseases symptoms, improving clinical results after the surgery (Mencucci, Boccalini, Caputo, & Favuzza, 2015).

#### **1.4.1 HA in drug delivery systems**

HA is soluble in water and used to form gel like lubricants. The length of HA chain, degree of cross-linking, presence of chemical modifications and the pH of the solvent, affect the viscosity of HA (Jin *et al.*, 2010; Price, Berry, & Navsaria, 2007). Tissue hydration process is controlled by the presence of HA and their interaction with collagen in the ECM. Due to these important biological functions and physicochemical properties, HA and its derivatives have been under a comprehensive investigation for drug delivery applications (Jin *et al.*, 2010). HA can be used in non-parenteral (ocular, nasal) and parenteral (gene delivery, sustained release, target specific delivery) delivery systems. HA has a considerable potential to be utilized for therapeutic drug delivery applications as nanocarrier supplement to enhance cellular uptake and therapeutic effects of the drugs.

HA is also effective for sustained release applications. HA was crosslinked with gelatin to form a hydrogel for sustained release of recombinant thrombomodulin (rhTM) (an integral transmembrane protein expressed on the surface of endothelial cells reducing blood coagulation) for wound healing process in diabetic mice. rhTM-loaded hydrogels increased granulation, angiogenesis, tissue formation, and re-epithelization (Hsu *et al.*, 2019). In another study, HA-tyramine hydrogel conjugates were used to incorporate trastuzumab (the monoclonal anti-VEGF antibody that is used for stomach and breast cancer therapies) and hyaluronidase. In four weeks, degradation of hydrogels was observed and possessed sustained release of trastuzumab from the hydrogels. Thus, HA-tyramine conjugation provided a better pharmacokinetic profile of trastuzumab (Xu, Lee, Gao, Tan, & Kurisawa, 2015).

HA is a suitable drug carrier for different active molecules. HA may carry proteins, peptides, nucleic acids, and different anticancer agents to the tissues and cells (Huang & Huang, 2018). In 2001, it was shown that HA could be useful for sustained release of nanoparticles, peptide and protein drugs (Donald L. Elbert, 2001). Kumar *et al.* used electrostatic interactions between negatively charged HA and positively charged  $FE_2O_3$  nanoparticles for delivering peptides into A549 and HEK293 cells efficiently (Kumar *et al.*, 2007). In another study, HA-Mitomycin C conjugation was designed to compare anti-metastatic effect of HA-Mitomycin C complex and free Mitomycin C against lung carcinoma. It was shown that HA-Mitomycin C exhibited anti-

metastatic effect against the disease while free Mitomycin C showed no effects (Kazuo Akima, 1996).

The mucoadhesive properties of HA may increase the absorption of drugs and proteins in nasal and ocular surfaces. The high amount of -COOH groups present in HA structure contributes to hydrogen bond formation with biological substrates (Pritchard & Mariott, 1996). The increase in the drug bioavailability could be the reason for longer residence time of drug formulation on the mucosa. It has been demonstrated that HA shows penetration enhancement properties toward nasal mucosa (Edman, 1992). The nasal absorption of protein drugs was enhanced by HA modified with tetraglycine-L-octa arginine as an absorption enhancer (Tomono *et al.*, 2020). Nasal absorption of insulin was also significantly increased by designing HA ester microspheres for nasal delivery (L. Illurn, 1994).

Since HA is a tumor marker for prostate and carcinomas, it can be used to monitor the disease progression by binding to cell surface receptors found in tumor tissues of kidney, vessels, and liver (Vasvani *et al.*, 2020). Hence, HA can be used for a targeted drug delivery and theranostic systems. Xu *et al.* designed gold nanorod conjugated with HA and an antibody for photodynamic therapy. There are several diseases that can be treated by using drug delivery systems in which HA is used, such as respiratory diseases, wound healing, regenerative medicine (Li Liu, Gao, Lu, & Zhou, 2016), anti-inflammatory, and anti-aging medications (Sabine A. Eming, 2014) due to these distinctive properties (Jin *et al.*, 2010; Vasvani *et al.*, 2020).

#### **1.4.2 HA in Ophthalmology**

HA has important structural roles in all segments of the eye (Huerta Angeles & Nesporova, 2021) as being an endogenous substance that is present abundantly. HA is found in iris, lens, retina (RPE cells, Müller cells, retinal ganglion cells), and vitreous (Guter & Breunig, 2017). Hyaluronic acid, together with collagen, is one of the main components of vitreous providing viscosity and elasticity, respectively. HA interacts with collagen to link collagen molecules and stabilize the helical structures of collagens by electrostatic interaction between negatively charged polysaccharides and positively charged proteins (Del Amo *et al.*, 2017). The vitreous humor acts as a barrier limiting the distribution and diffusion of drug molecules and delivery systems (Del Amo *et al.*, 2017). The concentration of hyaluronic acid increases from the anterior to the posterior of the eye in the vitreous (Varela-Fernandez *et al.*, 2020). The amount of diffusion hindrance factor of the vitreous humor is small. Only the diffusion of anionic and

neutral molecules is not restrained in the vitreous by the vitreous components. Cationic molecules undergo charge interactions with HA, which decrease cationic-drug diffusion through vitreous humor. Xu *et al.* intravitreally injected a biodegradable nanoparticle to the back of the eye and measured the diffusion of the nanoparticles in the bovine vitreous compared to their diffusion in water using Stokes-Einstein equation. Diffusion coefficient of nanoparticles was two times lower than in water indicating a slower diffusion rate in vitreous (Xu *et al.*, 2013).

HA acts in the recovery of cornea, take part in maintenance of intraocular pressure (IOP), and has a role in migration of inflammatory cells. HA binds to CD44, Toll-like receptor (TLR) 4 and TLR 2 and stimulate inflammatory cells (Jiang, Liang, & Noble, 2011; Oh *et al.*, 2010). It promotes wound healing in corneal epithelial cells by providing cell migration, preventing inflammatory responses, and upregulating repair responses (Zhong *et al.*, 2016). Zhong *et al.* reported that the expression levels of inflammatory cytokines IL-1 $\beta$  and MMP-9 in human corneal epithelial cells (HCE) decrease after incubation in HA solution (Zhong *et al.*, 2016). HA's effective roles in wound healing, cell migration and angiogenesis provide a synergistic effect as an ophthalmic therapeutic agent. So far, HA has been utilized in a number of ophthalmological applications including treatment of dry eye (Bielory & Wagle, 2017), corneal wound healing (Carlson, Kao, & Ogundele, 2018), drug delivery (Dovedytis, Liu, & Bartlett, 2020), ophthalmic viscosurgical devices (Arshinoff & Jafari, 2005), comfort agent of contact lenses (M. George, Khong, & Maltseva, 2019), vitreous substitutes (Chatterjee *et al.*, 2021), and intracameral injections to the anterior chamber of the eye (Chan *et al.*, 2019).

To increase the precorneal duration of therapeutics in topical administrations, the mucosal adhesion features of HA can be used in the forms of gels, viscous solutions, inserts, and nanocarriers (X. Zhang *et al.*, 2021). In this sense, HA can be used as a material for drug conjugations in topical administration. In 2009, Oh *et al.* designed anti-Flt1 peptide-HA conjugate to treat corneal neovascularization and *in vivo* biological activity of the conjugate was confirmed (Oh, Park, Choi, Joo, & Hahn, 2009). In 2015, Beack *et al.* conjugated Flt1 peptide and HA and it was observed that the conjugate was absorbed and retained on the corneal epithelium after topical administration in mice model (Oh *et al.*, 2011).

### **1.5 Nanogels**

Nanogels are 3D hydrogels that are made of hydrophilic polymer network with sizes in the nanoscale (Li, Maciel, Rodrigues, Shi, & Tomas, 2015). Nanogels are named according to the

cross-linking method. When nanogels are synthesized via physical or chemical crosslinking, they are called physically or chemically cross-linked nanogels, respectively (Soni, Desale, & Bronich, 2016). Compared to microgels, nanogels are more advantageous for reaching body areas, which results in an improved bioavailability.

Nanogels swell in water and can encompass 30% of weight of biological molecules and drugs via electrostatic, hydrophobic, and/or van der Waals interactions, also they can make covalent bonds with polymer chains (Soni *et al.*, 2016). Nanogels can entrap therapeutics in large amounts with no change in their biological activity after loading. The release of entrapped drug occurs as a result of hydrolytic degradation of polymeric network (Sivaram, Rajitha, Maya, Jayakumar, & Sabitha, 2015). The amount or type of polymer, drug or nanogel charge, and environmental factors such as pH, temperature, and ions, are the factors to control the drug release from the nanogels (Buwalda *et al.*, 2017; Kompella, Amrite, Pacha Ravi, & Durazo, 2013).

### **1.5.1 Nanogels in Ophthalmology**

In topical ocular drug delivery systems, the major goal is to deliver optimal drug concentration to the target site. To achieve this, several drug delivery systems have been developed that can increase the residence time on the eye, such as medical gels. These gels are designed in liquid forms, and they are stimuli-responsive against the physical, chemical, and biological stimuli (Gan, Gan, Zhu, Zhang, & Zhu, 2009; Makwana, Patel, & Parmar, 2016). Nanogels for ocular delivery become important systems due to their many critical properties, such as their capacity to entrap large amounts of drug, sustained release and ability to prolong the corneal residence time (Sivaram *et al.*, 2015).

For instance, Brannigan *et al.* synthesized poly((2-dimethylamino) ethyl methacrylate) nanogels and quarternized with acryloyl chloride to increase mucoadhesivity. Synthesized nanogels showed good mucoadhesive properties on bovine conjunctival tissues and they provided a sustained release of pilocarpine hydrochloride more than 6 hours (Brannigan & Khutoryanskiy, 2017). Wang *et al.* developed a therapeutic ophthalmic contact lenses loaded with zwitterionic nanogels made of poly (sulfobetaine methacrylate) (PSBMA). The ophthalmic drug levofloxacin was encapsulated into the nanogels for sustained release. The contact lenses that are loaded with nanogels show a considerable potential to be used for the treatment of ocular diseases (Wang, 2021).

In addition to synthetic polymer based nanogels, natural materials were also employed in ocular drug delivery applications. Chitosan and hyaluronic acid are the two widely used polysaccharides for nanogel engineering. Buosi *et al.* developed a high molecular weight chitosan nanogel, which is crosslinked with sodium tripolyphosphate. It was observed that the nanogels did not show cytotoxic or inflammatory effect on human retinal pigment epithelial cells (ARPE-19), which constitutes the outer blood-retinal barrier (Buosi, 2020).

For ocular delivery of ferulic acid, a pluronic micelle- hyaluronan nanogel formulation was designed for corneal wound healing. Compared to the rapid release from micelles, micelle-nanogel formulation sustained the release time up to 2 days, which promoted the fibroblast growth in damaged cornea (Grimaudo *et al.*, 2020). Zhang *et al.* aimed an antibiotic release system to prevent the possible post-surgical adhesion. HA was conjugated with ciprofloxacin and vancomycin to be used for sustained release of antibiotics (Zhang, 2020). A similar approach was used by Ito *et al.* by synthesizing an HA nanogel by the conjugation with dexamethasone via an ester linkage and modification with aldehyde groups to increase crosslinking by means of hydrazone (Mero, 2014).

## **2. Aim of the study**

Aim of the study is to develop a nanodrug formulation that is cost-effective compared to monoclonal antibodies, can pass anatomical and physiological barriers and target retina through topical administration. The first component of the nanodrug formulation is the anti-VEGF peptide, HRH, which would eliminate neovascularization with anti-angiogenic activity on HUVEC cells. As the nanogel material, HA is chosen due to its mucoadhesive properties, abundant presence in the vitreous and interactions with CD44 receptors in retina. HA also provides high encapsulation efficiency of HRH and provide sustained release through covalent cross-linking of polysaccharides chains introduced by DVS. For an effective treatment, nanogel is required to reach to the back of the eye either through transcorneal, transconjunctival or transscleral penetration. To enhance ocular tissue penetration of the nanogel, the most effective cell penetrating peptide for ocular tissues, penetratin is incorporated into the system (de Cogan *et al.*, 2017). The final nanogel formulation is composed HA stabilized by the presence of DVS and Cholesterol, encapsulating HRH peptide, and decorated by CPP (**Figure 7**).

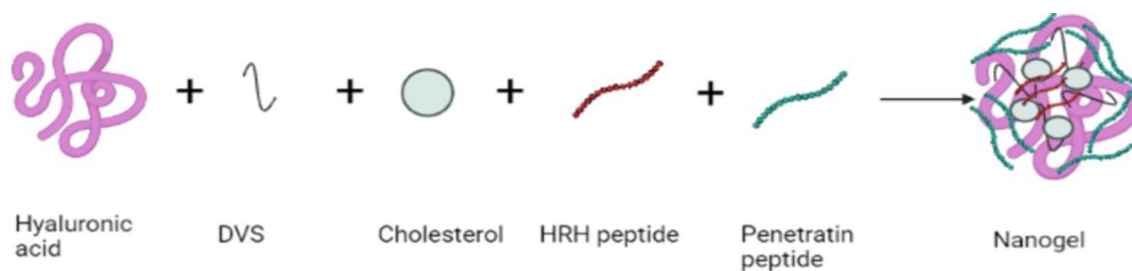


**Figure 7. Nanogel formulation composed of HA, HRH peptide, and CPP.** Nanogel formation is triggered with cholesterol hydrophobic core, then HRH is incorporated into the nanogel. Eventually, CPP is coated onto the nanogel surface. DVS was used to enhance the long-term stability of nanogel. The figure was drawn by Paint 3D.

### 3. Materials

HA with molecular weight of 21-40 kDa was purchased from Biomaterials LLC (USA). HRH peptide (FITC-Ahx-HRHTKQRHTALH-NH<sub>2</sub>, 2024 Da) and penetratin peptide (NH<sub>2</sub>-RQIKIWFQNRRMKWKK-COOH, 2247 Da) were purchased from RS Synthesis (Louisville, USA). Cholesterol was purchased from BioChemica Ltd., (UK). Divinyl sulfone (DVS) and cell counting kit-8 (CCK-8) were purchased from Sigma Aldrich (Tokyo, Japan). Vascular cell basal medium was purchased from ATCC (USA). DMEM F-12 was purchased from PanBiotech (Aidenbach, Germany). HUVECs (CRL-1730, ATCC) and ARPE-19 cells (CRL-2302, ATCC) were purchased from ATCC (USA). Poly-L-lysine (PLL) with molecular weight of 150-300 kDa was purchased from Sigma Aldrich (Tokyo, Japan). Live/dead cell imaging kit was purchased from Thermo Fisher Scientific (USA).

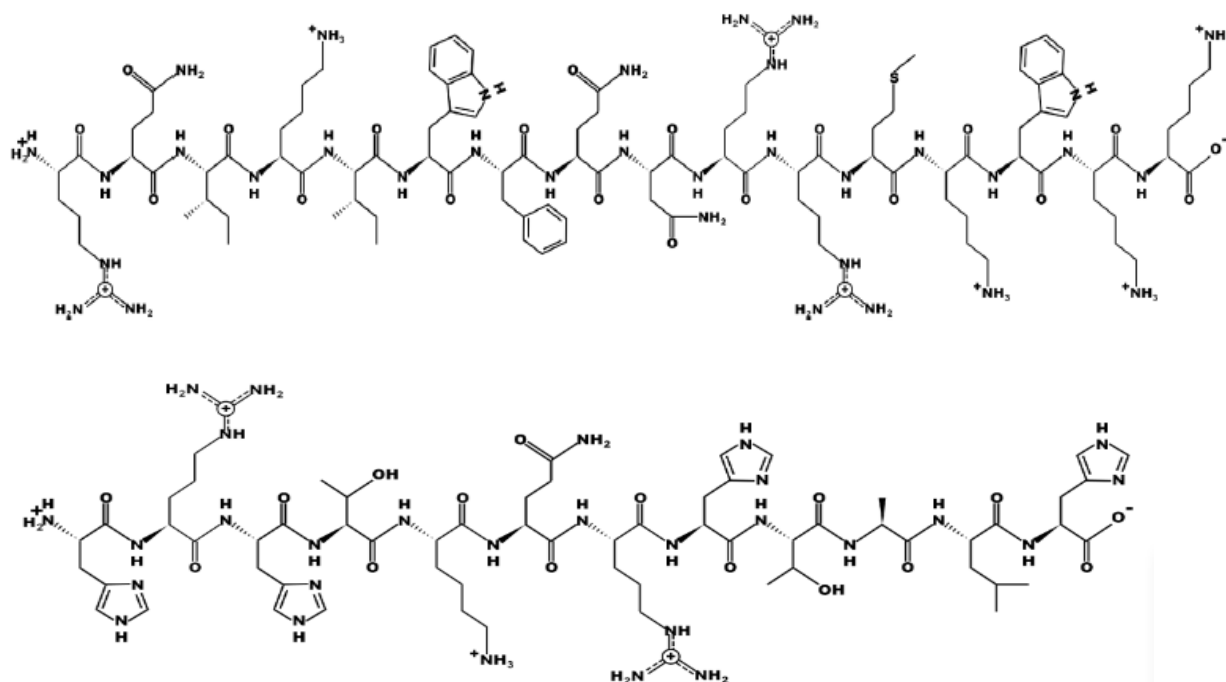


**Figure 8. Chemical structure of penetration peptide (top) and HRH peptide (bottom).** It is a highly positively charged peptide with 3 arginine residues within its 16 amino acid composition. The figures were drawn by PepDraw.com.

#### 4. Methods

**Cell culture.** Adherent cultures of human umbilical vein endothelial cells (HUVE cells) and Spontaneously Arising Retinal Pigment Epithelium (ARPE-19) cells were maintained at 37°C and 5% CO<sub>2</sub> and in mediums supplemented with 10% fetal bovine serum, 1% pen-strep, and antibiotics, Human Vascular Basal Medium and DMEM F-12, respectively. 2,5x10<sup>5</sup> HUVECs and 2,5x10<sup>5</sup> ARPE-19 cells were seeded into T-25 flasks. Both cell lines reach confluency in 4 days. 1x10<sup>6</sup> cells were frozen and stocked in liquid nitrogen with each passage for both cell lines.

**Preparation of HRH and penetration peptide solutions for cell viability assay.** 1mg/mL HRH peptide stock solution (494 μM) was prepared and diluted to 25 μM, 50 μM, 75 μM, 100 μM, and 150 μM free HRH peptide solutions to treat HUVECs and ARPE-19 cells. 1 mg/mL cell penetrating peptide stock solution (445 μM) was prepared and diluted to 25 μM, 50 μM, 75 μM, 100 μM, and 150 μM free CPP solutions to treat HUVECs and ARPE-19 cells.

**HA-Poly-L-lysine (PLL) formulation and synthesis.** 1 mg HA (21-40 kDa) was dissolved in 1 mL sterile water and sonicated for 30 minutes. 0.1 mL PLL (0.01%) was diluted ten-times in 0.9 mL of sterile water to achieve PLL: HA monomer ratio of 2:1. PLL solution was added dropwise into the HA solution and the mixture was stirred for 3 hours. The reaction was carried out at different temperatures and pH (Tračuma & Loca, 2020). Experiments were repeated three times and averages for particle size, charge and PDI are given in Table 2 with one representative graph. Different pH values investigated were pH 6, 9, 7.4, and 7 for HA, pH 6 for PLL (Hyukjin Lee, 2007). The reactions were also carried out at different temperatures, 25°C or 37°C. Even though body temperature is about 37°C, eye temperature is not as high as body temperature. Therefore, experiments were conducted at two temperature values.

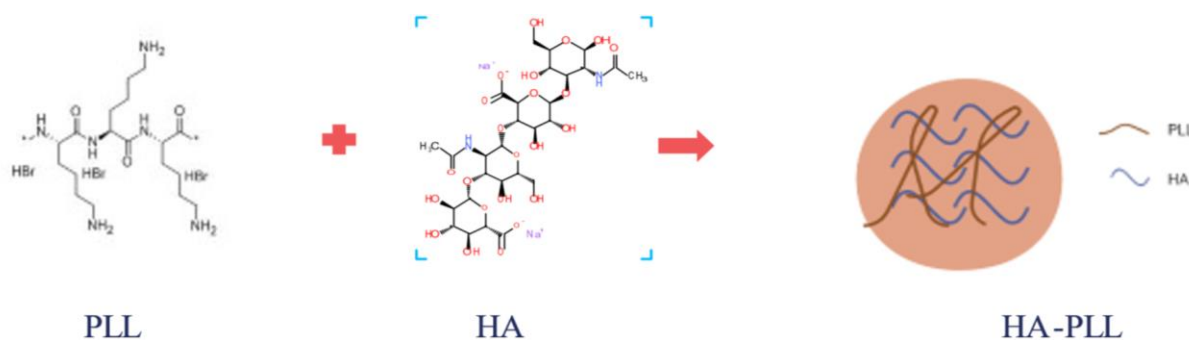


**Figure 9. Schematic representation of HA-PLL nanogel formation.** PLL and HA were electrostatically interacted at different pH values and temperatures to form a nanosized gel. Negatively charged HA (due to its COO group) interacts with positively charged PLL (due to its NH<sub>2</sub> group). Drawn by Chem4word.

**HA-EDC/NHS-Cholesterol-PLL formulation and synthesis.** 1mg HA (21-40 kDa) was dissolved in 1 mL sterile water ( $3.3 \times 10^{-5}$  M) and sonicated for 30 minutes to provide homogenization in nanogel size. EDC/NHS chemistry was used for crosslinking HA to PLL. EDC and NHS are used to make covalent bond between HA and PLL by activating COOH group of HA to bind to NH<sub>2</sub> of PLL (**Figure 10**). EDC ( $1 \times 10^{-3}$  M) and NHS ( $1 \times 10^{-3}$  M) were added to HA solution, (HA: EDC: NHS molar ratio is 1:0.033:0.033) stirred for 24 hours and dialyzed with 6-8 kDa cellulose dialysis membrane (Thermofisher Scientific, USA) against water, overnight. 3.15 mg cholesterol was dissolved in 120  $\mu$ L toluene, added dropwise to the solution, mixed for 6 hours at 25°C and 700 rpm and dialyzed against water/toluene (3:1 v/v) (Wei, Senanayake, Warren, & Vinogradov, 2013). 0.1 mL PLL (0.01%) was diluted ten-times in 0.9 mL of sterile water to achieve PLL/HA with 2:1 monomer ratio. PLL solution was added dropwise into HA solution and the mixture was stirred for 3 hours (Hyukjin Lee, 2007). The reaction was carried out at 25°C and pH 6 (**Figure 10**). Experiments were repeated three times and the data obtained from DLS measurements averages are given in the **Table 3** and one representative graph.

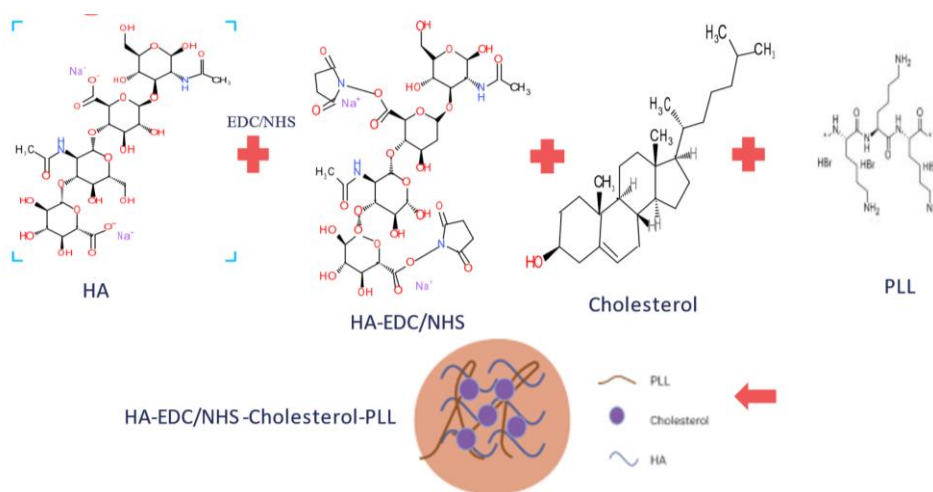


**Figure 10. Chemically crosslinked HA, cholesterol, and PLL nanogel formation** that was generated by using EDC/NHS crosslinker for higher stability. EDC/NHS chemistry was used to introduce covalent bond between HA and PLL by activating COOH group of HA to bind to NH<sub>2</sub> of PLL. Drawn by Chem4Word.

**HA-Cholesterol-PLL formulation and synthesis.** 1 mg of HA (21-40 kDa) was dissolved in 1 mL sterile water and sonicated for 30 minutes. 3.15 mg cholesterol was dissolved in toluene, added dropwise to the solution (**Figure 11**), mixed for 6 hours and dialyzed with 6-8 kDa cellulose dialysis membrane (Thermofisher scientific, USA) against water/toluene (3:1 v/v) (Wei *et al.*, 2013), overnight. 0.1 mL PLL (0.01%) was diluted ten-times in 0.9 mL of sterile water to achieve PLL/HA monomer ratios to 2:1. PLL solution was added dropwise into HA solution and the mixture was stirred for 3 hours (Hyukjin Lee, 2007). The reaction was carried

out at 25°C and pH 7.4. Experiments were repeated three times and averages are given in the **Table 3** and one representative graph.

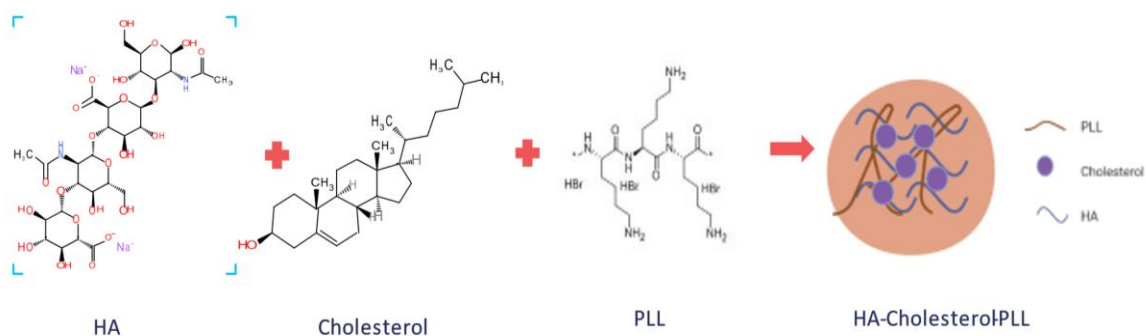


**Figure 11. HA, cholesterol, and PLL nanogel generation.** HA and PLL electrostatically interacted, and cholesterol were used for increasing nanogel formation. Drawn by Chem4Word.

**HA-DVS-PLL Nanogel formulation and synthesis.** 1 mg of HA (21-40 kDa) was dissolved in 1 mL sterile water and sonicated for 30 minutes. The pH of the solution was adjusted to either 6 or 11. The optimum pH value of DVS to crosslink the nanogel components is 11. Then, HA was mixed with 0.2  $\mu$ L DVS for 6 hours for crosslinking (HA: DVS 1:1 molar ratio) (**Figure 12**) (Lai, 2014). After 6 hours of mixing, 0.1 mL of 0.01% PLL solution was ten times diluted in sterile water to arrange PLL/HA monomer ratio 2:1 and added dropwise into HA solution and the mixture was stirred for 3 hours (Hyukjin Lee, 2007). The reaction was carried out at 25°C and pH 7.4. Experiments were repeated three times and DLS measurement data were given as averages in the **Table 4** and one representative graph.

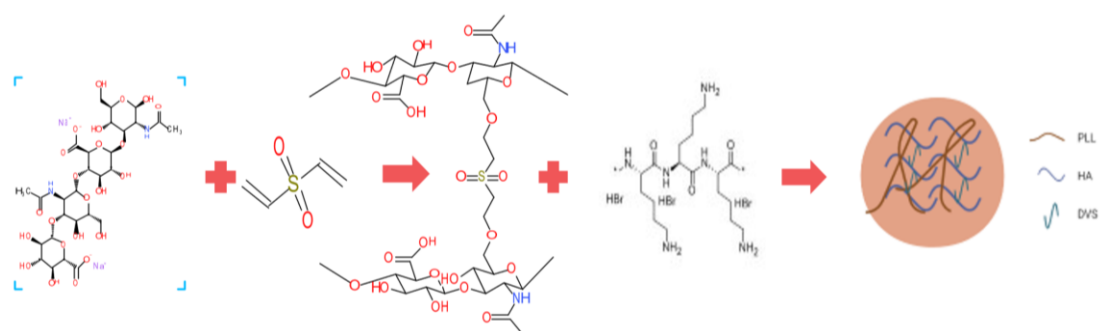


**Figure 12. HA-DVS-PLL nanogel generation.** DVS crosslinks HAs with N-acetyl glucosamines and increases the nanogel stability. PLL and HA interacts electrostatically. Drawn by Chem4Word.

**HA-EDC/NHS-Cholesterol-HRH-CPP nanogel formulation and synthesis.** 1 mg HA (21-40 kDa) was dissolved in sterile water (1mL) to achieve a 1mg/mL HA solution with 30 seconds of vortex. The pH of the solution was adjusted to 6. EDC/NHS chemistry was used for crosslinking HA to HRH peptide (**Figure 13**). EDC and NHS were added to HA solution, (HA: EDC: NHS molar ratio is 1:0.03:0.03) stirred for 24 hours and dialyzed with 6-8 kDa cellulose

dialysis membrane (Thermofisher Scientific, USA) against water (Wei *et al.*, 2013). 3.15 mg cholesterol and 0.2 mg of HRH peptide were dissolved in 120  $\mu\text{l}$  toluene and 200  $\mu\text{l}$  sterile water, respectively (Wei *et al.*, 2013; Zhang *et al.*, 2017). In the following step, they were added to HA-EDC/NHS solution and mixed for 6 hours (HA: HRH molar ratio is 1:1). The mixture was dialyzed overnight against water/toluene (3:1 v/v) and 0.8 mg penetratin peptide was dissolved in 0.4 mL sterile water and added to the solution. (HA: HRH: CPP molar ratio is 0.33:1:1.8). The formulation was stored at +4  $^{\circ}\text{C}$  until use. Experiments were repeated three times and DLS measurement data averages are given in the Table and one representative graph.

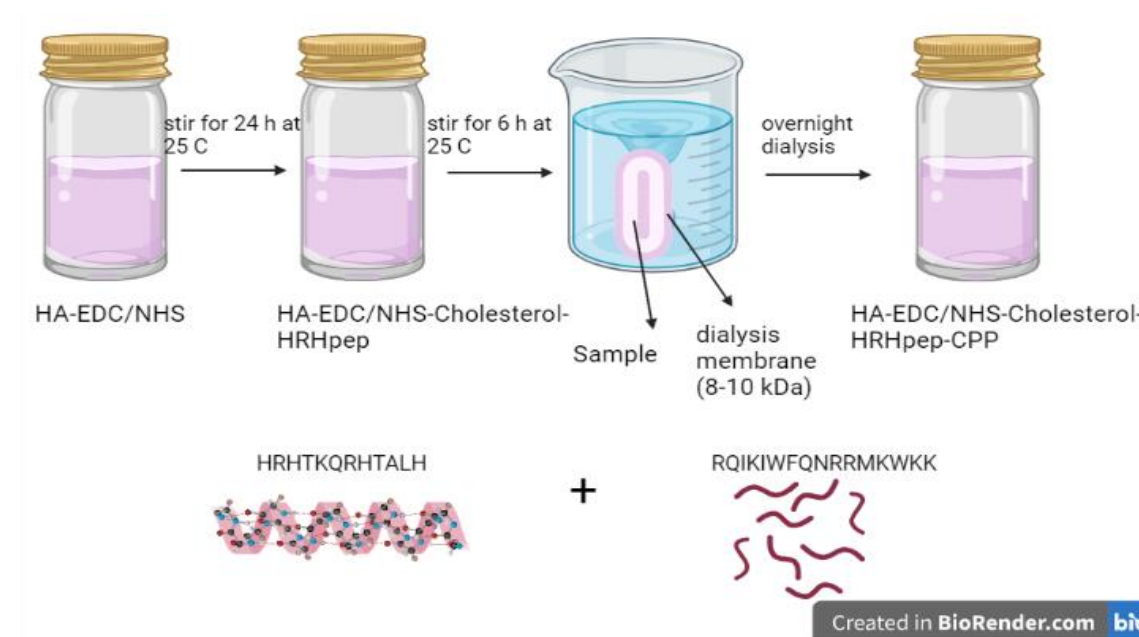


**Figure 13. HA-EDC/NHS-Cholesterol-HRH-CPP nanogel generation.** To activate the COOH groups of HA, EDC/NHS chemistry was used by stirring HA and EDC/NHS for 24 hours. Cholesterol and HRH were added to the HA-EDC/NHS solution together for HRH to be encapsulated in the structure. Solution was dialyzed for overnight against water/toluene to remove toluene that cholesterol was dissolved in. In the last step, penetratin peptide was added to the formulation to generate an outer layer for enhancing penetration. The figure was drawn by BioRender.com.

**HA-DVS-Cholesterol-HRH-CPP nanogel formulation and synthesis.** 1 mg HA (21-40 kDa) was dissolved in 1 mL sterile water to achieve a 1mg/mL HA solution with 30 seconds of vortex. The pH of the HA solution was adjusted to >11 and HA was mixed with 0.2  $\mu\text{L}$  DVS for 3 hours for crosslinking (HA: DVS 1:1 molar ratio) (Lai, 2014). After 3 hours of mixing, 3.15 mg cholesterol, 0.2 mg of HRH peptide were dissolved in 120  $\mu\text{L}$  toluene and 0.2 mL sterile water, respectively (Wei *et al.*, 2013; Zhang *et al.*, 2017). In the following step, they were added to HA-DVS solution and mixed for 6 hours (HA: HRH molar ratio is 0.33:1). The mixture was dialyzed overnight with 6-8 kDa cellulose dialysis membrane (Thermofisher scientific, USA) against water/toluene (3:1 v/v) and 0.4 mg penetratin peptide was dissolved in 0.8 mL of sterile water and added to the solution. (HA: HRH: CPP 0.33:1:1.8 molar ratio).

The formulation was stored at +4 °C until use. Experiments were repeated three times and DLS data averages are given in the Table and one representative graph. Experimental schematic is given at **Figure 14**.

**HA-DVS-Cholesterol-HRH-CPP nanogel formulation and synthesis (Nanogel 1).** 1 mg HA (10 kDa) was dissolved in sterile water (1mL) to achieve a 1 mL HA solution with 30 seconds of vortex. The pH of the HA solution was adjusted to >11 and HA was mixed with 0.2 μL DVS for 3 hours for crosslinking (HA: DVS 1:1 molar ratio). After 3 hours of mixing, 3.15 mg cholesterol, 0.2 mg of HRH peptide were dissolved in toluene and sterile water, respectively (Wei *et al.*, 2013; Zhang *et al.*, 2017). In the following step, they were added to HA-DVS solution and mixed for 6 hours. The mixture was dialyzed overnight against water/toluene (3:1 V/V) and 0.4 mg of penetratin peptide was added to the solution. (HA: HRH: CPP molar ratio is 1:1:1.8). The formulation was stored at +4 °C until use. Experiments were repeated three times and averages are given in the Table and one representative graph.

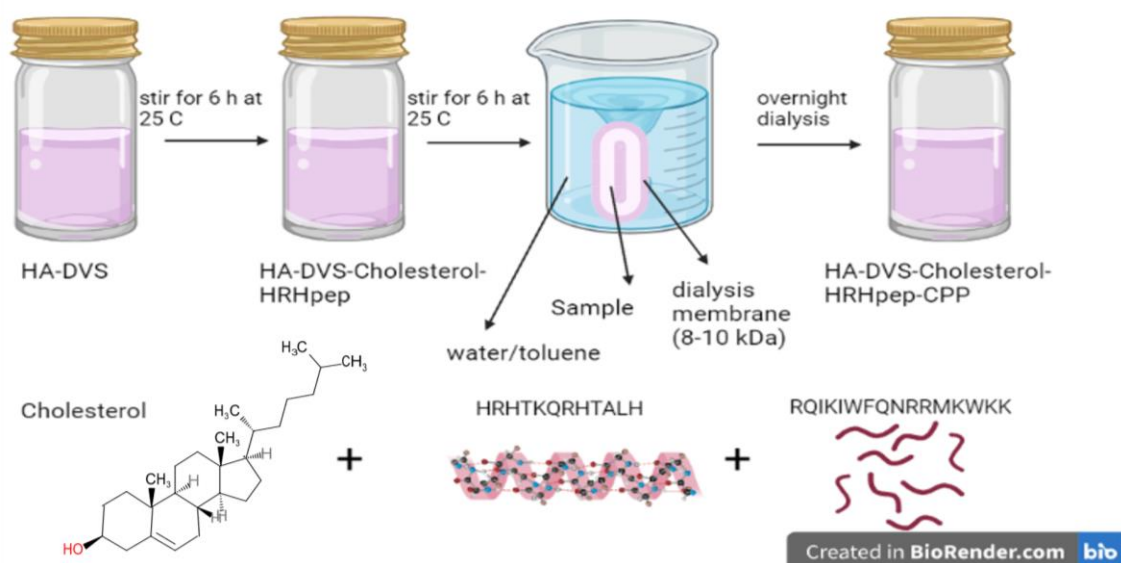


**Figure 14. HA-DVS-Cholesterol-HRH-CPP nanogel generation.** DVS was used to crosslink HAs and stirred for 6 hours. After that, cholesterol and HRH were added to the HA-DVS solution together for HRH to be encapsulated in the structure. Solution was dialyzed for overnight against water/toluene to get rid of toluene that cholesterol was dissolved in. In the last step, penetratin peptide was added to the formulation to generate an outer layer peptide for enhancing penetration. The figure was drawn by BioRender and Chem4Word.

**HA-DVS-Cholesterol-HRH-CPP nanogel formulation and synthesis (Nanogel 2).** 1 mg HA (8-15 kDa) was dissolved in sterile water (1mL) to achieve a 1 mL HA solution with 30 seconds of vortex. The pH of the HA solution was adjusted to >11 and HA was mixed with 0.2 μL DVS for 3 hours for crosslinking (HA: DVS 1:1 molar ratio) (Lai, 2014). After 3 hours of mixing, 3.15 mg cholesterol, 0.2 mg of HRH peptide were dissolved in toluene and sterile

water, respectively (Wei *et al.*, 2013). In the following step, they were added to HA-DVS solution and mixed for 6 hours. The mixture was dialyzed overnight against water/toluene (3:1 V/V) and 0.4 mg of penetratin peptide was added to the solution. (HA: HRH: CPP molar ratio is 1:1:1.8). To remove toluene and DVS from the nanogels, they were freeze-dried (Cool-safe, Scanvac) for 24 hours at -96 °C under 0.007 mbar vacuum. After freeze-drying, nanogel was dissolved in 1 mL DPBS and stored at +4 °C until use. Experiments were repeated three times and averages are given in the Table and one representative graph.

#### **4.1 Nanogel Characterization**

The interactions were characterized by particle size, distribution, and charge. Size and size distribution was measured with dynamic light scattering (DLS), which is a characterization method determining the size distribution profile of small particles in suspension (Malvern Zetasizer Nano ZS, UK) at 25°C with three measurements. 40 µL samples were put into disposable microcuvettes. Surface charge of the particles were measured by using 1 mL sample in Zetasizer® cuvettes (Malvern,UK) under DLS by using Zeta Potential measurements. Morphology and size distribution of particles were finally visualized under scanning electron microscope (SEM), which is a technique that determines the structure of samples by scanning it with beam of electrons, analysis at 25°C. Samples were prepared by drop casting 7 µL sample on SEM grids and sputter coated with Au/Pd using 40 mA for 80 s. Samples were observed with Jeol Leo Supra VP35 Field Emission Scanning Electron Microscope (Zeiss, Germany). Observation was made using 3 kV accelerating voltage and Secondary electron and in-lens detectors simultaneously. To investigate the chemical bonds between the components of nanogels, FTIR spectroscopy (Thermo Fisher Scientific, USA) was used for analysis of samples at 25 °C with 128 scanning in Omnic software.

**Encapsulation efficacy and drug release profile of nanogels.** Drug encapsulation efficacy and drug release profile of nanogels were calculated for the nanogel generated HA with 10 kDa molecular weight.

To see the release profile, nanogels containing FITC fluorophore, were dialyzed with dialysis membrane against PBS by stirring at 700 rpm and 25°C in 25 mL PBS and samples were taken from PBS after 30 minutes, 1 hour, 2 hours, 4, 8, 24, 48, and 72, 96, 120, 144, 168, and 192 hours to investigate the amount of drug released from dialysis membrane by using fluorescence spectrometer TECAN infinite F200 pro (TECAN AG, Switzerland). Sample was taken from nanogel 2 after 30 minutes, 1 hours, 2 hours, 4, 8, and 24 hours and measured under fluorescent

spectroscopy. Calibration curve was drawn by HRH peptide samples with different concentrations (0,0001 mg/mL, 0,0005 mg/mL, 0,001 mg/mL, 0,025 mg/mL, 0,05 mg/mL, and 0,1 mg/mL) and an equation was generated with the curve. To calculate the encapsulation efficacy of nanogel, it was centrifuged twice, and supernatants were measured under fluorescence spectroscopy measuring the FITC-tag of HRH. Encapsulation efficiency is calculated as percent drug obtained after centrifugation compared to initial drug loaded.

**Cell proliferation assays on HUVEC and ARPE-19.** Cell proliferation analysis for HUVEC and ARPE-19 cells were conducted by using CCK-8 assay.  $1 \times 10^4$  HUVEC and  $1 \times 10^4$  ARPE-19 cells were seeded per 96-well plate and incubated at 37°C and %5 CO<sub>2</sub> overnight. After incubation, cells were treated with 20 µL nanogel formulation HA: HRH: CPP; 1:1:1.8 molar ratio and were incubated for 96 hours. After 96 hours of incubation, CCK-8 assay was performed by adding 10 µL CCK-8 agent into each well and cells were incubated for 4 hours. Then, the absorbance measurement was performed at 450 nm by using microplate reader (Bio-rad, USA). The experiment was repeated as at least three biological replicates.

CCK-8 assay is the assay using WST-8 (2-(2-methoxy-4-nitrophenyl)-3-(4-nitrophenyl)-5-(2,4-disulfophenyl)-2H-tetrazolium, monosodium salt), producing a water-soluble formazan dye upon bioreduction in the presence of an electron carrier, 1-Methoxy PMS. CCK-8 assay is a colorimetric assay to determine the cell viability in cell proliferation and cytotoxicity assays. The amount of formazan dye due to the dehydrogenase activity in cells is proportional to the number of living cells. CCK-8 assay is a more sensitive colorimetric assay compared to MTT and MTS assays, which determine the mitochondrial activation.

**Live/dead cell assay.** To determine whether HA, HRH peptide, penetration peptide, and nanogel formulation are toxic on ARPE-19 cells or HUVE cells. ARPE-19 and HUVE cells were seeded to each cover slip placed into each well. After 96 hours of treatment of ARPE-19 cells and HUVE cells with HA, peptides, and nanogel separately, live/dead cell assay was performed by adding 1 mL of calcein solution to 1 µL of propidium iodide (PI) and vortex for 30 seconds. Live/dead cell assay working solution was added into each well with the same amount of volume that cells were cultured, and cells were incubated for 15 minutes. Next, cells were washed with DPBS three times and monitored under LSCM (**Figure 32**).

Live/dead cells assay is a highly sensitive assay, which is used to determine the viability of live cells based on intracellular esterase activity and plasma membrane integrity, and dead cells or membrane damaged cells. Virtually non-fluorescent dye is converted into a fluorescent calcein

(green) with high esterase activity of live cells, while dead or damaged cells are stained into red color with propidium iodide dye (Hu, 2022).

**Co-culture experiments.** To determine the proliferation capabilities of ARPE-19 and HUVE cells in vascular cell basal medium and DMEM F-12 mediums, cells were co-cultured in well plates. HUVECs were seeded in 12-well plates whereas ARPE-19 cells were seeded to the trans-well insert membranes. When they reach confluency, HUVECs were stained with crystal violet, and ARPE-19 cells with DAPI to be investigated under the light microscopy and laser scanning confocal microscopy (LSCM), respectively. Cells were examined with five different culture conditions to determine the optimum conditions of co-culture of two cell lines (**Figure 15**). ARPE-19 cells were fixed with paraformaldehyde (PFA) for 10 minutes and washed by DPBS three times. Then ARPE-19 cells were stained with DAPI for 15 minutes under dark condition and investigated under LSCM. The HUVEC growth medium was aspirated and washed with DPBS three times. Crystal violet was added into the HUVECs and incubated for 15 minutes. After incubation, cells were washed with DPBS again and pictured under the microscope (Skottman *et al.*, 2017).

**Transepithelial/transendothelial electrical resistance (TEER) measurement.** TEER measurement is a non-invasive measure of the tightness of epithelial cell barriers. TEER measurement device functions in indicating barrier integrity of epithelial tissues and is useful to assess ion transport and permeability of tight junctions. TEER is measured by placing two chopstick electrodes on each side of confluent cell layer. A current is applied, and the barrier resistance is measured. In the experiment setup, ARPE-19 cells were seeded into 12-well insert membrane and HUVECs were seeded into the 12- well plate.

## 5. Results

### 5.1 Cell proliferation ability of co-cultured ARPE-19 and HUVE cells

ARPE-19 and HUVE cells were co-cultured to investigate their proliferation performance within their own cell culture medium or within each other's medium.  $1 \times 10^4$  HUVECs and ARPE-19 cells were seeded with different combinations into the wells and trans well insert membranes, respectively. After 24 hours of incubation, cells were stained for proper visualization and cell counts were obtained for quantitate analysis (**Figure 15**).

Results indicated that HUVECs showed the highest proliferation in their own medium, human vascular cell basal medium. On the other hand, it was seen that ARPE-19 can also survive in vascular basal cell medium as well as their own medium, DMEM-F12. High amount of growth

factors present in vascular basal cell medium might be the reason of ARPE-19 cells proliferating fast in vascular basal cell medium. HUVECs did not show an efficient proliferation in DMEM-F12 and the reason of ability difference to proliferate in DMEM-F12 and human vascular cell basal medium for HUVECs can be that HUVECs are endothelial cells, which would be more sensitive compared to epithelial cells such as ARPE-19.

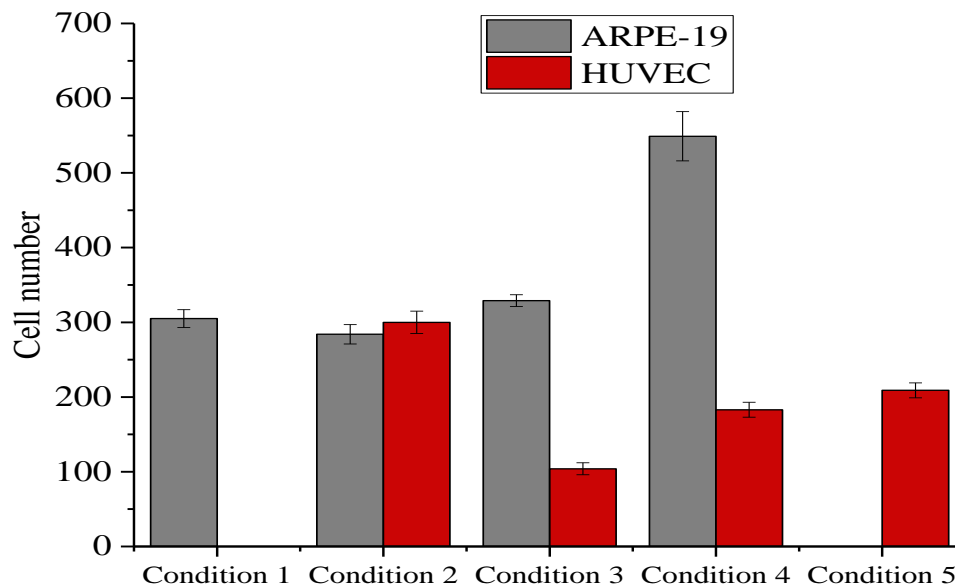
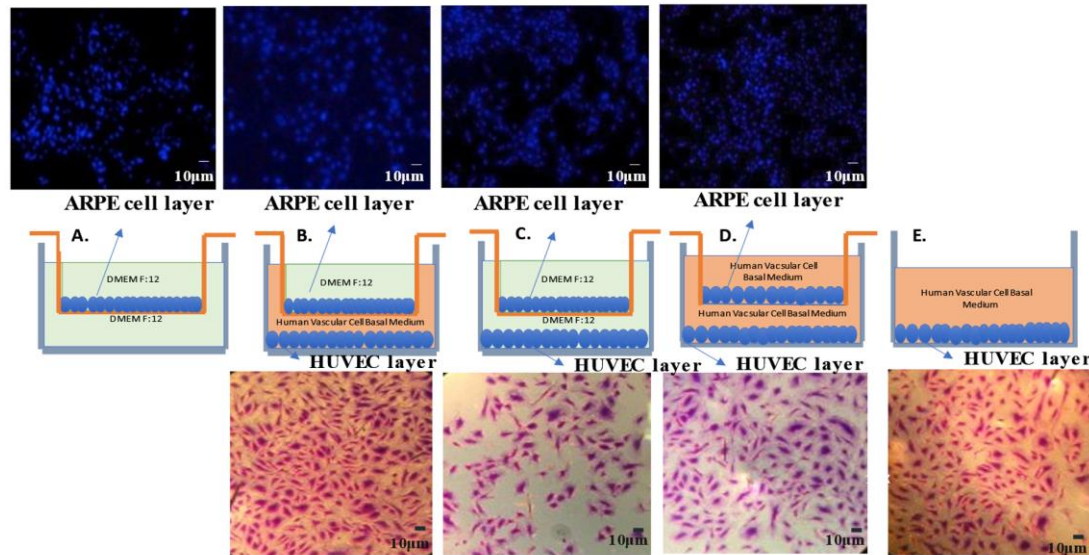


**Figure 15. Co-culture experiments on ARPE-19 and HUVEC cells in different culture media conditions and numbers of ARPE-19 cells and HUVEC cells.**  $5 \times 10^3$  ARPE-19 cells were seeded in inserts whereas  $5 \times 10^3$  cells were seeded into the wells. A) APRE-19 cells cultured in DMEM-F12, B) ARPE-19 cells were cultured in DMEM-F12 and HUVECs were cultured in basal medium, C) both cells were cultured in DMEM-F12, D) both cells were cultured in basal medium, E) HUVECs were cultured in basal medium. After 24 hours of incubation, cells were stained with DAPI and crystal violet for HUVECs and ARPE-19 cells, respectively. Cells were counted via Image J after capturing the images from 24 hr incubated cells with different culture mediums and given as in the graph. ARPE-19 cells cultured in DMEM-F12 (condition 1), ARPE-19 cells were cultured in DMEM-F12 and HUVECs were cultured in basal medium (condition 2), both cells were cultured in DMEM-

F12 (condition 3), both cells were cultured in basal medium (condition 4), and HUVECs were cultured in basal medium (condition 5). Cell numbers were counted from three image of each sample and the average cell number was given as for each condition (n=2).

## 5.2 Cell Viability Assay with bioactive peptides (HRH and CPP)

To investigate the inhibitory effect of HRH and penetration peptides on HUVECs and ARPE-19 cell proliferation, cell viability was investigated with CCK-8. The results showed that HUVE cell proliferation decreased with increasing HRH concentration, indicating that HRH peptide has an inhibitory effect on HUVE cell proliferation. On the other hand, penetratin peptide did not show any effect on cell proliferation. When ARPE-19 cells were treated with HRH and penetratin at the same peptide concentrations, not significant effect on cell proliferation was observed (**Figure 33**).

These data provided the assurance that HRH and penetratin would be used as effective anti-VEGF agent and cell penetrating peptide for the nanogel formulation.

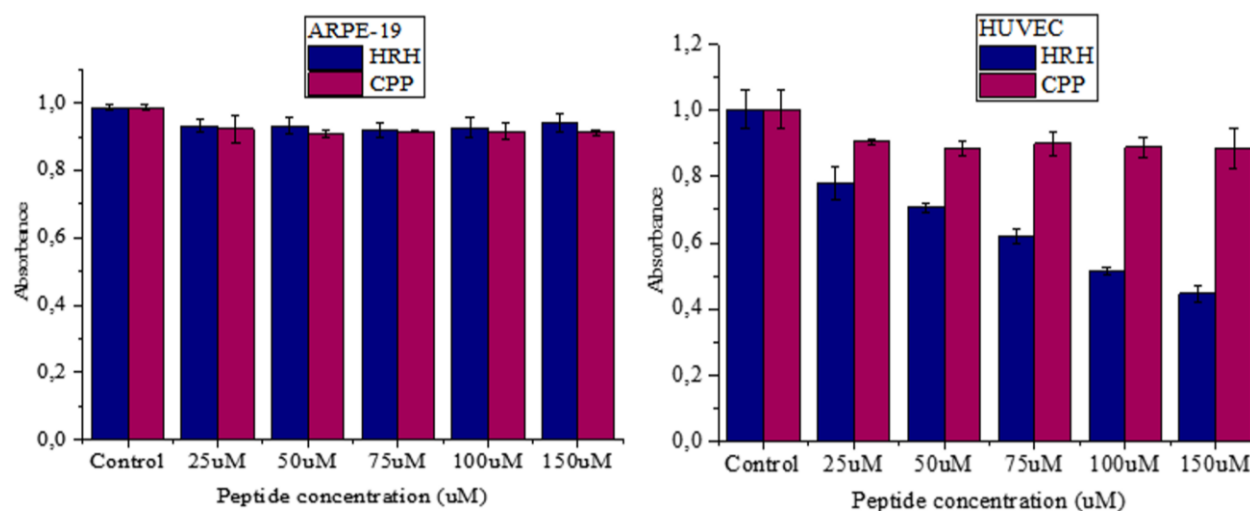


**Figure 16. CCK-8 on HUVECs and ARPE-19 cells treated with different concentrations of HRH peptide and CPP.** Cells were 80% confluency at the initiation of the study. Analysis was performed on cell cultures treated with the peptides for 96 hr at 37°C. It was observed that mitochondrial activity of HUVECs decreased with increasing HRH peptide concentration, resulting in decreasing of the absorbance value, while increasing penetratin peptide concentration showed no inhibitory effect on the absorbance values of HUVECs. Moreover, ARPE-19 cells were not affected by the treatment of HRH peptide or penetratin peptide. Experiments were repeated as three biological replicates (n=3).

## 5.3 Nanogel generation

### 5.3.1 HA-Poly-L-lysine (PLL) formulation

To optimize the nanogel formulation, HA was either electrostatically interacted or chemically crosslinked at different temperatures and buffer pH. Before all experiments, HA was sonicated for 30 minutes to minimize the possible HA aggregations.

As given in **Table 2** and **Figure 17**, HA-PLL interactions at pH 7.4 and 25°C was optimum for nanogel formation. Average size was 128.35 nm at 25°C with the lowest PDI number. This size and homogeneity were also confirmed with SEM analysis (**Figure 18**). However, HA-PLL interactions show low stability at all conditions and nanogels' hydrodynamic radius were increased around 30% within the following 24 hours. Therefore, further optimizations were considered.

**Table 2. DLS analysis of HA-PLL interactions at different pH at 25 °C and 37°C.** Size data is given as an average of three biological experiments. Within each experiment three measurements were taken. HA and PLL were interacted at different pH values and temperatures with 2:1 monomer ratio to observe the size of nanogels at different conditions. The sizes of HA-PLL interactions were 128.35 nm and 138.1 nm at 25°C and 37°C, respectively, which indicates that nanogels are smaller in size at 25°C. Since pH 7.4 is the neutral pH, the following experiments were conducted at pH 7.4 and 25°C.

	Size (d.nm ± S.D)	PDI	pH	Temp.	Zeta Potential (mV)	PLL: HA monomer ratio	Size after 24 hours	PDI after 24 hours
HA-PLL	128.35 ±10	0.104	7.4	25 °C	-3.77	2:1	168.04	0.144
HA-PLL	264.2 ±16	0.270	6	25 °C	-5.53	2:1	212.6	0.407
HA-PLL	121.3 ±10	0.166	9	25 °C	-8.73	2:1	164.1	0.190
HA-PLL	110.0 ±8	0.134	7 for HA, 6 for PLL	25 °C	-4.99	2:1	149.7	0.228
HA-PLL	138.1 ±12	0.160	7.4	37 °C	-3.55	2:1	161.2	0.249
HA-PLL	127.7 ±14	0.270	6	37 °C	-13.1	2:1	191.2	0.164
HA-PLL	151.9 ±12	0.259	9	37 °C	-14.0	2:1	154.5	0.205
HA-PLL	119.9 ±8	0.228	7 for HA, 6 for PLL	37 °C	-12.9	2:1	156.0	0.183

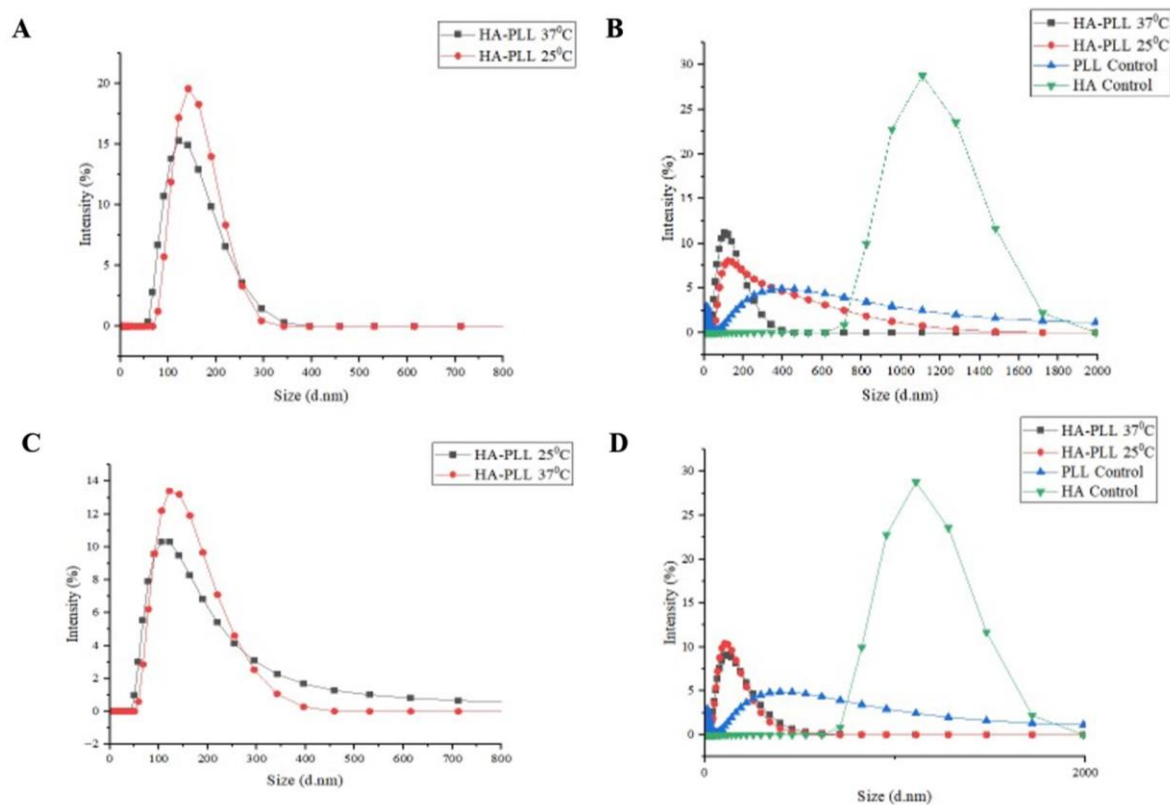


**Figure 17. Representative DLS data of HA-PLL nanogel formation** at 25°C and 37°C at pH 7.4 (A), 6 (B), 9 (C), and 6 for PLL and 7 for HA (D). For both experiments PLL and HA was measured as the control in relevant pH buffers. At pH 7.4, nanogels were generated at 128.35 nm and 138.1 nm on average sizes at 25°C and 37°C (A), while the size was bigger at pH 6 at 25°C ( $264.2 \pm 16$ ) and  $127.7 \pm 14$  at 37°C (B). At pH 9, smaller nanogels were generated at 25°C ( $121.3 \pm 10$ ) compared to nanogel sizes at 37°C (C). The sizes of nanogels that pH 7 for HA and 6 for PLL were  $110 \pm 8$  and  $119.9 \pm 8$  at both temperatures (D).

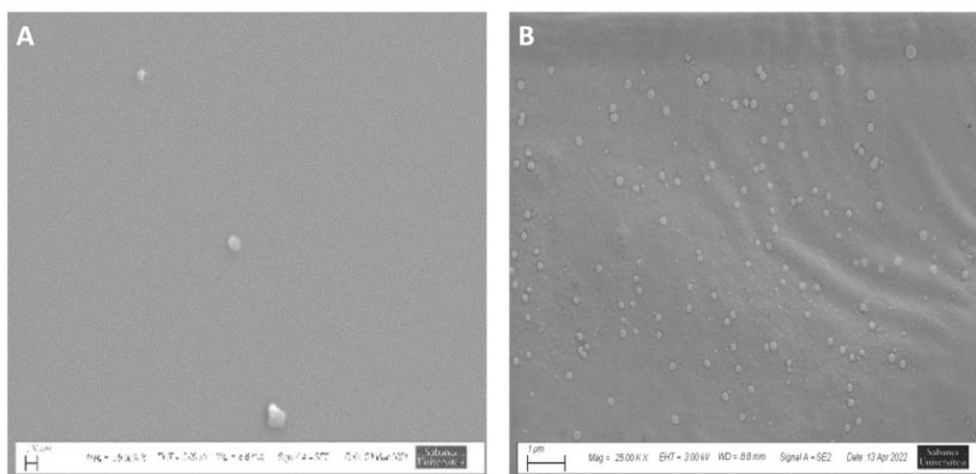


**Figure 18. SEM images of HA-PLL nanogels** generated at pH 7.4 and 25°C (A), or 37°C (B). HA-PLL interactions showed low homogeneity and low nanogel generation at both temperatures and neutral pH values. Samples were prepared with drop-casting 7  $\mu$ l of sample onto SEM grids, which were air-dried overnight and coated with Au/Pd using 40 mA for 80 s. Samples were observed with Jeol Leo Supra VP35 Field Emission Scanning Electron Microscope at 3 kV accelerating voltage. (n=3)

### 5.3.2. HA-Cholesterol-PLL and HA-EDC/NHS-Cholesterol-PLL formulations

To increase stability and generation of HA-PLL interactions, cholesterol and EDC-NHS chemical crosslinker were used. On the other hand, HA, cholesterol and PLL were mixed and electrostatically interacted. HA, cholesterol and PLL were interacted at 25°C and pH 6 with and without EDC/NHS crosslinker (pH 6 is the working pH value of EDC/NHS crosslinker). This result suggests whether crosslinker is an effective way for nanogel stabilization.

Nanostructures generated by using EDC-NHS chemistry, which produce amide bonds between HA and PLL showed higher stability and their hydrodynamic radius remained constant within 24 hours. Even though HA-cholesterol-PLL nanogels were smaller in size, when they were freshly synthesized, their size became bigger than nanogels stabilized with EDC-NHS crosslinker in 24 hours. This result proves that crosslinker is an effective way for nanogel stabilization. Both nanostructures were characterized with DLS, and SEM (Table 3, Figure 18, and Figure 19). DLS data showed that the average sizes of the nanogels, which are generated with and without crosslinker, were 143.1 nm and 117.1 nm, respectively. Additionally, nanogels stabilized with EDC/NHS resulted in higher homogeneity as can be followed both with lower PDI and SEM images.

**Table 3.** DLS analysis of HA-Cholesterol-PLL and HA-EDC/NHS-Cholesterol-PLL interactions at pH 7.4 and 25°C. Results are the average of three biological replicates.

	Size (d.nm ± S.D)	PDI	Size after 24 hours	PDI after 24 hours	Size after one week	PDI after one week
HA-Cholesterol-PLL	117.1 ± 12	0.132	134.8	0.088	159.6	0.128
HA-EDC/NHS-Cholesterol-PLL	143.1 ± 15	0.078	143.0	0.082	161.2	0.060

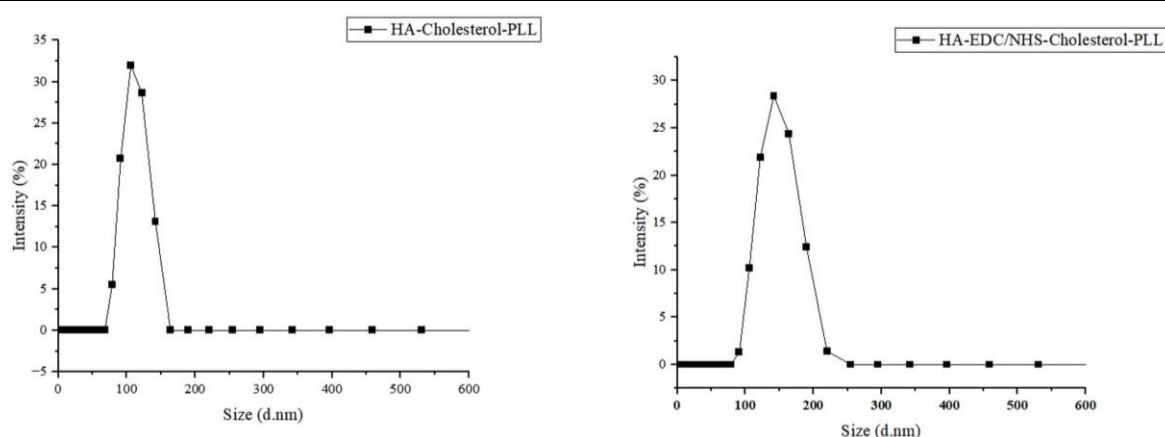


**Figure 19.** A representative DLS data of HA-Cholesterol-PLL and HA-EDC/NHS-Cholesterol-PLL nanogels at 25°C at pH 7.4. Nanogels generated with HA-Cholesterol-PLL are smaller in size (117.1 nm) compared to the nanogels generated with HA-EDC/NHS-Cholesterol-PLL (143.1 nm).

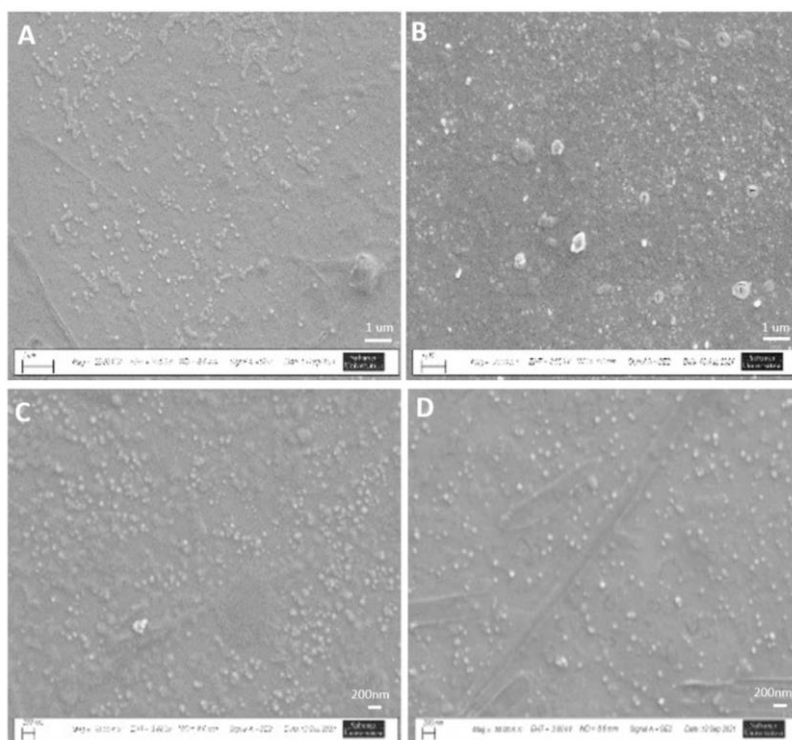


**Figure 20. SEM images of HA-Cholesterol-PLL nanogels synthesized at pH 7.4 (A and B) and HA-EDC/NHS-Cholesterol-PLL nanogels synthesized at pH 7.4 and 25 °C (C and D).** The average sizes of nanogels were measured as 112.8 nm for the nanogel generated without cross linker, and 131.2 nm for the nanogel synthesized with cross linker with more homogeneity. Samples were prepared with drop-casting 7  $\mu$ l of sample onto SEM grids, which were air-dried overnight and coated with Au/Pd using 40 mA for 80 s. Samples were observed with Jeol Leo Supra VP35 Field Emission Scanning Electron Microscope at 3 kV accelerating voltage. (n=3).

### 5.3.3. HA-DVS-PLL Nanogel formulation

As an alternative to EDC-NHS, DVS was used as the crosslinker for HA-PLL formulation. The reaction was carried out with 1:1 HA: DVS molar ratio and the ratio of HA:PLL was as in previous experiments (2:1 PLL:HA monomer ratio). HA and PLL were interacted with DVS crosslinker at either pH 6 or pH 11. The reason to make the interactions at pH 6 and pH 11 is that the best working pH value of DVS is 11 and PLL shows  $\beta$ -sheet structure and best folding at pH 6. Compared to HA-PLL electrostatic interaction, both HA-DVS-PLL interactions showed significantly higher stability and the hydrodynamic radius remained almost the same after 24 hours at pH 11, indicating that DVS is an effective crosslinker to stabilize the nanogel formulation (**Table 4 and Figure 21**). However, the size homogeneity of nanogels were low at both pH values (**Figure 20**).

**Table 4. DLS analysis of HA-DVS-PLL interactions at pH 6 and pH 11 at 25 °C.** Results are given as the average of three biological replicates. HA-DVS-PLL interacted at pH 11 was less stable compared to the nanogel generated at pH 6.

	Size (d.nm $\pm$ S.D)	PDI	pH	Size after 24 hours	PDI after 24 hours	Size after one week	PDI after one week
HA-DVS-PLL	135.7 $\pm$ 10	0.273	6	140.1	0.402	136.1	0.177
HA-DVS-PLL	151.0 $\pm$ 12	0.340	11	157.8	0.297	216.8	0.233

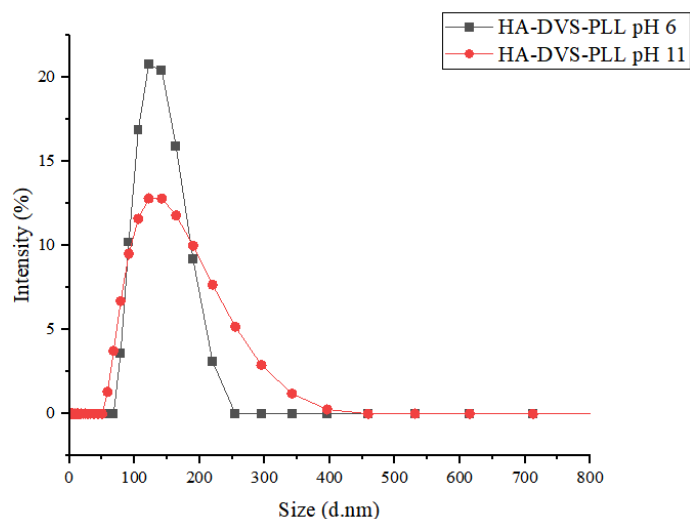


**Figure 21. Representative DLS data of HA-DVS-PLL nanogel formation at 25°C at pH 6 and 11. Nanogel formation at pH 6 was more than nanogel generated at pH 11.**

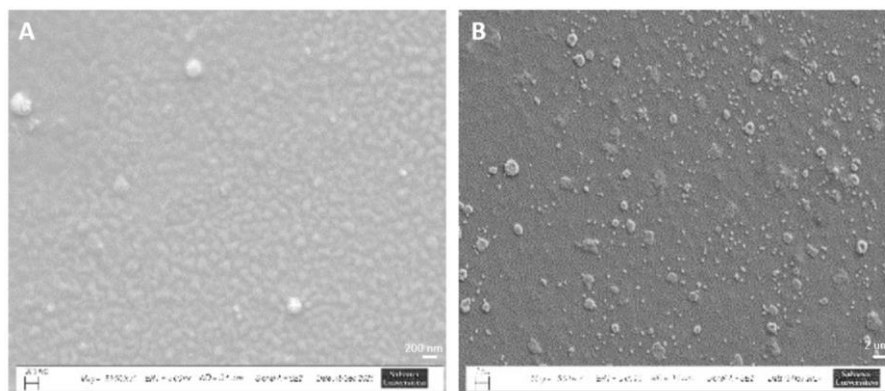


**Figure 22. SEM images of HA-DVS-PLL nanogels synthesized at pH 11 and 25°C. The size of nanogels was measured as 142.4 in average. Samples were prepared with drop-casting 7  $\mu$ l of sample onto SEM grids, which were air-dried overnight and coated with Au/Pd using 40 mA for 80 s. Samples were observed with Jeol Leo Supra VP35 Field Emission Scanning Electron Microscope (n=3).**

#### 5.3.4. HA-EDC/NHS-Cholesterol-HRH-CPP nanogel formulation

To investigate the size and stability of HA-cholesterol-HRH-CPP, EDC-NHS chemistry was used for nanogel synthesis. HA (10 kDa) was modified with EDC/NHS 1:0.4:0.4 molar ratio (**Figure 23**). Then HRH and finally CPP were added to HA structure to obtain an HA: HRH nanogel coated with CPP. The final molar ratio was 1:1:1.8 for HA: HRH: CPP. The formulation was stored at +4 °C until used for further analysis. Both DLS and SEM analysis showed that the size homogeneity was low (**Figure 24 and 25**), formulation was unstable, and the size of nanogel was too big (254.4 nm) to be able to penetrate through the ocular tissues. Thus, DVS was considered as an alternative to crosslink HAs.

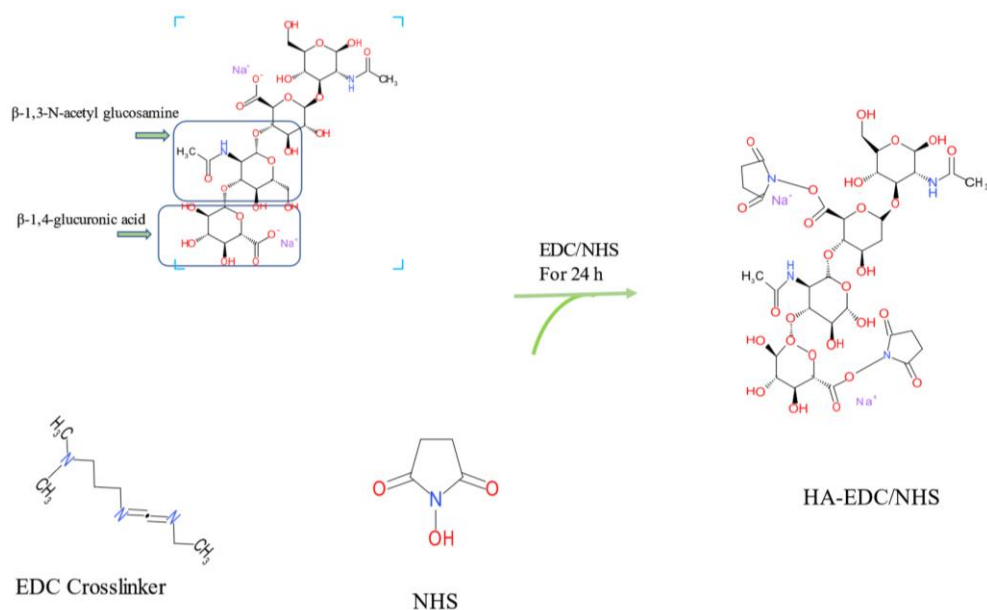


**Figure 23. The mechanism of HA-EDC/NHS interaction** (drawn at Chem4Word). EDC/NHS chemistry activates the COOH group of HA.

**Table 5. DLS analysis of HA-EDC/NHS-Cholesterol-HRH-CPP interactions** at pH 6. and 25°C. Data represents the average of three biological replicates.

	Size (d.nm ± S.D)	PDI	pH	Size after 24 hours	PDI after 24 hours	Size after one week	PDI after one week
HA-EDC/NHS-Cholesterol-HRH-CPP	254.4 ± 14	0.536	6	322.3	0.557	390.1	0.707

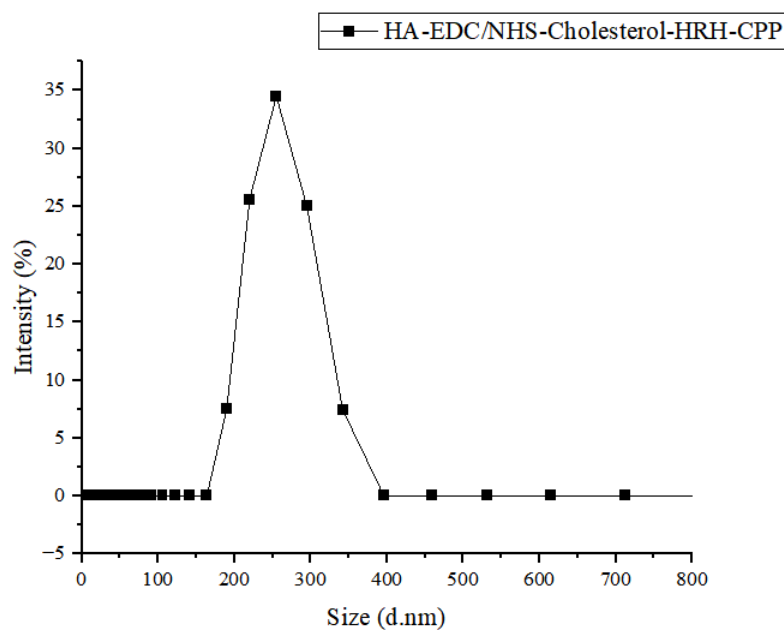


**Figure 24. A representative DLS data of HA-EDC/NHS-Cholesterol-HRH-CPP interaction** at 25°C at pH 6. The nanogel size was measured as 254.4 nm in average with low homogeneity and stability.

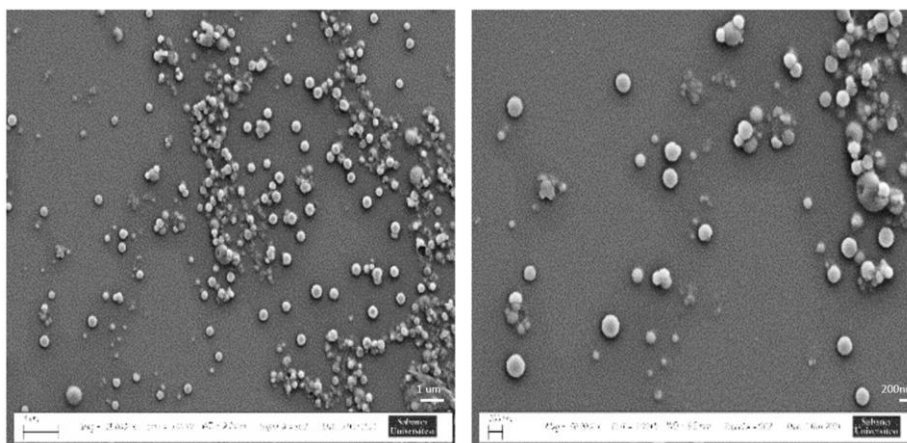


**Figure 25. SEM images of HA-EDC/NHS-Cholesterol-HRH-CPP nanogels** synthesized at pH 6 and 25°C. The nanogel size homogeneity was low even though nanogels were generated with relatively high intensity. The nanogel size was around 232,8 nm. Samples were prepared with drop-casting 7  $\mu$ l of sample onto SEM grids, which were air-dried overnight and coated with Au/Pd using 40 mA for 80 s. Samples were observed with Jeol Leo Supra VP35 Field Emission Scanning Electron Microscope (n=3).

### 5.3.5. HA-DVS-Cholesterol-HRH-CPP nanogel formulation

HA was crosslinked by using DVS to increase the stability of the formulation (Nurettin Sahiner, 2008) by mixing 24 hours at 700 rpm. Cholesterol was used to compose a hydrophobic core in the nanogel, HRH peptide was used as an anti-VEGF agent against vascularization in the eye and penetratin peptide is used to enhance the capability of cell penetration of the nanogel formulation. To achieve the optimum size of the nanogel, three HA with different molecular weights, 10 kDa, 8-15 kDa, or 21-40 kDa, were used.

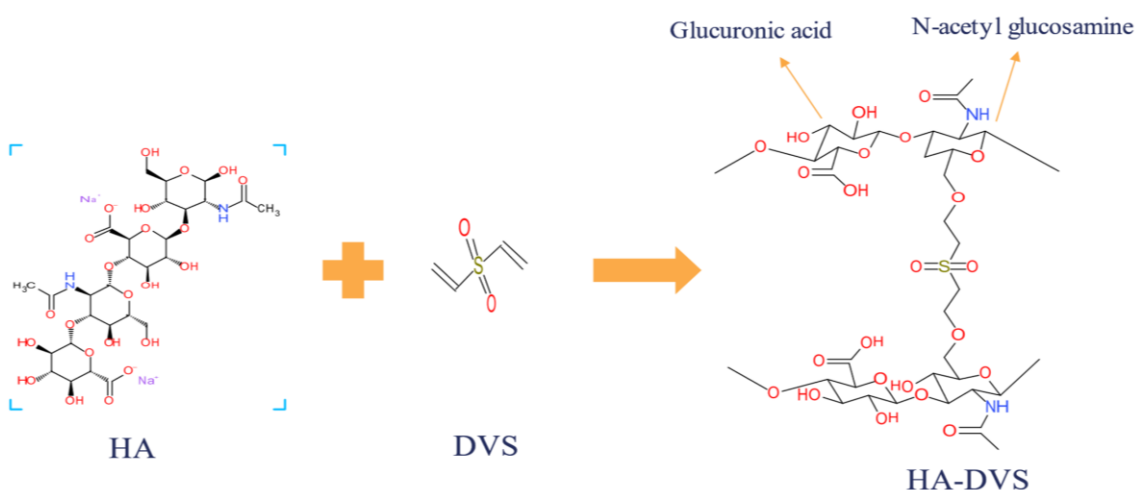


**Figure 26. HA-DVS crosslinking mechanism.** (Drawn at Chem4Word.). By using DVS crosslinker, two HA monomers bind to each other with N-acetyl glucosamine.

The nanogels synthesized with 10 kDa and 8-15 kDa HAs (nanogel 1 and nanogel 2) showed smaller sizes (134 nm and 138 nm, respectively) compared to nanogels with 20-41 kDa (323

nm) HA and they showed higher stability (**Table 6**). Nanogel formulations were further characterized by SEM and FTIR analysis (**Figure 28 and 29**).

The size of nanogels generated with 21-40 kDa HA was too big compared to the nanogel 1 and nanogel 2 formulation including 10 kDa and 8-15 kDa HA (**Table 6**). This result might be due to the molecular weight of HA utilized (21-40 kDa), because the size was small enough either DVS or EDC/NHS was used as the cross-linker. To make the nanogel size smaller, two HA in lower molecular weights were used for nanogel generation. Nanogel formulations synthesized with 10 kDa and 8-15 kDa HA was smaller in size in both SEM and DLS analysis (**Table 6, Figure 27 and 28**).

**Table 6. DLS analysis of HA-DVS-Cholesterol-HRH-CPP interactions** at pH 6 and pH 11, and 25 °C. The nanogel synthesized with 20-41 kDa HA showed a bigger size at both pH values and optimum size and stability were achieved with the nanogels synthesized with 10 kDa and 8-15 kDa. Data represents the average of three biological replicates.

	Size (d.nm ± S.D)	PDI	pH	Zeta Potential mV	Size after 24 hours	PDI after 24 hours
HA (21-40kDa)-DVS-Chol-HRH-CPP	450.8 ± 20	0.228	6	-4.99	427.7	0.703
HA (21-40 kDa)-DVS-Chol-HRH-CPP	323.5 ± 19	0.390	11	-7.89	368.5	0.570
HA-DVS-Cholesterol-HRH-CPP (Nanogel 1)	134.8 ± 8	0.343	11	-7.91	141.7	0.962
HA-DVS-Cholesterol-HRH-CPP (Nanogel 2)	138.8 ± 10	0.717	11	-7.83	149.1	0.812

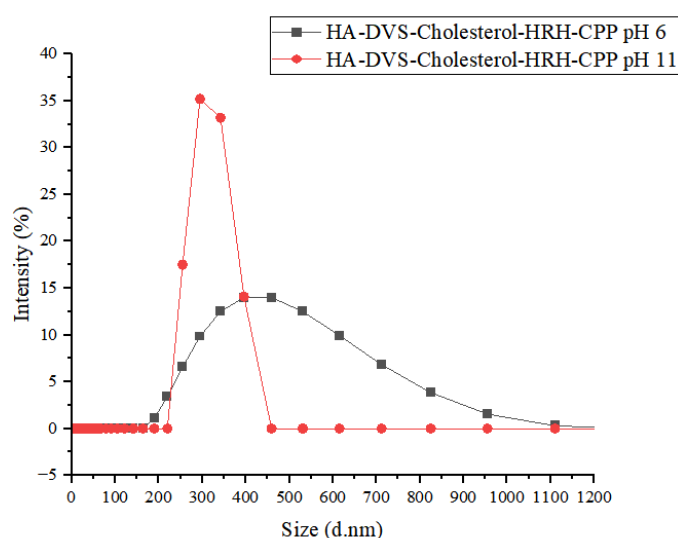


**Figure 27. A representative DLS data of HA-DVS-Cholesterol-HRH-CPP interaction** at 25°C at pH 6 (a) and pH 11 (b). nanogels generated by using 21-40 kDa HA were too big to penetrate the eye at both pH 6 and 11 (450.8 nm and 323.5 nm in average, respectively) with low stability, and nanogel generation and homogeneity was low at pH 6.

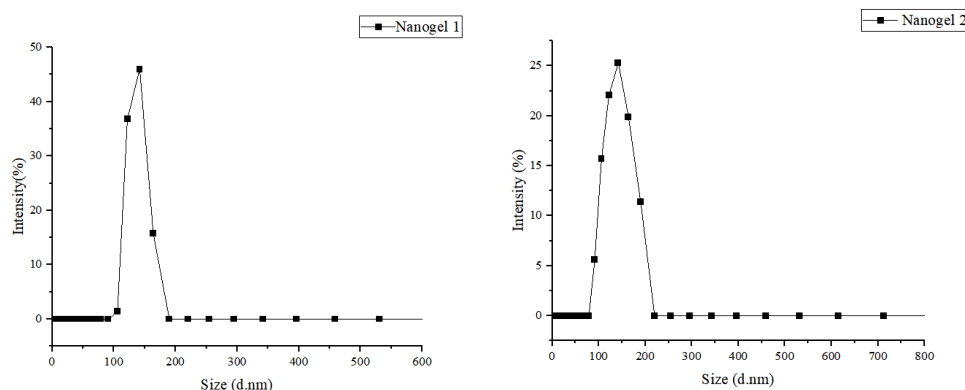


**Figure 28.** A representative DLS data of HA-DVS-Cholesterol-HRH-CPP interactions at pH 11 (nanogel 1 and 2, respectively). Nanogel 1 and nanogel 2 were synthesized with relatively higher stability and lower sizes (134.8 nm and 138.8 nm, respectively). After 24 hours, the sizes of both nanogels were slightly increased, indicating that nanogels shows a stability.

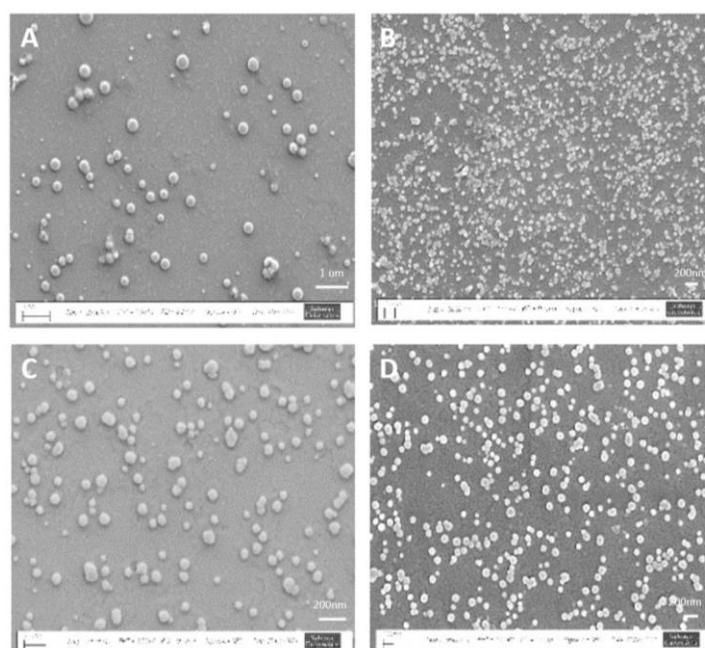


**Figure 29.** SEM images of HA (21-40 kDa)-DVS-Cholesterol-HRH-CPP nanogels synthesized at pH 11 (A) and pH 6 (B), Nanogel 1 (C), and nanogel 2 (D) at 25 °C. Nanogel 1 and nanogel 2 were observed in spherical shape with 230-350 nm for nanogels generated by using 21-40 kDa HA, and 80-200 nm which is parallel with DLS data. At pH 6, nanogel generation was lower compared to nanogel generated by using 21-40 kDa HA at pH 11. Samples were observed with Jeol Leo Supra VP35 Field Emission Scanning Electron Microscope at 3 kV accelerating voltage (n=3).

FTIR analysis was performed at 25°C and 0.5 bar nitrogen pressure with 128 times scanning for both nanogel 1 and nanogel 2. The results showed that the crosslink between HA and DVS (Vasi, Popa, Butnaru, Dodi, & Verestiuc, 2014) and between HA and HRH (Mallamace, 2015) and CPP peptides were occurred. The FTIR spectrum of nanogels (**Figure 30**) showed the following characteristics bands: the peak located at 3280  $\text{cm}^{-1}$  is associated with the intra- and intermolecular stretching vibration of -OH group, 1375  $\text{cm}^{-1}$  and 1530  $\text{cm}^{-1}$  are associated with intermolecular interaction with peptides (amide III and amide II, respectively), while the peak from 1020  $\text{cm}^{-1}$  is associated with the C-O-C bond from HA (Vasi *et al.*, 2014).

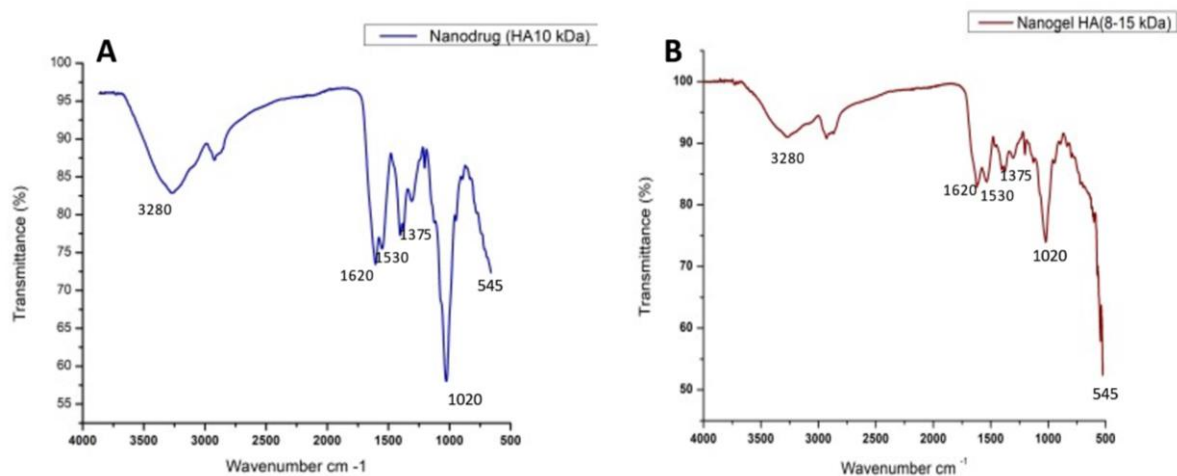


**Figure 30. FTIR analysis** of nanogel 1 (A) and nanogel 2 (B) nanogels generated at pH 11 and 25°C. Data was obtained by using and ATR-FTIR (Thermo Fisher Scientific, USA) at 25 °C with 128 scanning in Omnic software. The peak located at 3280  $\text{cm}^{-1}$  represents the intra- and intermolecular stretching vibration of -OH group, 1375  $\text{cm}^{-1}$  and 1530  $\text{cm}^{-1}$  are associated with intermolecular interaction with peptides (amide III and amide II, respectively), and the peak from 1020  $\text{cm}^{-1}$  is associated with the C-O-C bond from HA.

#### 5.4 Encapsulation Efficacy and Release Profile of Nanogels

Encapsulation efficacy of nanogels were calculated as 65 % and 53 % for nanogel 1 and nanogel 2, respectively. Drug release profile of both nanogels were obtained by using fluorescent spectroscopy (**Figure 31**). According to the equation and fluorescent intensity values, drug release profile was obtained for each nanogel.

Both nanogel formulations showed a burst effect in the first hour with HRH release of 10 and 15% from nanogel 1 and nanogel 2, respectively. Release profile was steadier the following 24 hours. At the end of 24 hours only 16% of HRH was released from nanogel 1 whereas 36% of drug was released from nanogel 2.

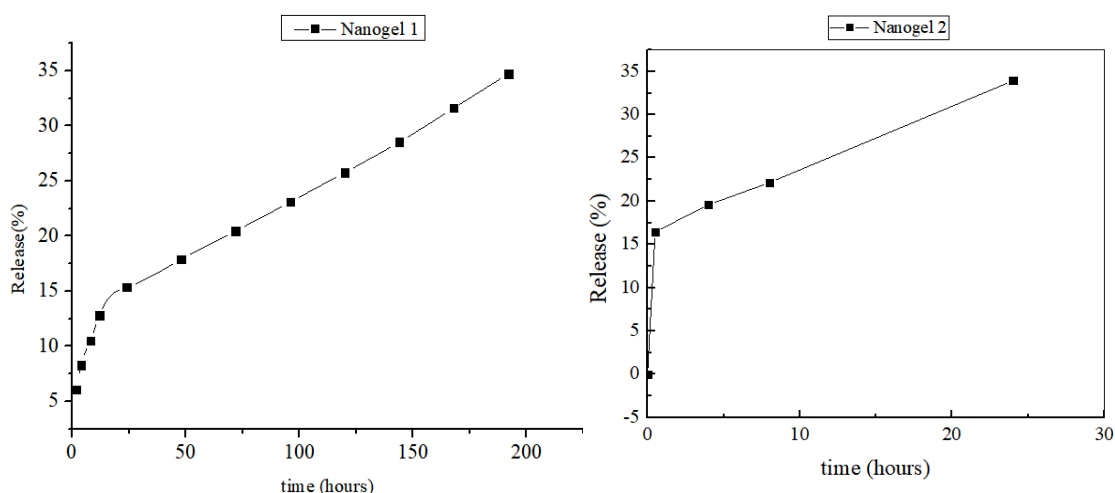


**Figure 31. Nanogel release profiles.** 34.72 % of nanogel 1 is released within 192 hours, while 33,93 % of nanogel 2 is released within 24 hours (n=3).

### 5.5 Treatment of HUVECs and ARPE-19 cells with nanodrug formulation

Depending on the data observed on nanogel formulations with DVS and EDC/NHS crosslinkers, nanogels formulated with DVS were found to be smaller than EDC/HNS stabilized ones. Therefore, the studies were continued with DVS cross-linker. When 10kDa and 8-15kDa HA was used in nanogel-1 and nanogel-2 forms, nanogel-1 resulted in slightly smaller size (134 nm vs 138 nm) and slightly higher encapsulation efficacy with 65%. Therefore, nanogel-1 was chosen for further studies.

To investigate the effect of nanodrug-1 formulation on proliferation of ARPE-19 cells and HUVECs, both cells were treated with 20  $\mu$ L nanogel. Overnight cultures were treated with HA: HRH: CPP nanogel at 1:1:1.8 molar ratio for 96 hours at 37°C, 5% CO<sub>2</sub>. 20  $\mu$ L nanogel is composed of 20  $\mu$ M HA, 20  $\mu$ M HRH and 36  $\mu$ M CPP. To follow the effect of HA, HRH and CPP, individually, free molecules at the same concentrations with nanogel is also investigated using live/dead assay (**Figure 32**). Cell proliferation was observed with optical microscope every day and at end of 96 hours of incubation, cells were treated with Calcein/PI, where live cells were stained in green and dead cells were stained in red. It was clear that neither of the peptide or the nanogel were toxic for HUVE or ARPE-19 cells and despite the differences in proliferations, cells were alive.

Nanodrug formulations containing anti-VEGF, HRH peptide at 20  $\mu$ M, showed inhibitory effects on HUVE cell proliferation (**Figure 33**). The amount of inhibition was almost 50%, which is higher than our initial experiments with different HRH concentrations, where a 25% inhibition was observed for 25  $\mu$ M HRH (**Figure 16**). This difference would have arisen from

the higher passage number of HUVE cells and new batch of HRH production. A similar inhibition difference was also observed for ARPE-19 cells compared to our initial experiments (**Figure 16**), suggesting a variation in cellular health in further passage numbers. In this experimental series with ARPE-19, some non-significant effect of HA and CPP was also evident.

Anti-VEGF peptide within the nanogel formulation showed a slightly higher inhibitory effect on HUVE cells, with around 70% decrease in proliferation compared to control cells. HRH peptide in nanogel form may exhibit synergistic effect, which would be explained with the presence of HA and CPP. The mechanism how nanogel affects HUVE cells should be investigated further with apoptosis markers and VEGF-R interactions. Meanwhile, no toxicity on ARPE-19 cells were observed (**Figure 32, Figure 33**).

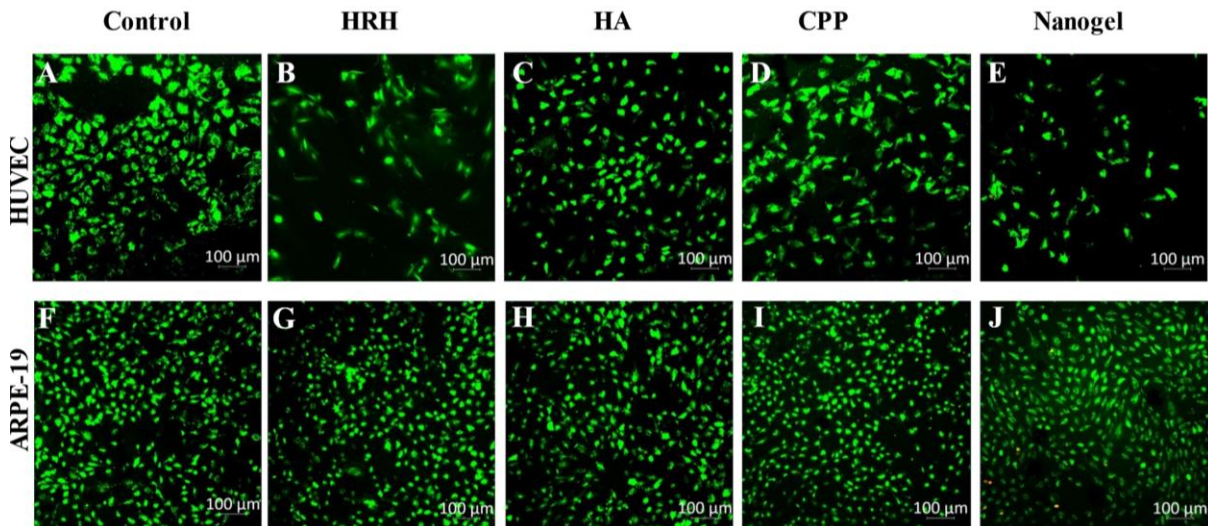


**Figure 32.** A representative data of HUVECs treated with nanogel, which contain 20  $\mu$ M HRH peptide, and ARPE-19 cells (J) treated with nanogel and incubated for 96 hours at 37°C and % 5 CO<sub>2</sub>. ARPE-19 cells treated with HRH (20 $\mu$ M), HA (20  $\mu$ M), and CPP (36  $\mu$ M) (G, H, I) respectively. HUVECs treated with HRH (20  $\mu$ M), HA (20  $\mu$ M), and CPP (36  $\mu$ M) (B, C, D, respectively). Control HUVECs, (A) and ARPE-19 cells (F). The proliferation of HUVE cells (C and D) and ARPE-19 cells (H, I) treated with HA and penetratin peptide, were not inhibited and cells stayed confluent. HUVE cells treated with HRH peptide and nanogel showed inhibition in their proliferation during the treatment time (B, E, respectively), while ARPE-19 cells' proliferation was not affected after treatment with HRH peptide and nanogel (G, J, respectively). Images were taken after 96 hours incubation with the bioagent by using an AxioPrimo inverted light microscopy (n=3).

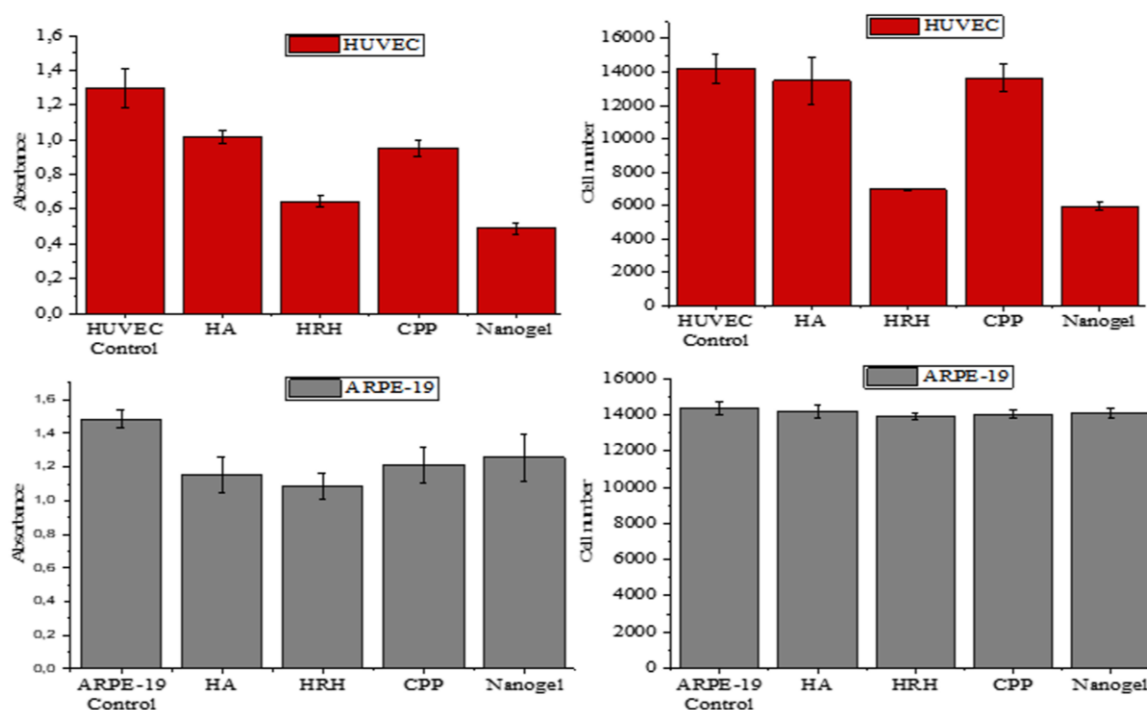


**Figure 33.** CCK-8 assays and cell numbers of HUVECs (A and B) and ARPE-19 cells (C and D) treated with HA (20  $\mu$ M), nanodrug formulations (with 20  $\mu$ M HRH peptide) and penetratin peptide (36  $\mu$ M) and free HRH peptide (20  $\mu$ M). Analysis was performed following 24hr incubation with the bioagent. CCK-8 kit was used and the measurements were conducted by using ELISA plate reader at 450 nm (n=4).

To further evaluate the effect of peptides incorporated into the nanogels, only HRH and only CPP peptide nanogels were prepared. These nanogels contain 0.6 mg HRH or 0.6 mg CPP instead of a combination of 0.2 mg HRH and 0.4 mg of CPP. Also, the original nanogel containing both peptides were evaluated in the same experiment. According to the data obtained from three independent experiments, nanogels composed of CPP peptide didn't show any effect on HUVE cell proliferation. Whereas nanogel prepared with only HRH peptide showed a drastic inhibition on HUVE cells. The inhibition was more than 50% in this case, which would be a direct result of higher HRH amount in the formulation (**Figure 34**). Neither nanogel formulation effected ARPE-19 cells significantly. Nanogel, which is prepared with 0.2 mg HRH peptide and 0.4 mg CPP inhibited the HUVEC proliferation, while nanogel has almost no inhibitory effect on ARPE-19 cells.

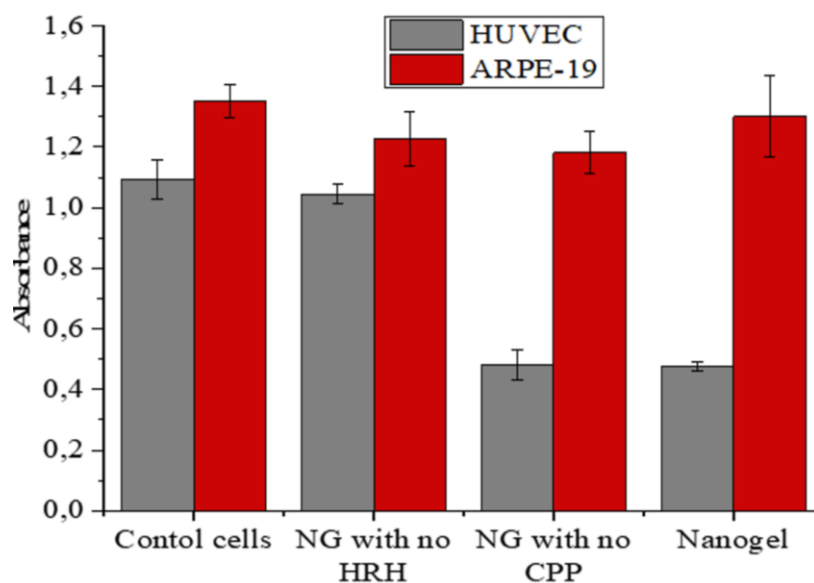


**Figure 34.** CCK-8 assay was performed on HUVECS and ARPE-19 cells. Nanogel with no HRH and with no CPP were added to both cells to investigate the effects of CPP or HRH peptides on the proliferation of ARPE-19 and HUVECs. Also, nanogel, which consists of both HRH and CPP peptides were administered to both cells. The proliferation of ARPE-19 was not negatively affected by all types of nanogel administration, while nanogels with no CPP and regular nanogels showed an inhibitory effect on HUVEC proliferation. HUVEC proliferation was not affected by the nanogel with no HRH peptide.

### 5.6 Penetration of Nanogel Formulations through the ARPE-19 cell layer

A TEER measurement device was designed (**Figure 35**) by a teammate Abuzer Alp Yetişgin and Bülent Köroğlu (SUNUM) and used to measure cell confluency of ARPE-19 cell layer. The device is briefly composed of two chopstick electrodes and indicators, showing current and voltage of cell containing mediums.

At the initiation of the experiments,  $1 \times 10^4$  ARPE-19 and  $1 \times 10^4$  HUVECs were seeded in trans-well insert and well, respectively. TEER measurements were performed at 60 mA current and 6 mV voltage as the cells became confluent. The expected resistance of confluent cell layer was 160-250  $\Omega$  with a steady curve (Oliveira, 2019, Kosma, 2016). In the next step, cells seeded in insert membranes were treated with 20  $\mu$ L nanogel formulations and TEER measurements have been taken daily to determine the resistance of cells. **Table 7** and **Figure 36** show that ARPE-19 cells reached confluency in 5 days and nanogels were administered and cells were incubated for 5 more days. TEER value reached to 189  $\Omega$  at the end of 5<sup>th</sup> day of culture on ARPE-19 cell layer. It was initiated with 161.1  $\Omega$  and the gradual increase was stopped at day 5 indicating the formation of confluent cell layer.

At day 5, nanogel formulation was administered to ARPE-19 cell layer and TEER measurements continued every day. For the following 5 days, there was no drastic decrease in resistance indicating the preservation (without any disruption such as tear or cell death) of confluent ARPE-19 layer despite nanogel treatment. This was pre-requisite, since with this

study the penetration of nanogel from confluent ARPE-19 layer to HUVEC layer is being investigated.

Every day after initiating the treatment with nanogel formulation, cells were stained to follow cell proliferation and effect of nanogel on both ARPE-19 and HUVE cells. Cell staining results confirmed the TEER measurements and showed that ARPE-19 confluency was not affected by nanogel treatment. HUVE cell layer, on the other hand, seem to be disrupted day by day and cell proliferation was inhibited. Thus, it was possible to say that nanogel penetrated throughout the insert membrane and ARPE-19 layer and reached the HUVE cells to affect their proliferation (**Figure 37**).



**Figure 35. TEER measurement device designed in the laboratory.** The device composes of a standard USB charger, USB extension cord, and a microcontroller, two standard multimeters to measure alternating current and voltage as root mean square, telephone extension cord with a RJ14 female connector including six pins with the inner four wired, two short cables, a luster terminal, wire and ferrules, and soldering lugs.

**Table 7. TEER measurements of cocultured cells after nanogel treatment.** ARPE-19 cells were seeded into the insert membrane and HUVE cells were seeded into the trans well plates. TEER measurements were taken until the cells reached the confluency. Nanogel administered on ARPE-19 cells and incubated for four days and the resistances of ARPE-19 cells treated with nanogels did not decrease, indicating that the cell confluency remains stable. TEER measurement was taken every day to follow confluent ARPE-19 cell layer.

	A (mA)	V (mV)	$\Omega$	$\Omega.cm^2$
Cultured ARPE-19 without nanogel treatment day 1	0.18	29	161.1	180.44
Cultured ARPE-19 without nanogel treatment day 2	0.18	31	172.2	192.864
Cultured ARPE-19 without nanogel treatment day 3	0.18	33	183.33	205.296
Cultured ARPE-19 without nanogel treatment day 4	0.19	36	189.47	212.2
Cultured ARPE-19 without nanogel treatment day 5	0.19	36	189.47	212.2
Nanogel addition day-1	0.18	36	200	224
Nanogel addition day-2	0.18	35	194.44	217.77
Nanogel addition day-3	0.18	35	194.44	217.77

Nanogel addition day-4	0.19	36	189.47	212.2
Nanogel addition day-5	0.18	36	200	223

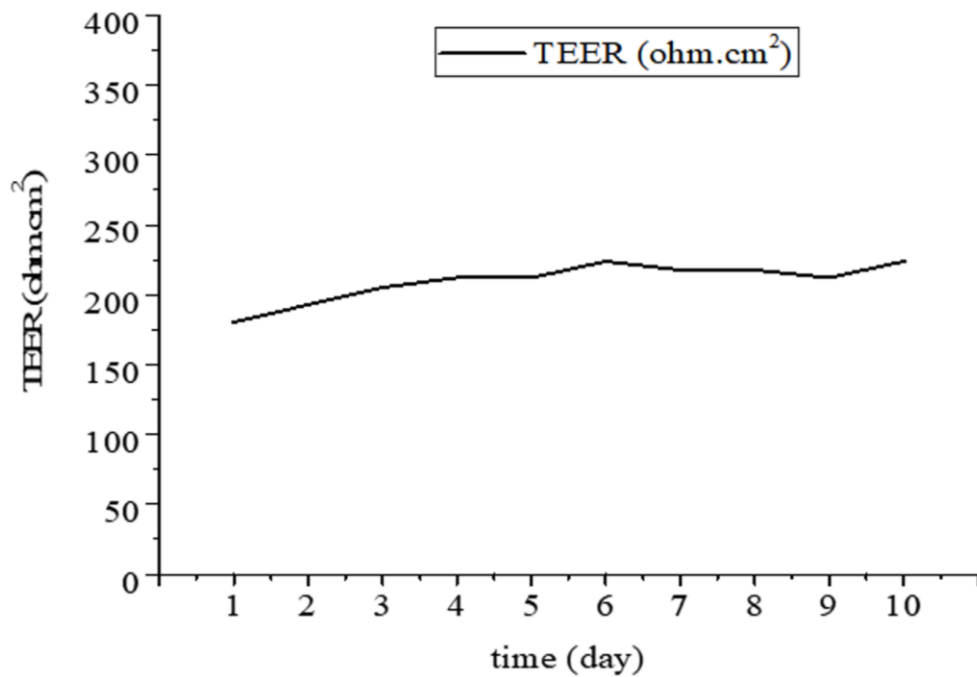


**Figure 36.** TEER measurements of ARPE-19 treated with nanogel. Measurements have been started with cell seeding (days 1 to 5) and continued after the nanodrug treatment initiation (days 6-10). The resistance of ARPE-19 cells reached to 189 mV in three days and then they were treated with nanogel. Cell resistance did not decrease, furthermore showed a slight increase.

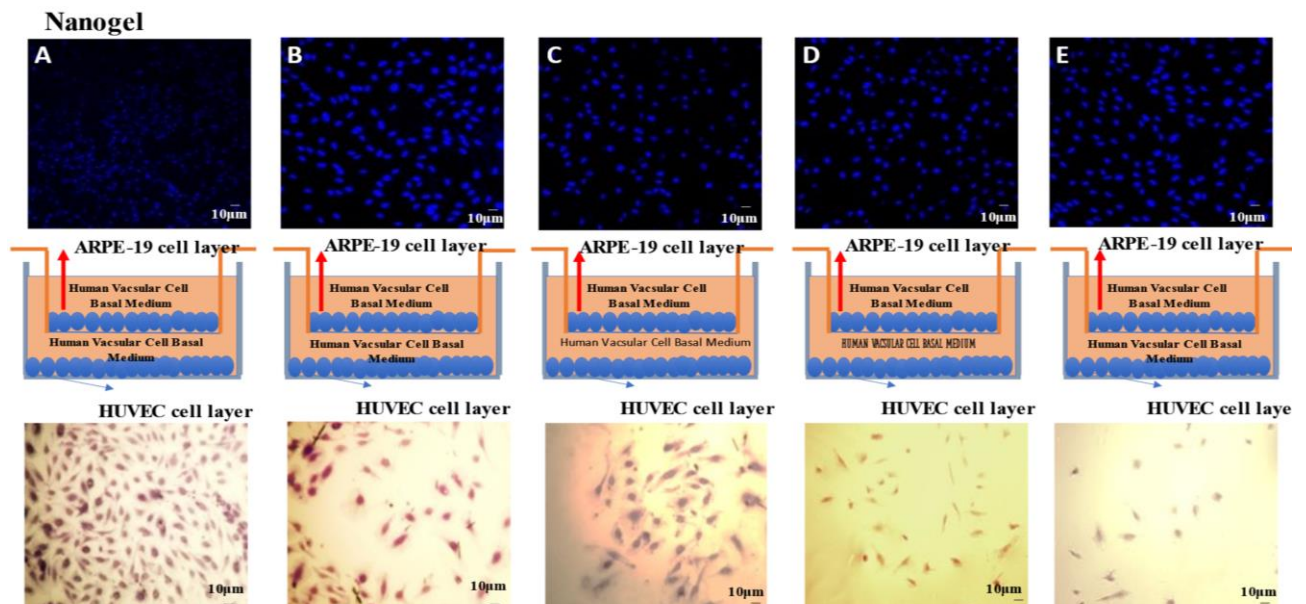


**Figure 37.** The images of ARPE-19 and HUVECs treated with nanogel. ARPE-19 confluency remained the same after five days of treatment, while HUVEC proliferation was inhibited by nanogels that penetrated through the insert membranes and reached the HUVEC cell layers. Therefore, HUVEC confluency decreased over time.

### 5.7. Nanogel penetration to ARPE-19 and HUVE cells

To evaluate the penetration to ARPE-19 and HUVE cells, nanogels were prepared with rhodamine and their entrance to the cells were monitored under LSCM. Rhodamine provided a red color to the nanogels, and their endosome mediated entrance was monitored with staining the cells with an early endosome marker, Rab-5, simultaneously.

Initially, nanogels were prepared with the original formulation containing HA, HRH and CPP. They have been found to enter both ARPE-19 and HUVE cells in 15 min. The nanogel was co-localized with the endosome marker Rab-5 in both cell types. This initial result was not encouraging considering that HRH should recognize the cell surface receptor VEGF-R to initiate the cascade for anti-angiogenesis. It was speculated that the CPP coating around the nanogel would be the primary reason for nanogel internalization and if HRH would be released from the nanogel, then it would interact with VEGF-R.

Therefore, a second experiment was conducted with nanogels containing only HRH peptide. With HRH nanogels, on the other hand, internalization was observed after 24<sup>th</sup> hour of nanogel administration. In ARPE-19 cells, HRH nanogel entrance was limited and co-localized with endosomal marker. However, HUVE cell internalization of HRH nanogel was not endosome mediated and was lower compared to ARPE-19 cells. Thus, it can be said that HRH is being selectively internalized by HUVE cells.

To quantify the amount of average nanogel penetration per cell, the red dots were counted in 45 ARPE-19 cells and 45 HUVE cells by Image J software. The number of red dots present in ARPE-19 cells, which are treated with nanogel with and without CPP was higher than that of HUVE cells treated with the same nanogel, which supports the LSCM data (**Figure 38**). To clarify that the nanogels penetrating to ARPE-19 cells by endosome marker Rab5, yellow dots, which correspond to the entrance of nanogel to ARPE-19 cells with endosomal marker were counted. **Figure 40** shows that the number of yellow dots counted inside ARPE-19 cells is slightly less than red dots, indicating that nanogels penetrate to ARPE-19 cells with endosomal marker Rab5. On the other hand, the number of counted yellow dots, which corresponds to that the nanogel penetration to HUVE cells with endosome marker was much less than the red dots. This might be speculated that nanogel is internalized by HUVE cells selectively.

**Figure 37. The images of ARPE-19 and HUVECs treated with nanogel**

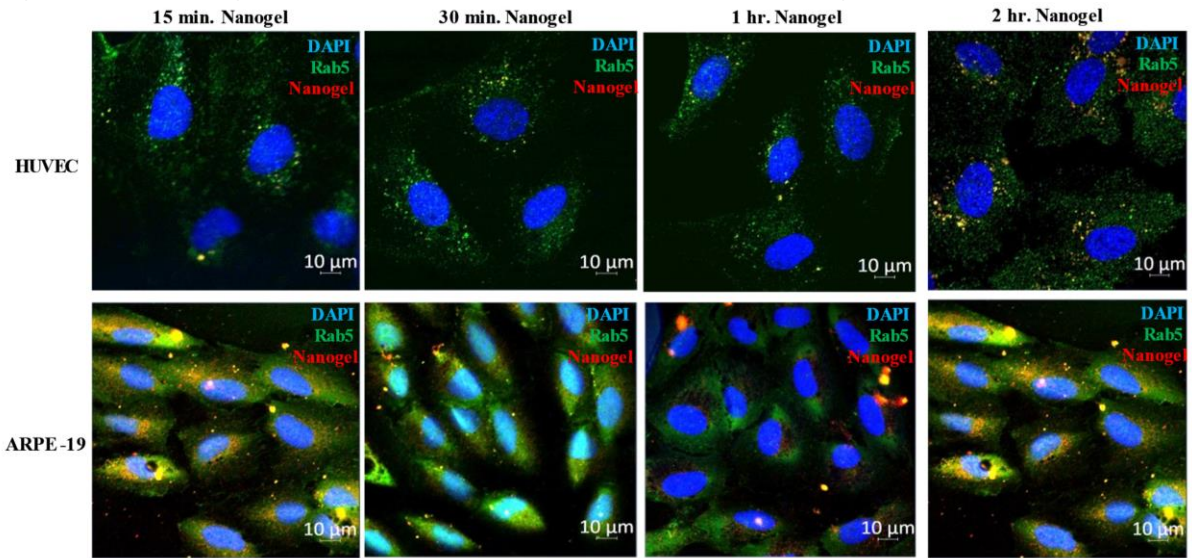


**Figure 38. HUVEC and ARPE-19 cells treated with nanogel containing CPP. Nanogels showed a fast penetration to the cells in 15 minutes and following times given in the figure (n=3).**

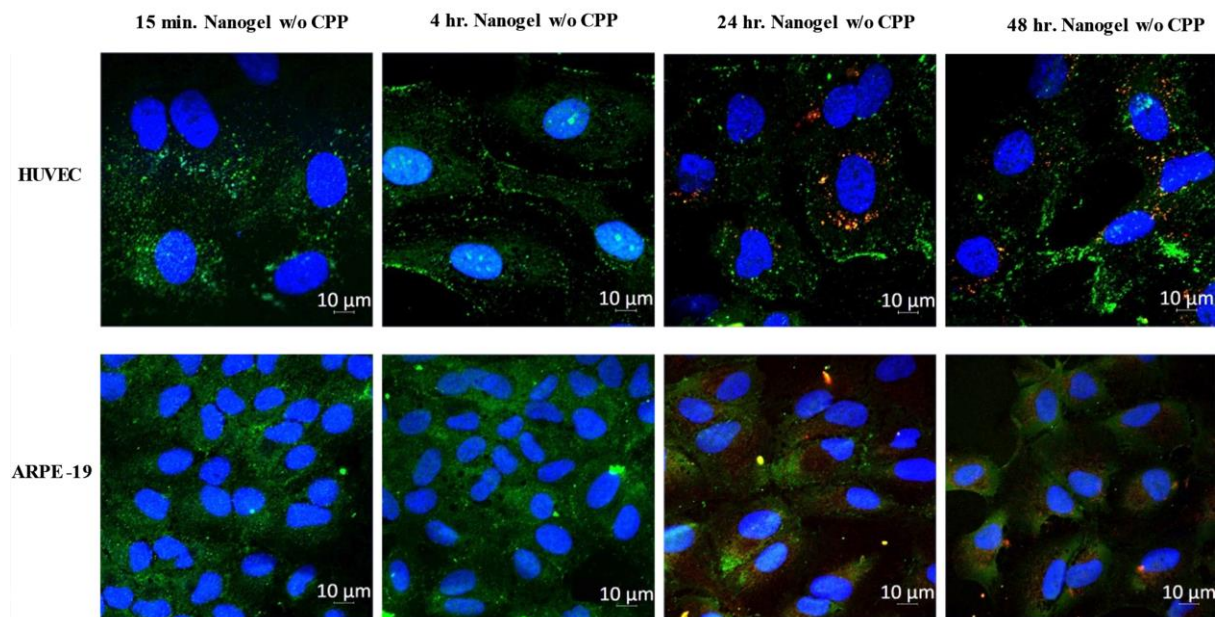


**Figure 39. HUVEC and ARPE-19 cells treated with nanogel with no CPP. Nanogels with no CPP were not able to penetrate into the cells during the first 4 hours. After 24 hours, nanogels penetrated the cells (n=3).**

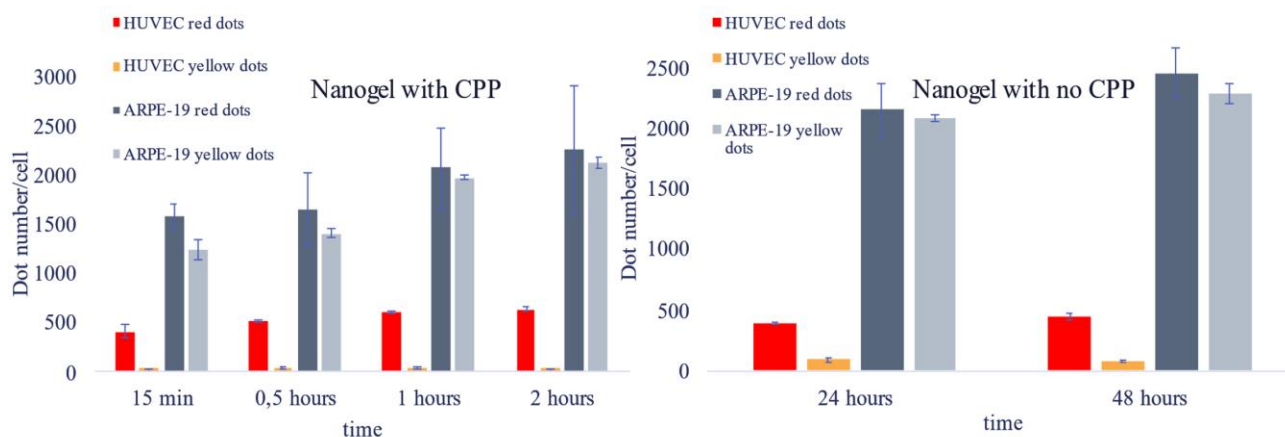


**Figure 40.** The red dots representing the amount of nanogels that penetrated the HUVE cells and ARPE-19 cells were counted to calculate the average amount of nanogel penetration per cell. Nanogels labeled with rhodamine showed a higher penetration to HUVECs than that of penetration to ARPE-19 cells, according to the LSCM microscope images. Yellow dots counted in ARPE-19 cells was marginally less than red dots, indicating that the internalization of nanogel to ARPE-19 cells is with endosome mediated (n=3).

## 6. Discussion

In this study, we generated a nanogel formulation composed of HA as the nano-carrier, HRH as the active therapeutic molecule and penetratin as the tissue penetrating agent. The nanogel formation was triggered with the addition of hydrophobic cholesterol core and stabilized by using different cross-linking strategies. The final nanogel was characterized for stability, HRH entrapment efficiency and drug release before *in vitro* activity evaluations on HUVE cells. Nanogels were evaluated both on HUVE cells and ARPE-19 cells and in their co-culture to observe the passage of nanogel from continues ARPE-19 layer to the HUVE cell layer.

Initially, ARPE-19 and HUVE cells were co-cultured to investigate their proliferation performance within their own cell culture medium or within each other's medium (**Figure 15**). ARPE-19 cells showed an efficient proliferation when co-cultured with HUVE cells in basal medium. The reason of ARPE-19 cells proliferating fast might be the high amount of growth factors present in human vascular cell basal medium. HUVE cells did not proliferate efficiently in DMEM-F12 and the reason of ability difference to proliferate in DMEM-F12 and human vascular cell basal medium for HUVE cells can be that HUVE cells are endothelial cells, which are more sensitive compared to epithelial cells such as ARPE-19.

As the second part of the study, nanogels were formulated. HA was chosen for this study for being a biocompatible, negatively charged glycosaminoglycan that can make electrostatic interaction with positively charged peptides. The chemical structure of HA is the same across all species, thus a rejection possibility of an implant or any potential immunologic reactions is

found to be negligible (Rah, 2011). HA can be considered as a perfect molecule for drug release because of its high loading capacity and enhanced drug release time due to its cohesiveness. The active therapeutic agent of this study, HRH peptide is a novel and positively charged anti-VEGF molecule, which has high affinity to VEGF-Fc proteins (Zhang *et al.*, 2017). Compared to antibodies utilized for AMD treatment, HRH peptide is a smaller agent, leading to a higher potential to penetrate the eye.

Due to high positive charge of HRH peptide, it was expected to electrostatically interact with negatively charged HA and form a stable nanogel. To test this hypothesis PLL, which is cost effective compared to HRH and similarly charged, is used. HA-PLL nanogels were formed with 21-40 kDa HA at 2:1, PLL: HA monomer ratio. Nanogel formation was observed in a preferred size range, 100-200 nm, for tissue targeting. However, stability and generation of interactions was low probably due to weakness of electrostatic interactions. Also, the size of the nanogels was increased after 24 hours even though the size (168 nm) was suitable for internalization to eye (Gupta *et al.*, 2013; Kamaledin, 2017) in the first day of generation. The size of nanostructures would be increased because of the distance between atoms increases with the temperature (Chang *et al.*, 2021). Additionally, swelling of nanogel by water penetration result in increased size.

To increase the stability of the formed nanogels, cholesterol and EDC/NHS chemistry were introduced. Cholesterol is a compound containing a hydrocarbon tail and a sterol nucleus consisting of four hydrocarbon rings. In generation of nanogel, cholesterol was considered as a compound to generate a hydrophobic core in nanogel structure and increase the nanogel formation. EDC/NHS chemistry was used to increase the stability of nanogels by crosslinking HA and PLL. EDC and NHS were added to the sample at the same time. EDC/NHS chemistry activates COOH groups of HA to introduce covalent bonds with NH<sub>2</sub> groups of PLL. HA-Cholesterol-PLL formulation showed more nanogel formation compared to HA-PLL interaction as can be seen in **Figure 18**. Nanogel generated with EDC/NHS crosslinker was more stable and the size remained the same within 24 hours (143 nm size). When the sizes were compared between crosslinked and non-crosslinked formulations, HA-cholesterol-PLL interaction is found to be more compact with 117 nm size compared to 128.35 nm. Here, hydrophobic tails can be closer to each other because of the sole electrostatic interaction between HA and PLL. Nanogel generated with EDC/NHS chemistry was larger in size probably because EDC/NHS may enforce the order structure to be spherical and provide constant bond distances.

As an alternative crosslinking strategy, DVS was also tested. DVS crosslinks the COOH groups present in the N-acetyl glucose amine in HA. DVS crosslinking stabilized the HA within its own structure and thereby increases the entrapment efficiency of loaded cargo. HA, DVS, and PLL was used to generate a nanogel initially at two pH values: pH 11 and pH 6. Since free DVS and the solvent, toluene, used during the synthesis might be toxic to the mammalian cells, DVS was removed from the formulation by freeze drying after generation of nanogel. Nanogels showed low homogeneity at both pH values (**Table 6**). On the other hand, nanogel stability was high at pH 6. The heterogeneity of the nanogel might be due to the unreacted and heterogeneously distributed HRH peptides, which is simply entrapped into the nanogel. Also, the size of the HA molecule might be effective on DVS crosslinking efficiency.

Keeping in mind that both EDC/NHS and DVS crosslinking strategies should be further optimized for the novel nanogel, HA-HRH-CPP nanogel formulations have been generated. In this final formulation, penetratin peptide was also added to enhance the penetration of nanogel into the eye. This CPP is shown to provide corneal tissue penetration and carry antibodies into the posterior segment of eye (de Cogan *et al.*, 2017). CPP was added to the formulation lastly to coat the surface of the nanogel and be present at the outermost layer to be effective in tissue penetration (**Figure 7**).

Firstly, EDC/NHS chemistry was used. The generated nanogel formation was high, however, the size of nanogel was too big with 254 nm to penetrate the eye at pH 6. Despite high homogeneity, nanogel was not stable within 24 hours (**Table 5**). Secondly, nanogels were generated with DVS at different molar ratios (i) 1:1 HA-DVS and (ii) 1:1:1.8 HA:HRH:CPP. The size of nanogel was too big (450 nm) to penetrate the eye at both pH 11 and 6 (**Table 6**). The reasons of big nanogel sizes could be molar ratios of positive and negative charges within the system, peptide concentration, or molecular weight of HA used in the formulation.

To optimize the size of the nanogels, molecular weight of HA was changed and 8-15 kDa and 10 kDa HA were used in nanodrug generation. Both experiments were conducted at pH 11, the optimum working pH value of DVS. The sizes of nanogels generated with 10 kDa (nanogel 1) and 8-15 kDa HA (nanogel 2) were 134.8 and 138.8, respectively, which are suitable sizes for ocular tissue targeting (Gupta *et al.*, 2013). Moreover, the nanodrug sizes did not show a considerable change within 24 hours. Therefore, nanogel formulation was optimized at pH 11, 25°C with 1:1:1.8 HA: HRH: CPP molar ratio.

To prevent possible toluene toxicity to ARPE-19 and HUVE cells, nanogel was freeze dried after generation and dissolved in DPBS before treatment. Previous experiment showed that DVS or toluene shows toxic effect on both ARPE-19 cells and HUVECs. To remove toluene and DVS from the nanogels, they were freeze-dried (Cool-safe, Scanvac) for 24 hours at -96°C under 0.007 mbar vacuum. After freeze-drying, nanogel was dissolved in 1 mL DPBS and stored at +4 °C until use.

Further characterizations of the nanogel 1 and 2 were shown that entrapment efficiency was 65% for nanogel 1 and 53% for nanogel 2. Meanwhile 34,72% of HRH was released from nanogel 1 within 192 hours, and 36% of HRH was released from nanogel 2 within 24 hours. (**Figure 31**). This entrapment and release ratios can be considered as suitable since drug release within 24-48 hours are acceptable for topical drug delivery (Johannsdottir *et al.*, 2018; Wang *et al.*, 2021). However, the drug concentration within the vitreous should be measured to make the conclusion.

As the final part of the study, *in vitro* evaluation of HA, HRH peptide, penetratin peptide and nanogel 1 were performed. The viability of ARPE-19 cells and HUVE cells was investigated by live/dead cell assay and monitored by LSCM (**Figure 32**). Cytotoxicity assay was performed by CCK-8 assay (**Figure 33**). CCK-8 assay was performed on cells instead of MTS or MTT assays because these assays are based on the measurement of mitochondrial activity and HRH peptide induces mitochondrial activity of cells. Therefore, HRH peptide interferes MTS and MTT assays about indication of cell viability by showing fluctuations in absorbance values (Kuang Tzu Huang & University of California, 2004).

HA and penetratin peptide showed no toxic effect on either ARPE-19 and HUVE cells, while nanogel 1 and HRH peptide inhibited the proliferation of HUVE cells and did not show a negative impact on ARPE-19 proliferation (**Figure 32 and 33**). For further investigation of the effects of peptides formulated in the nanogels, CCK-8 assay was performed on ARPE-19 and HUVECs, which are administrated with only HRH (no CPP) and only CPP (no HRH) peptide nanogels. The results revealed that neither form of the nanogels is cytotoxic on ARPE-19 cells. Nanogels that does not contain HRH do not cause significant decrease in HUVEC proliferation, while there is around 50% decrease in the proliferation of HUVECs that are treated with only HRH (no CPP) peptide nanogels. The results indicates that CPP peptide is not toxic for either of the cells and HRH peptide inhibits HUVEC proliferation (**Figure 34**).

To mimic the retinal penetration of nanogel formulation, ARPE-19 cells and HUVE cells were seeded into inserts and wells, respectively. During reaching the confluency, the resistance of cell monolayer was measured by TEER measurement every day. At day 5, when the cell layer was confluent and the TEER measurement was around 189.47  $\Omega$ , nanodrug formulation was added to ARPE-19 cell compartment and incubated for 96 hours. Cell resistance did not decrease throughout the nanodrug treatment, even increased slightly, indicating that ARPE-19 cells' proliferation is not negatively affected by nanogel, and the cell monolayer is intact. Despite no change on ARPE-19 proliferation, HUVE cell proliferation is affected (**Figure 36**). Since the nanogel was added to the ARPE-19 compartment of the trans-well plate, only if it was penetrated across the insert membrane and reach to HUVE cell layer, nanogel can show direct inhibition on HUVE cell proliferation. These in vitro studies indicate the passage of HRH peptide containing nanodrug through ARPE-19 cell layer and effect HUVE cell proliferation.

To identify the cell penetration mechanism of nanogels, the original formulation containing HA, HRH and CPP was followed with endosomal marker within the cell. The nanogel was able to enter both ARPE-19 and HUVE cells within 15 min. and co-localized with the endosome marker Rab-5 in both cell types (**Figure 38**). On the other hand, with HRH nanogels that does not contain any CPP to mediate cell penetration, internalization was observed around 24<sup>th</sup> hour of nanogel administration (**Figure 39**). In ARPE-19 cells, HRH nanogel entrance was co-localized with endosomal marker. However, HUVE cell internalization of HRH nanogel was not endosome mediated and was much lower compared to ARPE-19 cells. Thus, it can be said that HRH is being selectively internalized by HUVE cells. Compared to the number of red and yellow dots, it might be said that the entrance of nanogels to ARPE-19 cells is endosome mediated, while the number of yellow dots counted in HUVE cells is much less than red dots, indicating that nanogel is not internalized by endosome, it is selectively internalized into HUVE cells (**Figure 40**).

## 7 Conclusion and Future Perspective

In this study, a nanodrug formulation and its effects on HUVECs and ARPE-19 cells were investigated. Besides of non-toxic effects of DVS, cholesterol, HA, and penetratin peptide, on HUVECs and ARPE-19 cells, HRH peptide showed an inhibitory effect on the proliferation of HUVECs in the coculture experiments (Zhang *et al.*, 2017). Thus, designed formulation showed an inhibitory effect on the proliferation of HUVECs. Once we tested this formulation's effect on VEGF signaling, it could be validated as a possible candidate for AMD treatment.

However, future studies with *ex vivo* and *in vivo* models will be required to confirm the efficiency of the nanodrugs.

## 8 References

- A. Joliot, C. P., H. Deagostini-Bazit, and A. Prochiantz. (1991). Antennapedia homeobox peptide regulates neural morphogenesis. *Neurobiology*, 88.
- Al-Kinani, A. A., Zidan, G., Elsaïd, N., Seyfoddin, A., Alani, A. W. G., & Alany, R. G. (2018). Ophthalmic gels: Past, present and future. *Adv Drug Deliv Rev*, 126, 113-126. doi: 10.1016/j.addr.2017.12.017
- Arshinoff, S. A., & Jafari, M. (2005). New classification of ophthalmic viscosurgical devices--2005. *J Cataract Refract Surg*, 31(11), 2167-2171. doi: 10.1016/j.jcrs.2005.08.056
- Becker, L. C., Bergfeld, W. F., Belsito, D. V., Klaassen, C. D., Marks, J. G., Jr., Shank, R. C., . . . Andersen, F. A. (2009). Final report of the safety assessment of hyaluronic acid, potassium hyaluronate, and sodium hyaluronate. *Int J Toxicol*, 28(4 Suppl), 5-67. doi:10.1177/1091581809337738
- Berrin Erdag, K. B. B., Asli Kumbasar, Omur Celikbicak, Gabrielle Zeder-Lutz, Danièle Altschuh, Bekir Salih and Kemal Baysal. (2007). Novel Short Peptides Isolated from Phage Display Library Inhibit VEGF Activity. *Molecular Biotechnology*, 35.
- Bielory, L., & Wagle, P. (2017). Ocular surface lubricants. *Curr Opin Allergy Clin Immunol*, 17(5), 382-389. doi:10.1097/ACI.0000000000000392
- Brannigan, R. P., & Khutoryanskiy, V. V. (2017). Synthesis and evaluation of mucoadhesive acryloyl-quaternized PDMAEMA nanogels for ocular drug delivery. *Colloids Surf B Biointerfaces*, 155, 538-543. doi: 10.1016/j.colsurfb.2017.04.050
- Brechner, R. J., Rosenfeld, P. J., Babish, J. D., & Caplan, S. (2011). Pharmacotherapy for neovascular age-related macular degeneration: an analysis of the 100% 2008 medicare fee-for-service part B claims file. *Am J Ophthalmol*, 151(5), 887-895 e881. doi: 10.1016/j.ajo.2010.11.017
- Bremnes, R. M., Camps, C., & Sirera, R. (2006). Angiogenesis in non-small cell lung cancer: the prognostic impact of neoangiogenesis and the cytokines VEGF and bFGF in tumours and blood. *Lung Cancer*, 51(2), 143-158. doi: 10.1016/j.lungcan.2005.09.005
- Brynskov, T., Munch, I. C., Larsen, T. M., Erngaard, L., & Sorensen, T. L. (2020). Real-world 10-year experiences with intravitreal treatment with ranibizumab and aflibercept for neovascular age-related macular degeneration. *Acta Ophthalmol*, 98(2), 132-138. doi:10.1111/aos.14183
- Buwalda, S. J., Vermonden, T., & Hennink, W. E. (2017). Hydrogels for Therapeutic Delivery: Current Developments and Future Directions. *Biomacromolecules*, 18(2), 316-330. doi: 10.1021/acs.biomac.6b01604
- By Hugo Quiroz-Mercado, M. (2013). Integrin Peptide Therapy in Choroidal and Retinal Neovascularization. *Retina Today*.
- Byeon, S. H., Lee, S. C., Choi, S. H., Lee, H. K., Lee, J. H., Chu, Y. K., & Kwon, O. W. (2010). Vascular endothelial growth factor as an autocrine survival factor for retinal pigment epithelial cells under oxidative stress via the VEGF-R2/PI3K/Akt. *Invest Ophthalmol Vis Sci*, 51(2), 1190-1197. doi:10.1167/iovs.09-4144
- Campochiaro, P. A., & Akhlaq, A. (2020). Sustained suppression of VEGF for treatment of retinal/choroidal vascular diseases. *Prog Retin Eye Res*, 100921. doi: 10.1016/j.preteyeres.2020.100921

- Carlson, E., Kao, W. W. Y., & Ogundele, A. (2018). Impact of Hyaluronic Acid-Containing Artificial Tear Products on Reepithelialization in an In Vivo Corneal Wound Model. *J Ocul Pharmacol Ther*, *34*(4), 360-364. doi:10.1089/jop.2017.0080
- Chan, K. C., Yu, Y., Ng, S. H., Mak, H. K., Yip, Y. W. Y., van der Merwe, Y., Leung, C. K. S. (2019). Intracameral injection of a chemically cross-linked hydrogel to study chronic neurodegeneration in glaucoma. *Acta Biomater*, *94*, 219-231. doi: 10.1016/j.actbio.2019.06.005
- Chang, J. H., Garg, N. K., Lunde, E., Han, K. Y., Jain, S., & Azar, D. T. (2012). Corneal neovascularization: an anti-VEGF therapy review. *Surv Ophthalmol*, *57*(5), 415-429. doi: 10.1016/j.survophthal.2012.01.007
- Chatterjee, S., Hui, P. C., Siu, W. S., Kan, C. W., Leung, P. C., Wanxue, C., & Chiou, J. C. (2021). Influence of pH-responsive compounds synthesized from chitosan and hyaluronic acid on dual-responsive (pH/temperature) hydrogel drug delivery systems of Cortex Moutan. *Int J Biol Macromol*, *168*, 163-174. doi: 10.1016/j.ijbiomac.2020.12.035
- Cheung, N., Wong, I. Y., & Wong, T. Y. (2014). Ocular anti-VEGF therapy for diabetic retinopathy: overview of clinical efficacy and evolving applications. *Diabetes Care*, *37*(4), 900-905. doi:10.2337/dc13-1990
- Comparison of Age-related Macular Degeneration Treatments Trials Research, G., Martin, D. F., Maguire, M. G., Fine, S. L., Ying, G. S., Jaffe, G. J., Ferris, F. L., 3rd. (2012). Ranibizumab and bevacizumab for treatment of neovascular age-related macular degeneration: two-year results. *Ophthalmology*, *119*(7), 1388-1398. doi: 10.1016/j.ophtha.2012.03.053
- Cunningham, E. T., Jr., Adamis, A. P., Altaweel, M., Aiello, L. P., Bressler, N. M., D'Amico, D. J., Macugen Diabetic Retinopathy Study, G. (2005). A phase II randomized double-masked trial of pegaptanib, an anti-vascular endothelial growth factor aptamer, for diabetic macular edema. *Ophthalmology*, *112*(10), 1747-1757. doi: 10.1016/j.ophtha.2005.06.007
- de Cogan, F., Hill, L. J., Lynch, A., Morgan-Warren, P. J., Lechner, J., Berwick, M. R., Logan, A. (2017). Topical Delivery of Anti-VEGF Drugs to the Ocular Posterior Segment Using Cell-Penetrating Peptides. *Invest Ophthalmol Vis Sci*, *58*(5), 2578-2590. doi:10.1167/iovs.16-20072
- de Jong, E. K., Geerlings, M. J., & den Hollander, A. I. (2020). Age-related macular degeneration. In *Genetics and Genomics of Eye Disease* (pp. 155-180).
- Deng, Y., Qiao, L., Du, M., Qu, C., Wan, L., Li, J., & Huang, L. (2021). Age-related macular degeneration: Epidemiology, genetics, pathophysiology, diagnosis, and targeted therapy. *Genes & Diseases*. doi: 10.1016/j.gendis.2021.02.009
- Derakhshankhah, H., & Jafari, S. (2018). Cell penetrating peptides: A concise review with emphasis on biomedical applications. *Biomed Pharmacother*, *108*, 1090-1096. doi: 10.1016/j.biopha.2018.09.097
- Deshayes, S., Morris, M. C., Divita, G., & Heitz, F. (2006). Interactions of amphipathic carrier peptides with membrane components in relation with their ability to deliver therapeutics. *J Pept Sci*, *12*(12), 758-765. doi:10.1002/psc.810
- Donald L. Elbert, A. B. P., Matthias P. Lutolf, Sven Halstenberg, Jeffrey A. Hubbell. (2001). Protein delivery from materials formed by self-selective conjugate addition reactions. *Journal of Controlled Release*, *76*.
- Dong-Goo Bae, T.-D. K., Ge Li, Wan-HeeYoon, and Chi-Bom Chae. (2005). Anti-Flt1Peptide, a Vascular Endothelial Growth Factor Receptor 1- Specific Hexapeptide, Inhibits Tumor Growth and Metastasis. *Clin Cancer Res*, *11*.
- Dovedy, M., Liu, Z. J., & Bartlett, S. (2020). Hyaluronic acid and its biomedical applications: A review. *Engineered Regeneration*, *1*, 102-113. doi: 10.1016/j.engreg.2020.10.001
- Duchardt, F., Ruttekolk, I. R., Verdurmen, W. P. R., Lortat-Jacob, H., Burck, J., Hufnagel, H., . . . Brock, R. (2009). A cell-penetrating peptide derived from human lactoferrin with conformation-dependent uptake efficiency. *J Biol Chem*, *284*(52), 36099-36108. doi:10.1074/jbc.M109.036426

- Dugel, P. U., Jaffe, G. J., Sallstig, P., Warburton, J., Weichselberger, A., Wieland, M., & Singerman, L. (2017). Brolucizumab Versus Aflibercept in Participants with Neovascular Age-Related Macular Degeneration: A Randomized Trial. *Ophthalmology*, *124*(9), 1296-1304. doi: 10.1016/j.ophtha.2017.03.057
- Edman, L. R. a. P. (1992). Effect of polymers and microspheres on the nasal absorption of insulin in rats. *International Journal of Pharmaceutics*, *83*.
- Fang, G., Yang, X., Wang, Q., Zhang, A., & Tang, B. (2021). Hydrogels-based ophthalmic drug delivery systems for treatment of ocular diseases. *Materials Science and Engineering: C*, *127*. doi: 10.1016/j.msec.2021.112212
- Ferrara, N., & Adamis, A. P. (2016). Ten years of anti-vascular endothelial growth factor therapy. *Nat Rev Drug Discov*, *15*(6), 385-403. doi:10.1038/nrd.2015.17
- Ferrington, D. A., Fisher, C. R., & Kowluru, R. A. (2020). Mitochondrial Defects Drive Degenerative Retinal Diseases. *Trends Mol Med*, *26*(1), 105-118. doi: 10.1016/j.molmed.2019.10.008
- Frenkel, R. E. P., Mani, L., Toler, A. R., & Frenkel, M. P. C. (2007). Intraocular Pressure Effects of Pegaptanib (Macugen) Injections in Patients With and Without Glaucoma. *American Journal of Ophthalmology*, *143*(6), 1034-1035. doi: 10.1016/j.ajo.2007.01.052
- Gan, L., Gan, Y., Zhu, C., Zhang, X., & Zhu, J. (2009). Novel microemulsion in situ electrolyte-triggered gelling system for ophthalmic delivery of lipophilic cyclosporine A: in vitro and in vivo results. *Int J Pharm*, *365*(1-2), 143-149. doi: 10.1016/j.ijpharm.2008.08.004
- Gastone G., C. a. P. J., DeMacro Jr. (1994). Anatomy and Physiology of the visual system. *Journal of Clinical Neurophysiology*, *11*.
- Gaudreault, J., Fei, D., Rusit, J., Suboc, P., & Shiu, V. (2005). Preclinical pharmacokinetics of Ranibizumab (rhuFabV2) after a single intravitreal administration. *Invest Ophthalmol Vis Sci*, *46*(2), 726-733. doi:10.1167/iovs.04-0601
- George, M., Khong, K., & Maltseva, I. (2019). Hyaluronic Acid (HA) Release of HA-Containing Lens Care Solutions with Silicone Hydrogel Lenses. *Contact Lens and Anterior Eye*, *42*(6), e17-e18. doi: 10.1016/j.clae.2019.10.059
- George Silva, L. P., Roman Galetto, Julianne Smith, Guillermo Montoya, Philippe Duchateau and Frédéric Pâques. (2011). Meganucleases and Other Tools for Targeted Genome Engineering Prospectives and Challenges for Gene Therapy. *current gene therapy*, *11*.
- George, S. M., Lu, F., Rao, M., Leach, L. L., & Gross, J. M. (2021). The retinal pigment epithelium: Development, injury responses, and regenerative potential in mammalian and non-mammalian systems. *Prog Retin Eye Res*, 100969. doi: 10.1016/j.preteyeres.2021.100969
- Gote, V., Sikder, S., Sicotte, J., & Pal, D. (2019). Ocular Drug Delivery: Present Innovations and Future Challenges. *J Pharmacol Exp Ther*, *370*(3), 602-624. doi:10.1124/jpet.119.256933
- Grimaudo, M. A., Amato, G., Carbone, C., Diaz-Rodriguez, P., Musumeci, T., Concheiro, A., . . . Puglisi, G. (2020). Micelle-nanogel platform for ferulic acid ocular delivery. *Int J Pharm*, *576*, 118986. doi: 10.1016/j.ijpharm.2019.118986
- Group, A.-R. E. D. S. R. (2005). Risk Factors for the Incidence of Advanced Age-Related Macular Degeneration in the Age-Related Eye Disease Study (AREDS)AREDS report no. 19. *Ophthalmology*, *112*(4), 533-539.e531. doi:10.1016/j.ophtha.2004.10.047
- Grunewald, F. S., Prota, A. E., Giese, A., & Ballmer-Hofer, K. (2010). Structure-function analysis of VEGF receptor activation and the role of coreceptors in angiogenic signaling. *Biochim Biophys Acta*, *1804*(3), 567-580. doi:10.1016/j.bbapap.2009.09.002
- Guter, M., & Breunig, M. (2017). Hyaluronan as a promising excipient for ocular drug delivery. *Eur J Pharm Biopharm*, *113*, 34-49. doi: 10.1016/j.ejpb.2016.11.035
- Ho, A. C., Busbee, B. G., Regillo, C. D., Wieland, M. R., Van Everen, S. A., Li, Z., . . . Group, H. S. (2014). Twenty-four-month efficacy and safety of 0.5 mg or 2.0 mg ranibizumab in patients with subfoveal neovascular age-related macular degeneration. *Ophthalmology*, *121*(11), 2181-2192. doi: 10.1016/j.ophtha.2014.05.009

- Hsu, Y. Y., Liu, K. L., Yeh, H. H., Lin, H. R., Wu, H. L., & Tsai, J. C. (2019). Sustained release of recombinant thrombomodulin from cross-linked gelatin/hyaluronic acid hydrogels potentiate wound healing in diabetic mice. *Eur J Pharm Biopharm*, *135*, 61-71. doi: 10.1016/j.ejpb.2018.12.007
- Huang, G., & Huang, H. (2018). Hyaluronic acid-based biopharmaceutical delivery and tumor-targeted drug delivery system. *J Control Release*, *278*, 122-126. doi: 10.1016/j.jconrel.2018.04.015
- Huerta Angeles, G., & Nesporova, K. (2021). Hyaluronan and its derivatives for ophthalmology: Recent advances and future perspectives. *Carbohydr Polym*, *259*, 117697. doi: 10.1016/j.carbpol.2021.117697
- Jae Kyung Choi, M. Y. L. L., MD, MPH; Jun Woong Moon, MD; Hyun Jin Shin, MD; Belong Cho, MD, PhD. (2010). Diabetes Mellitus and Early Age-related Macular Degeneration. *Epidemiology*, *129*.
- Jain, A., Shah, S. G., & Chugh, A. (2015). Cell penetrating peptides as efficient nanocarriers for delivery of antifungal compound, natamycin for the treatment of fungal keratitis. *Pharm Res*, *32*(6), 1920-1930. doi:10.1007/s11095-014-1586-x
- Jiang, D., Liang, J., & Noble, P. W. (2011). Hyaluronan as an immune regulator in human diseases. *Physiol Rev*, *91*(1), 221-264. doi:10.1152/physrev.00052.2009
- Jin, Y.-J., Ubonvan, T., & Kim, D.-D. (2010). Hyaluronic Acid in Drug Delivery Systems. *Journal of Pharmaceutical Investigation*, *40*(suppl), 33-43. doi:10.4333/kps.2010.40.S.033
- Johanna M. Seddon, M., ScM; Sarah George, MPH; Bernard Rosner, (2006). Cigarette Smoking, Fish Consumption, Omega-3 fatty acid intake, and associations with age-related macular degeneration. *Epidemiology*.
- John E. Park, G.-A. K., and Napoleone Ferrara. (1993). The Vascular Endothelial Growth Factor (VEGF) Isoforms: Differential Deposition into the Subepithelial Extracellular Matrix and Bioactivity of Extracellular Matrix-bound VEGF. *Molecular Biology of the Cell*, *4*.
- Jumelle, C., Gholizadeh, S., Annabi, N., & Dana, R. (2020). Advances and limitations of drug delivery systems formulated as eye drops. *J Control Release*, *321*, 1-22. doi: 10.1016/j.jconrel.2020.01.057
- Jussara S. Michaloski, A. R. R., Leila S. Magalhães, Caio C. Cambui, Ricardo J. Giordano\*. (2016). Discovery of pan-VEGF inhibitory peptides directed to the extracellular ligand-binding domains of the VEGF receptors. *Science Advances*, *2*.
- Kanazawa, T., Morisaki, K., Suzuki, S., & Takashima, Y. (2014). Prolongation of life in rats with malignant glioma by intranasal siRNA/drug codelivery to the brain with cell-penetrating peptide-modified micelles. *Mol Pharm*, *11*(5), 1471-1478. doi:10.1021/mp400644e
- Kärt Padari†, K. K., Annely Lorents†, Mattias Hällbrink§, Miguel Manoll, Maria C. Pedroso de Limall, and Margus Pooga. (2010). S413-PV Cell-Penetrating Peptide Forms Nanoparticle-Like Structures to Gain Entry into Cells. *Bioconjugate Chemistry*, *21*.
- Kazuo Akima, H. I. Y. I., ' Kayoko Matsuo, ' Nobutoshi Watari, ' Mitsuo Yanagi: Hiroo Hagif Kazumi Osmihaf Akikuni Yagita? Yutaka Atomif and Isao Tatekawa' (1996). Evaluation of Antitumor Activities of Hyaluronate binding antitumor drugs synthesis, characterization and antitumor activity. *Journal of Drug Targeting*, *4*.
- Khanani, A. M., Patel, S. S., Ferrone, P. J., Osborne, A., Sahni, J., Grzeschik, S., . . . Dugel, P. U. (2020). Efficacy of Every Four Monthly and Quarterly Dosing of Faricimab vs Ranibizumab in Neovascular Age-Related Macular Degeneration: The STAIRWAY Phase 2 Randomized Clinical Trial. *JAMA Ophthalmol*, *138*(9), 964-972. doi:10.1001/jamaophthalmol.2020.2699
- Kim, A., Checkla, D. M., Dehazya, P., & Chen, W. (2003). Characterization of DNA-hyaluronan matrix for sustained gene transfer. *Journal of Controlled Release*, *90*(1), 81-95. doi:10.1016/s0168-3659(03)00175-5
- Kim, S. H., Lutz, R. J., Wang, N. S., & Robinson, M. R. (2007). Transport barriers in transscleral drug delivery for retinal diseases. *Ophthalmic Res*, *39*(5), 244-254. doi:10.1159/000108117

- Kinnunen, K., Petrovski, G., Moe, M. C., Berta, A., & Kaarniranta, K. (2012). Molecular mechanisms of retinal pigment epithelium damage and development of age-related macular degeneration. *Acta Ophthalmol*, *90*(4), 299-309. doi:10.1111/j.1755-3768.2011.02179.x
- Klein, C., Schaefer, W., Regula, J. T., Dumontet, C., Brinkmann, U., Bacac, M., & Umana, P. (2019). Engineering therapeutic bispecific antibodies using CrossMab technology. *Methods*, *154*, 21-31. doi: 10.1016/j.ymeth.2018.11.008
- Klettner, A., Kauppinen, A., Blasiak, J., Roider, J., Salminen, A., & Kaarniranta, K. (2013). Cellular and molecular mechanisms of age-related macular degeneration: from impaired autophagy to neovascularization. *Int J Biochem Cell Biol*, *45*(7), 1457-1467. doi: 10.1016/j.biocel.2013.04.013
- Klettner\*, A., & Roider, a. J. (2009). Treating Age-Related Macular Degeneration – Interaction of VEGF Antagonists with their Target. *Mini-Reviews in Medicinal Chemistry*, *9*.
- Kompella, U. B., Amrite, A. C., Pacha Ravi, R., & Durazo, S. A. (2013). Nanomedicines for back of the eye drug delivery, gene delivery, and imaging. *Prog Retin Eye Res*, *36*, 172-198. doi: 10.1016/j.preteyeres.2013.04.001
- Kompella, U. B., Hartman, R. R., & Patil, M. A. (2021). Extraocular, periorcular, and intraocular routes for sustained drug delivery for glaucoma. *Prog Retin Eye Res*, *82*, 100901. doi:10.1016/j.preteyeres.2020.100901
- Krebs, I., Lie, S., Stolba, U., Zeiler, F., Felke, S., & Binder, S. (2009). Efficacy of intravitreal bevacizumab (Avastin) therapy for early and advanced neovascular age-related macular degeneration. *Acta Ophthalmol*, *87*(6), 611-617. doi:10.1111/j.1755-3768.2008.01312.x
- Kumar, A., Sahoo, B., Montpetit, A., Behera, S., Lockey, R. F., & Mohapatra, S. S. (2007). Development of hyaluronic acid-Fe<sub>2</sub>O<sub>3</sub> hybrid magnetic nanoparticles for targeted delivery of peptides. *Nanomedicine*, *3*(2), 132-137. doi: 10.1016/j.nano.2007.03.001
- L. Illurn", N.F. Farraja, A.N. FisheP, I. Gill", M. Migliettab and L.M. Benedettib (1994). Hyaluronic acid ester microspheres as a nasal delivery system for insulin. *Journal of Controlled Release*, *29*.
- Lee, M. T., Hung, W. C., Chen, F. Y., & Huang, H. W. (2005). Many-body effect of antimicrobial peptides: on the correlation between lipid's spontaneous curvature and pore formation. *Biophys J*, *89*(6), 4006-4016. doi:10.1529/biophysj.105.068080
- Lesley, J., Hascall, V. C., Tammi, M., & Hyman, R. (2000). Hyaluronan Binding by Cell Surface CD44. *Journal of Biological Chemistry*, *275*(35), 26967-26975. doi:10.1016/s0021-9258(19)61467-5
- Li, C., Chen, R., Xu, M., Qiao, J., Yan, L., & Guo, X. D. (2018). Hyaluronic acid modified MPEG-b-PAE block copolymer aqueous micelles for efficient ophthalmic drug delivery of hydrophobic genistein. *Drug Deliv*, *25*(1), 1258-1265. doi:10.1080/10717544.2018.1474972
- Li, H., Xue, Y., Jia, B., Bai, Y., Zuo, Y., Wang, S., . . . Tang, H. (2018). The preparation of hyaluronic acid grafted pullulan polymers and their use in the formation of novel biocompatible wound healing film. *Carbohydr Polym*, *188*, 92-100. doi: 10.1016/j.carbpol.2018.01.102
- Li, Y., Maciel, D., Rodrigues, J., Shi, X., & Tomas, H. (2015). Biodegradable Polymer Nanogels for Drug/Nucleic Acid Delivery. *Chem Rev*, *115*(16), 8564-8608. doi:10.1021/cr500131f
- Liew, G., Joachim, N., Mitchell, P., Burlutsky, G., & Wang, J. J. (2016). Validating the AREDS Simplified Severity Scale of Age-Related Macular Degeneration with 5- and 10-Year Incident Data in a Population-Based Sample. *Ophthalmology*, *123*(9), 1874-1878. doi: 10.1016/j.optha.2016.05.043
- Lim, L. S., Cheung, C. M. G., Mitchell, P., & Wong, T. Y. (2011). Emerging evidence concerning systemic safety of anti-VEGF agents--should ophthalmologists be concerned? *Am J Ophthalmol*, *152*(3), 329-331. doi: 10.1016/j.ajo.2011.05.040
- Lim, L. S., Mitchell, P., Seddon, J. M., Holz, F. G., & Wong, T. Y. (2012). Age-related macular degeneration. *The Lancet*, *379*(9827), 1728-1738. doi:10.1016/s0140-6736(12)60282-7
- Liu, L., Gao, Q., Lu, X., & Zhou, H. (2016). In situ forming hydrogels based on chitosan for drug delivery and tissue regeneration. *Asian Journal of Pharmaceutical Sciences*, *11*(6), 673-683. doi: 10.1016/j.ajps.2016.07.001

- Liu, L., Yang, J., Xie, J., Luo, Z., Jiang, J., Yang, Y. Y., & Liu, S. (2013). The potent antimicrobial properties of cell penetrating peptide-conjugated silver nanoparticles with excellent selectivity for gram-positive bacteria over erythrocytes. *Nanoscale*, *5*(9), 3834-3840. doi:10.1039/c3nr34254a
- Lu, X., & Sun, X. (2015). Profile of conbercept in the treatment of neovascular age-related macular degeneration. *Drug Des Devel Ther*, *9*, 2311-2320. doi:10.2147/DDDT.S67536
- M.S.Pepper, N. F., L.Orci and R.Montesano (1992). Potent synergism between VEGF and basic fibroblast growth factor in the induction of angiogenesis in vitro. *BIOCHEMICAL AND BIOPHYSICAL RESEARCH COMMUNICATIONS*, *189*.
- Makwana, S. B., Patel, V. A., & Parmar, S. J. (2016). Development and characterization of in-situ gel for ophthalmic formulation containing ciprofloxacin hydrochloride. *Results Pharma Sci*, *6*, 1-6. doi: 10.1016/j.rinphs.2015.06.001
- Mandal, A., Pal, D., Agrahari, V., Trinh, H. M., Joseph, M., & Mitra, A. K. (2018). Ocular delivery of proteins and peptides: Challenges and novel formulation approaches. *Adv Drug Deliv Rev*, *126*, 67-95. doi: 10.1016/j.addr.2018.01.008
- Markham, A. (2019). Brolucizumab: First Approval. *Drugs*, *79*(18), 1997-2000. doi:10.1007/s40265-019-01231-9
- Matsui, T., Nishino, Y., Maeda, S., & Yamagishi, S. (2012). PEDF-derived peptide inhibits corneal angiogenesis by suppressing VEGF expression. *Microvasc Res*, *84*(1), 105-108. doi: 10.1016/j.mvr.2012.02.006
- Mencucci, R., Boccacini, C., Caputo, R., & Favuzza, E. (2015). Effect of a hyaluronic acid and carboxymethylcellulose ophthalmic solution on ocular comfort and tear-film instability after cataract surgery. *J Cataract Refract Surg*, *41*(8), 1699-1704. doi: 10.1016/j.jcrs.2014.12.056
- Misra, S., Heldin, P., Hascall, V. C., Karamanos, N. K., Skandalis, S. S., Markwald, R. R., & Ghatak, S. (2011). Hyaluronan-CD44 interactions as potential targets for cancer therapy. *FEBS J*, *278*(9), 1429-1443. doi:10.1111/j.1742-4658.2011.08071.x
- Moisseiev, E., & Loewenstein, A. (2020). Abicipar pegol-a novel anti-VEGF therapy with a long duration of action. *Eye (Lond)*, *34*(4), 605-606. doi:10.1038/s41433-019-0584-y
- Mueller, N. H., Ammar, D. A., & Petrash, J. M. (2013). Cell penetration peptides for enhanced entry of alphaB-crystallin into lens cells. *Invest Ophthalmol Vis Sci*, *54*(1), 2-8. doi:10.1167/iovs.12-10947
- Nayak, K., & Misra, M. (2018). A review on recent drug delivery systems for posterior segment of eye. *Biomed Pharmacother*, *107*, 1564-1582. doi: 10.1016/j.biopha.2018.08.138
- Ng, Y. S., Krilleke, D., & Shima, D. T. (2006). VEGF function in vascular pathogenesis. *Exp Cell Res*, *312*(5), 527-537. doi: 10.1016/j.yexcr.2005.11.008
- Oh, E. J., Choi, J. S., Kim, H., Joo, C. K., & Hahn, S. K. (2011). Anti-Flt1 peptide - hyaluronate conjugate for the treatment of retinal neovascularization and diabetic retinopathy. *Biomaterials*, *32*(11), 3115-3123. doi: 10.1016/j.biomaterials.2011.01.003
- Oh, E. J., Park, K., Choi, J. S., Joo, C. K., & Hahn, S. K. (2009). Synthesis, characterization, and preliminary assessment of anti-Flt1 peptide-hyaluronate conjugate for the treatment of corneal neovascularization. *Biomaterials*, *30*(30), 6026-6034. doi:10.1016/j.biomaterials.2009.07.024
- Oh, E. J., Park, K., Kim, K. S., Kim, J., Yang, J. A., Kong, J. H., . . . Hahn, S. K. (2010). Target specific and long-acting delivery of protein, peptide, and nucleotide therapeutics using hyaluronic acid derivatives. *J Control Release*, *141*(1), 2-12. doi: 10.1016/j.jconrel.2009.09.010
- Pabo\*t, A. F. a. C. (1988). Cellular Uptake of the Tat Protein from Human Immunodeficiency Virus. *Cell*, *55*.
- Park, J. S., Yi, S. W., Kim, H. J., & Park, K. H. (2016). Receptor-mediated gene delivery into human mesenchymal stem cells using hyaluronic acid-shielded polyethylenimine/pDNA nanogels. *Carbohydr Polym*, *136*, 791-802. doi: 10.1016/j.carbpol.2015.09.053

- Park, K. (2016). Ocular microparticle formulations for 6-month delivery of anti-VEGF. *J Control Release*, 244(Pt A), 136. doi: 10.1016/j.jconrel.2016.12.001
- Patel, A., Cholkar, K., Agrahari, V., & Mitra, A. K. (2013). Ocular drug delivery systems: An overview. *World J Pharmacol*, 2(2), 47-64. doi:10.5497/wjp.v2.i2.47
- Peng, L. H., Niu, J., Zhang, C. Z., Yu, W., Wu, J. H., Shan, Y. H., . . . Gao, J. Q. (2014). TAT conjugated cationic noble metal nanoparticles for gene delivery to epidermal stem cells. *Biomaterials*, 35(21), 5605-5618. doi: 10.1016/j.biomaterials.2014.03.062
- Perillo, E., Allard-Vannier, E., Falanga, A., Stiuso, P., Vitiello, M. T., Galdiero, M., . . . Chourpa, I. (2015). Quantitative and qualitative effect of gH625 on the nanoliposome-mediated delivery of mitoxantrone anticancer drug to HeLa cells. *Int J Pharm*, 488(1-2), 59-66. doi: 10.1016/j.ijpharm.2015.04.039
- Pescina, S., Govoni, P., Potenza, A., Padula, C., Santi, P., & Nicoli, S. (2015). Development of a convenient ex vivo model for the study of the transcorneal permeation of drugs: histological and permeability evaluation. *J Pharm Sci*, 104(1), 63-71. doi:10.1002/jps.24231
- Pescina, S., Ostacolo, C., Gomez-Monterrey, I. M., Sala, M., Bertamino, A., Sonvico, F., . . . Nicoli, S. (2018). Cell penetrating peptides in ocular drug delivery: State of the art. *J Control Release*, 284, 84-102. doi: 10.1016/j.jconrel.2018.06.023
- Pescina, S., Santi, P., Ferrari, G., Padula, C., Cavallini, P., Govoni, P., & Nicoli, S. (2012). Ex vivo models to evaluate the role of ocular melanin in trans-scleral drug delivery. *Eur J Pharm Sci*, 46(5), 475-483. doi: 10.1016/j.ejps.2012.03.013
- Ponta, H., Sherman, L., & Herrlich, P. A. (2003). CD44: from adhesion molecules to signalling regulators. *Nat Rev Mol Cell Biol*, 4(1), 33-45. doi:10.1038/nrm1004
- Price, R. D., Berry, M. G., & Navsaria, H. A. (2007). Hyaluronic acid: the scientific and clinical evidence. *J Plast Reconstr Aesthet Surg*, 60(10), 1110-1119. doi: 10.1016/j.bjps.2007.03.005
- Pritchard, K., Lansley, A. B., Martin, G. P., Heliwell, M., & Marriott, C., Benedetti, L. M. (1996). Evaluation of the bioadhesive properties of hyaluronan derivatives: Detachment weight and mucociliary transport rate studies. *International Journal of Pharmaceutics*, 129.
- Qin, Y., Tian, Y., Liu, Y., Li, D., Zhang, H., Yang, Y., . . . Gan, L. (2018). Hyaluronic acid-modified cationic niosomes for ocular gene delivery: improving transfection efficiency in retinal pigment epithelium. *J Pharm Pharmacol*, 70(9), 1139-1151. doi:10.1111/jphp.12940
- Rama D. Jager, M. D., William F. Mieler, M.D., and Joan W. Miller, M.D. (2008). Medical Progress Age-Related Macular Degeneration. *The New England Journal of Medicine*.
- Reissmann, S. (2014). Cell penetration: scope and limitations by the application of cell-penetrating peptides. *J Pept Sci*, 20(10), 760-784. doi:10.1002/psc.2672
- Roskoski, R., Jr. (2007). Vascular endothelial growth factor (VEGF) signaling in tumor progression. *Crit Rev Oncol Hematol*, 62(3), 179-213. doi: 10.1016/j.critrevonc.2007.01.006
- Roziing, M. P., Durhuus, J. A., Krogh Nielsen, M., Subhi, Y., Kirkwood, T. B., Westendorp, R. G., & Sorensen, T. L. (2020). Age-related macular degeneration: A two-level model hypothesis. *Prog Retin Eye Res*, 76, 100825. doi: 10.1016/j.preteyeres.2019.100825
- Rudolph L Juliano, R. A., Vidula Dixit and Hyun Min Kang. (2009). Cell-targeting and cell-penetrating peptides for delivery of therapeutic and imaging agents. *John Wiley & Sons, Inc*, 1. doi:10.1002/wnan.004
- Ruseska, I., & Zimmer, A. (2020). Internalization mechanisms of cell-penetrating peptides. *Beilstein J Nanotechnol*, 11, 101-123. doi:10.3762/bjnano.11.10
- Sabine A. Eming, 2,3\* Paul Martin,4,5\* Marjana Tomic-Canic6\*. (2014). Wound repair and regeneration Mechanisms, signaling, and translation. *Science Translational Medicine*, 6.
- Sahni, J., Dugel, P. U., Patel, S. S., Chittum, M. E., Berger, B., Del Valle Rubido, M., . . . Fauser, S. (2020). Safety and Efficacy of Different Doses and Regimens of Faricimab vs Ranibizumab in Neovascular Age-Related Macular Degeneration: The AVENUE Phase 2 Randomized Clinical Trial. *JAMA Ophthalmol*, 138(9), 955-963. doi:10.1001/jamaophthalmol.2020.2685

- Sharma, A., Kumar, N., Kuppermann, B. D., & Bandello, F. (2020). Abicipar pegol: the non-monoclonal antibody anti-VEGF. *Eye (Lond)*, *34*(5), 797-801. doi:10.1038/s41433-019-0607-8
- Shiroh Futaki, I. N., Tomoki Suzuki, Zhang Youjun, and Yukio Sugiura. (2002). Translocation of Branched-Chain Arginine Peptides through Cell Membranes flexibility in the spatial disposition of positive charges in membrane-permeable peptides. *Biochemistry*, *41*.
- Sivaram, A. J., Rajitha, P., Maya, S., Jayakumar, R., & Sabitha, M. (2015). Nanogels for delivery, imaging and therapy. *Wiley Interdiscip Rev Nanomed Nanobiotechnol*, *7*(4), 509-533. doi:10.1002/wnan.1328
- Soni, K. S., Desale, S. S., & Bronich, T. K. (2016). Nanogels: An overview of properties, biomedical applications and obstacles to clinical translation. *J Control Release*, *240*, 109-126. doi: 10.1016/j.jconrel.2015.11.009
- Srinivasan, S., Swaminathan, G., Kulothungan, V., Ganesan, S., Sharma, T., & Raman, R. (2017). Age-related macular degeneration in a South Indian population, with and without diabetes. *Eye (Lond)*, *31*(8), 1176-1183. doi:10.1038/eye.2017.47
- Stahl, A., Stumpp, M. T., Schlegel, A., Ekawardhani, S., Lehrling, C., Martin, G., . . . Binz, H. K. (2013). Highly potent VEGF-A-antagonistic DARPins as anti-angiogenic agents for topical and intravitreal applications. *Angiogenesis*, *16*(1), 101-111. doi:10.1007/s10456-012-9302-0
- Staurengi, G., Lai, T. Y. Y., Mitchell, P., Wolf, S., Wenzel, A., Li, J., . . . Group, P. S. (2018). Efficacy and Safety of Ranibizumab 0.5 mg for the Treatment of Macular Edema Resulting from Uncommon Causes: Twelve-Month Findings from PROMETHEUS. *Ophthalmology*, *125*(6), 850-862. doi: 10.1016/j.ophtha.2017.12.002
- Suda, K., Murakami, T., Gotoh, N., Fukuda, R., Hashida, Y., Hashida, M., . . . Yoshimura, N. (2017). High-density lipoprotein mutant eye drops for the treatment of posterior eye diseases. *J Control Release*, *266*, 301-309. doi: 10.1016/j.jconrel.2017.09.036
- Sun, X., Ma, P., Cao, X., Ning, L., Tian, Y., & Ren, C. (2009). Positive hyaluronan/PEI/DNA complexes as a target-specific intracellular delivery to malignant breast cancer. *Drug Deliv*, *16*(7), 357-362. doi:10.1080/10717540903059549
- Tai, L., Liu, C., Jiang, K., Chen, X., Wei, G., Lu, W., & Pan, W. (2017). Noninvasive delivery of oligonucleotide by penetratin-modified polyplexes to inhibit protein expression of intraocular tumor. *Nanomedicine*, *13*(6), 2091-2100. doi: 10.1016/j.nano.2017.04.011
- Terri Davis-Smyth, H. C., Jeanie Park, & Ferrara, L. G. P. a. N. (1996). The second immunoglobulin-like domain of the VEGF tyrosine kinase receptor Flt-1 determines ligand binding and may initiate a signal transduction cascade. *the EMBO Journal*, *15*.
- Tezel, A., & Fredrickson, G. H. (2008). The science of hyaluronic acid dermal fillers. *J Cosmet Laser Ther*, *10*(1), 35-42. doi:10.1080/14764170701774901
- Thakur, A., Scheinman, R. I., Rao, V. R., & Kompella, U. B. (2011). Pazopanib, a multitargeted tyrosine kinase inhibitor, reduces diabetic retinal vascular leukostasis and leakage. *Microvasc Res*, *82*(3), 346-350. doi: 10.1016/j.mvr.2011.09.001
- Thomas, C. J., Mirza, R. G., & Gill, M. K. (2021). Age-Related Macular Degeneration. *Med Clin North Am*, *105*(3), 473-491. doi: 10.1016/j.mcna.2021.01.003
- Tomono, T., Yagi, H., Ukawa, M., Ishizaki, S., Miwa, T., Nonomura, M., . . . Sakuma, S. (2020). Nasal absorption enhancement of protein drugs independent to their chemical properties in the presence of hyaluronic acid modified with tetraglycine-L-octaarginine. *Eur J Pharm Biopharm*, *154*, 186-194. doi: 10.1016/j.ejpb.2020.07.003
- Traynor, K. (2012). Aflibercept approved for macular degeneration. *Am J Health Syst Pharm*, *69*(1), 6. doi:10.2146/news120001
- Tsutomu Yasukawa†, Y. O., Hideya Kimura, Eiji Sakurai & Yasuhiko Tabata. (2006). Drug delivery from ocular implants. *Ashley Publications*.
- Urtti, A. (2006). Challenges and obstacles of ocular pharmacokinetics and drug delivery. *Adv Drug Deliv Rev*, *58*(11), 1131-1135. doi: 10.1016/j.addr.2006.07.027

- Valeria Cicatiello, I. A., Laura Tudisco, Valeria Tarallo, Luigi Formisano, Annamaria Sandomenico, Younghee Kim, Ana Bastos-Carvalho, Augusto Orlandi, Jayakrishna Ambati, Menotti Ruvo, Roberto Bianco, Sandro De Falco. (2015). Powerful anti-tumor and anti-angiogenic activity of a new antivascular EGF receptor-1 peptide in colorectal cancer models. *Oncotarget*, 6.
- Varma, R., Fraser-Bell, S., Tan, S., Klein, R., Azen, S. P., & Los Angeles Latino Eye Study, G. (2004). Prevalence of age-related macular degeneration in Latinos: the Los Angeles Latino eye study. *Ophthalmology*, 111(7), 1288-1297. doi: 10.1016/j.ophtha.2004.01.023
- Vasvani, S., Kulkarni, P., & Rawtani, D. (2020). Hyaluronic acid: A review on its biology, aspects of drug delivery, route of administrations and a special emphasis on its approved marketed products and recent clinical studies. *Int J Biol Macromol*, 151, 1012-1029. doi: 10.1016/j.ijbiomac.2019.11.066
- Virgili G, B. A. (2007). Laser photocoagulation for neovascular age-related macular degeneration. *Wiley*.
- Vives, E., Schmidt, J., & Pelegrin, A. (2008). Cell-penetrating and cell-targeting peptides in drug delivery. *Biochim Biophys Acta*, 1786(2), 126-138. doi: 10.1016/j.bbcan.2008.03.001
- Wang, Y., Lin, H., Lin, S., Qu, J., Xiao, J., Huang, Y., . . . Li, X. (2010). Cell-penetrating peptide TAT-mediated delivery of acidic FGF to retina and protection against ischemia-reperfusion injury in rats. *J Cell Mol Med*, 14(7), 1998-2005. doi:10.1111/j.1582-4934.2009.00786.x
- Xu, K., Lee, F., Gao, S., Tan, M. H., & Kurisawa, M. (2015). Hyaluronidase-incorporated hyaluronic acid-tyramine hydrogels for the sustained release of trastuzumab. *J Control Release*, 216, 47-55. doi: 10.1016/j.jconrel.2015.08.015
- Yehonathan Pouny, D. R., Amram Mor, Pierre Nicolas, and Yechiel Shai. (1992). Interaction of Antimicrobial Dermaseptin and Its Fluorescently Labeled Analogues with phospholipid membranes. *Biochemistry*, 49.
- ZARBIN, M. A. (1998). Age-related macular degeneration: Review of Pathogenesis. *European Journal of Ophthalmology*, 8, 199-205.
- Zhang, X., Wei, D., Xu, Y., & Zhu, Q. (2021). Hyaluronic acid in ocular drug delivery. *Carbohydr Polym*, 264, 118006. doi: 10.1016/j.carbpol.2021.118006
- Zhang, Y., He, B., Liu, K., Ning, L., Luo, D., Xu, K., . . . Xu, X. (2017). A novel peptide specifically binding to VEGF receptor suppresses angiogenesis in vitro and in vivo. *Signal Transduct Target Ther*, 2, 17010. doi:10.1038/sigtrans.2017.10
- Zhong, J., Deng, Y., Tian, B., Wang, B., Sun, Y., Huang, H., . . . Yuan, J. (2016). Hyaluronate Acid-Dependent Protection and Enhanced Corneal Wound Healing against Oxidative Damage in Corneal Epithelial Cells. *J Ophthalmol*, 2016, 6538051. doi:10.1155/2016/6538051
- Chakravarthy, U., Havilio, M., Syntosi, A., Pillai, N., Wilkes, E., Benyamini, G., . . . Sagkriotis, A. (2021). Impact of macular fluid volume fluctuations on visual acuity during anti-VEGF therapy in eyes with nAMD. *Eye (Lond)*, 35(11), 2983-2990. doi:10.1038/s41433-020-01354-4
- Chang, S., Qin, D., Yan, R., Zhang, M., Sui, B., Xu, H., . . . Qi, C. (2021). Temperature and pH Dual Responsive Nanogels of Modified Sodium Alginate and NIPAM for Berberine Loading and Release. *ACS Omega*, 6(2), 1119-1128. doi:10.1021/acsomega.0c03965
- Ciulla, T. A., Hussain, R. M., Pollack, J. S., & Williams, D. F. (2020). Visual Acuity Outcomes and Anti-Vascular Endothelial Growth Factor Therapy Intensity in Neovascular Age-Related Macular Degeneration Patients: A Real-World Analysis of 49 485 Eyes. *Ophthalmol Retina*, 4(1), 19-30. doi:10.1016/j.oret.2019.05.017
- de Cogan, F., Hill, L. J., Lynch, A., Morgan-Warren, P. J., Lechner, J., Berwick, M. R., . . . Logan, A. (2017). Topical Delivery of Anti-VEGF Drugs to the Ocular Posterior Segment Using Cell-Penetrating Peptides. *Invest Ophthalmol Vis Sci*, 58(5), 2578-2590. doi:10.1167/iovs.16-20072
- Del Amo, E. M., Rimpela, A. K., Heikkinen, E., Kari, O. K., Ramsay, E., Lajunen, T., . . . Urtti, A. (2017). Pharmacokinetic aspects of retinal drug delivery. *Prog Retin Eye Res*, 57, 134-185. doi:10.1016/j.preteyeres.2016.12.001

- Dugel, P. U., Koh, A., Ogura, Y., Jaffe, G. J., Schmidt-Erfurth, U., Brown, D. M., . . . Investigators, H. S. (2020). HAWK and HARRIER: Phase 3, Multicenter, Randomized, Double-Masked Trials of Brolicizumab for Neovascular Age-Related Macular Degeneration. *Ophthalmology*, *127*(1), 72-84. doi:10.1016/j.ophtha.2019.04.017
- Evans, J. R., & Lawrenson, J. G. (2017). Antioxidant vitamin and mineral supplements for preventing age-related macular degeneration. *Cochrane Database Syst Rev*, *7*, CD000253. doi:10.1002/14651858.CD000253.pub4
- Feher, J., Kovacs, I., Artico, M., Cavallotti, C., Papale, A., & Balacco Gabrieli, C. (2006). Mitochondrial alterations of retinal pigment epithelium in age-related macular degeneration. *Neurobiol Aging*, *27*(7), 983-993. doi:10.1016/j.neurobiolaging.2005.05.012
- Finger, R. P., Daien, V., Eldem, B. M., Talks, J. S., Korobelnik, J. F., Mitchell, P., . . . Carrasco, J. (2020). Anti-vascular endothelial growth factor in neovascular age-related macular degeneration - a systematic review of the impact of anti-VEGF on patient outcomes and healthcare systems. *BMC Ophthalmol*, *20*(1), 294. doi:10.1186/s12886-020-01554-2
- Guo, X., Hutcheon, A. E., & Zieske, J. D. (2004). Transduction of functionally active TAT fusion proteins into cornea. *Exp Eye Res*, *78*(5), 997-1005. doi:10.1016/j.exer.2003.12.010
- Gupta, H., Aqil, M., Khar, R. K., Ali, A., Bhatnagar, A., & Mittal, G. (2013). Nanoparticles laden in situ gel of levofloxacin for enhanced ocular retention. *Drug Deliv*, *20*(7), 306-309. doi:10.3109/10717544.2013.838712
- Huang, Y., Zhu, Y., Cai, D., Guo, Q., Wang, J., Lei, L., . . . Shi, S. (2022). Penetrating-peptide-mediated non-invasive Axitinib delivery for anti-neovascularisation. *J Control Release*, *347*, 449-459. doi:10.1016/j.jconrel.2022.05.009
- Hyukjin Lee, Y. J., and Tae Gwan Park. (2007). Shell Cross-Linked Hyaluronic Acid/Polylysine Layer-by-Layer Polyelectrolyte Microcapsules Prepared by Removal of Reducible Hyaluronic Acid Microgel Cores. *Biomacromolecules*, *8*.
- Johannsdottir, S., Jansook, P., Stefansson, E., Kristinsdottir, I. M., Fulop, Z., Asgrimsdottir, G. M., . . . Loftsson, T. (2018). Topical drug delivery to the posterior segment of the eye: Dexamethasone concentrations in various eye tissues after topical administration for up to 15 days to rabbits. *Journal of Drug Delivery Science and Technology*, *45*, 449-454. doi:10.1016/j.jddst.2018.04.007
- Kamaleddin, M. A. (2017). Nano-ophthalmology: Applications and considerations. *Nanomedicine*, *13*(4), 1459-1472. doi:10.1016/j.nano.2017.02.007
- Kim, L. A., & D'Amore, P. A. (2012). A brief history of anti-VEGF for the treatment of ocular angiogenesis. *Am J Pathol*, *181*(2), 376-379. doi:10.1016/j.ajpath.2012.06.006
- Kuang Tzu Huang, Y. H. C., and Ameae M. Walker, & University of California, R., CA, USA. (2004). Inaccuracies in MTS assays: major distorting effects of medium, serum albumin, and fatty acids. *BioTechniques*, *37*.
- Lai, J. Y. (2014). Relationship between structure and cytocompatibility of divinyl sulfone cross-linked hyaluronic acid. *Carbohydr Polym*, *101*, 203-212. doi:10.1016/j.carbpol.2013.09.060
- Layek, B., Lipp, L., & Singh, J. (2015). Cell Penetrating Peptide Conjugated Chitosan for Enhanced Delivery of Nucleic Acid. *Int J Mol Sci*, *16*(12), 28912-28930. doi:10.3390/ijms161226142
- Mitchell, P., Liew, G., Gopinath, B., & Wong, T. Y. (2018). Age-related macular degeneration. *The Lancet*, *392*(10153), 1147-1159. doi:10.1016/s0140-6736(18)31550-2
- Nurettin Sahiner, X. J. (2008). One-Step Synthesis of Hyaluronic Acid-Based (Sub)micron Hydrogel Particles\_ Process Optimization and Preliminary Characterization. *Turk J Chem*, *32*.
- Pescina, S., Ostacolo, C., Gomez-Monterrey, I. M., Sala, M., Bertamino, A., Sonvico, F., . . . Nicoli, S. (2018). Cell penetrating peptides in ocular drug delivery: State of the art. *J Control Release*, *284*, 84-102. doi:10.1016/j.jconrel.2018.06.023
- Rah, M. J. (2011). A review of hyaluronan and its ophthalmic applications. *Optometry*, *82*(1), 38-43. doi:10.1016/j.optm.2010.08.003

- Schargus, M., & Frings, A. (2020). Issues with Intravitreal Administration of Anti-VEGF Drugs. *Clin Ophthalmol*, 14, 897-904. doi:10.2147/OPTH.S207978
- Sharaf, M. G., Cetinel, S., Heckler, L., Damji, K., Unsworth, L., & Montemagno, C. (2014). Nanotechnology-Based Approaches for Ophthalmology Applications: Therapeutic and Diagnostic Strategies. *Asia Pac J Ophthalmol (Phila)*, 3(3), 172-180. doi:10.1097/APO.000000000000059
- Skottman, H., Muranen, J., Lahdekorpi, H., Pajula, E., Makela, K., Koivusalo, L., . . . Juuti-Uusitalo, K. (2017). Contacting co-culture of human retinal microvascular endothelial cells alters barrier function of human embryonic stem cell derived retinal pigment epithelial cells. *Exp Cell Res*, 359(1), 101-111. doi:10.1016/j.yexcr.2017.08.004
- Su, W., Sun, S., Tian, B., Tai, P. W. L., Luo, Y., Ko, J., . . . Lin, H. (2021). Efficacious, safe, and stable inhibition of corneal neovascularization by AAV-vectored anti-VEGF therapeutics. *Mol Ther Methods Clin Dev*, 22, 107-121. doi:10.1016/j.omtm.2021.06.007
- Tračuma, E., & Loca, D. (2020). Hyaluronic Acid/Polylysine Composites for Local Drug Delivery: A Review. *Key Engineering Materials*, 850, 213-218. doi:10.4028/[www.scientific.net/KEM.850.213](http://www.scientific.net/KEM.850.213)
- Varela-Fernandez, R., Diaz-Tome, V., Luaces-Rodriguez, A., Conde-Penedo, A., Garcia-Otero, X., Luzardo-Alvarez, A., . . . Otero-Espinar, F. J. (2020). Drug Delivery to the Posterior Segment of the Eye: Biopharmaceutic and Pharmacokinetic Considerations. *Pharmaceutics*, 12(3). doi:10.3390/pharmaceutics12030269
- Vasi, A. M., Popa, M. I., Butnaru, M., Dodi, G., & Verestiuc, L. (2014). Chemical functionalization of hyaluronic acid for drug delivery applications. *Mater Sci Eng C Mater Biol Appl*, 38, 177-185. doi:10.1016/j.msec.2014.01.052
- Wang, J., Li, B., Huang, D., Norat, P., Grannonico, M., Cooper, R. C., . . . Yang, H. (2021). Nano-in-Nano Dendrimer Gel Particles for Efficient Topical Delivery of Antiglaucoma Drugs into the Eye. *Chem Eng J*, 425. doi:10.1016/j.cej.2021.130498
- Wei, X., Senanayake, T. H., Warren, G., & Vinogradov, S. V. (2013). Hyaluronic acid-based nanogel-drug conjugates with enhanced anticancer activity designed for the targeting of CD44-positive and drug-resistant tumors. *Bioconjug Chem*, 24(4), 658-668. doi:10.1021/bc300632w
- Xu, Q., Boylan, N. J., Suk, J. S., Wang, Y. Y., Nance, E. A., Yang, J. C., . . . Hanes, J. (2013). Nanoparticle diffusion in, and microrheology of, the bovine vitreous ex vivo. *J Control Release*, 167(1), 76-84. doi:10.1016/j.jconrel.2013.01.018
- Yi, L. J., Feng; Lili, Yang; Hongfeng, Tang; Ji, Jin; Xun, Xu. (2014). Anti-inflammatory effects of a synthetic peptide derived from pigment epithelium-derived factor on H2O2-induced corneal injury in vitro. *Chinese Medical Journal*, 127. doi:10.3760/cma.j.issn.0366-6999.20132571
- Zhang, Y., He, B., Liu, K., Ning, L., Luo, D., Xu, K., . . . Xu, X. (2017). A novel peptide specifically binding to VEGF receptor suppresses angiogenesis in vitro and in vivo. *Signal Transduct Target Ther*, 2, 17010. doi:10.1038/sigtrans.2017.10
- Zhao, Y., & Singh, R. P. (2018). The role of anti-vascular endothelial growth factor (anti-VEGF) in the management of proliferative diabetic retinopathy. *Drugs Context*, 7, 212532. doi:10.7573/dic.212532

## **Appendix**

**Copy right clearance to use image 2: Multimodal imaging of AMD.**

**ELSEVIER LICENSE  
TERMS AND CONDITIONS**

Jan 25, 2022

---

This Agreement between Sabanci University -- hande sutova ("You") and Elsevier ("Elsevier") consists of your license details and the terms and conditions provided by Elsevier and Copyright Clearance Center.

License Number 5222100880834

License date Jan 04, 2022

Licensed Content  
Publisher ElsevierLicensed Content  
Publication The Lancet

Licensed Content Title Age-related macular degeneration

Licensed Content Author Paul Mitchell, Gerald Liew, Bamini Gopinath, Tien Y Wong

Licensed Content Date 29 September–5 October 2018

Licensed Content Volume 392

<https://s100.copyright.com/CustomAdmin/PLF.jsp?ref=ed209bad-f15a-44ad-8aaf-58463b2b4245>

<https://documentcloud.adobe.com/link/review?uri=urn:aaid:scds:US:b5957bb2-dd36-34c3-8b47-8ac18f309c96>